TITLE

The exocyst complex controls multiple events in the pathway of regulated exocytosis

Sofía Suárez Freire[1, 2], Sebastián Pérez-Pandolfo[1, 2], Sabrina M. Fresco[1], Julián Valinoti[1], Eleonora Sorianello[2, 3], Pablo Wappner[1, 2, 4] * and Mariana Melani[1, 2, 4] *

[1] Fundación Instituto Leloir, Buenos Aires, Argentina.

[2] Consejo Nacional De Investigaciones Científicas Y Técnicas (CONICET), Buenos Aires, Argentina.

[3] Laboratorio de Regulación Hipofisaria. Instituto de Medicina y Biología Experimental (IBYME-CONICET), 1428 Buenos Aires, Argentina.

[4] Departamento De Fisiología, Biología Molecular Y Celular, Facultad De Ciencias Exactas Y Naturales, Universidad De Buenos Aires, Buenos Aires, Argentina.

*Corresponding authors

pwappner@leloir.org.ar

mmelani@leloir.org.ar

ABSTRACT

Eukaryotic cells depend on exocytosis to direct intracellularly synthesized material towards the extracellular space or the plasma membrane, so exocytosis constitutes a basic function for cellular homeostasis and communication between cells. The secretory pathway includes biogenesis of secretory granules (SGs), their maturation and fusion with the plasma membrane (exocytosis), resulting in release of SG content to the extracellular space. The larval salivary gland of *Drosophila melanogaster* is an excellent model for studying exocytosis. This gland synthesizes mucins that are packaged in SGs that sprout from the *trans*-Golgi network and then undergo a maturation process that involves homotypic fusion, condensation and acidification. Finally, mature SGs are directed to the apical domain of the plasma membrane with which they fuse, releasing their content into the gland lumen. The exocyst is a hetero-octameric complex that participates in tethering of vesicles to the plasma membrane during constitutive exocytosis. By precise temperature-dependent gradual activation of the Gal4-UAS expression system, we have induced different levels of silencing of exocyst complex subunits, and identified three temporarily distinctive steps of the regulated exocytic pathway where the exocyst is critically required: SG biogenesis, SG maturation and SG exocytosis. Our results shed light on previously unidentified functions of the exocyst along the exocytic pathway. We propose that the exocyst acts as a general tethering factor in various steps of this cellular process.

INTRODUCTION

Protein secretion is a fundamental process for communication between eukaryotic cells and therefore, for organismal homeostasis, reproduction and survival. Two types of secretory processes can be distinguished based on the rate and mode of regulation of secretory vesicle release: Constitutive secretion and regulated secretion (Morgan, 1995). In constitutive secretion, secretory vesicles are exocytosed as they are produced. This process takes place in all eukaryotic cells, mainly to maintain homeostasis of the plasma membrane and the extracellular matrix. In contrast, regulated secretion takes place in specialized cell types, such as endocrine and exocrine cells, as well as in cells of the immune system such as platelets and neutrophils (Aggarwal, Jennings, Manning, & Cameron, 2023; Ley et al., 2018). These cell types produce specialized secretory vesicles known as secretory granules (SGs), which are released in response to specific stimuli (Kogel & Gerdes, 2010). SGs sprout from the *trans*-Golgi network (TGN) as immature vesicles, incompetent for fusion with the plasma membrane. Maturation of SGs involves homotypic fusion and acquisition of membrane proteins, which are required for SG delivery and fusion with the plasma membrane. Finally, stimulus-driven fusion of SGs with the plasma membrane results in cargo release to the extracellular milieu (Omar-Hmeadi & Idevall-Hagren, 2021; Sugita, 2008).

The salivary gland of *Drosophila melanogaster* larvae provides several advantages for the identification of regulators of SG biogenesis, maturation and exocytosis (Burgess et al., 2012; de la Riva-Carrasco et al., 2021; Neuman & Bashirullah, 2018; Rousso, Schejter, & Shilo, 2016). At late third larval instar, salivary glands synthesize a series of mucins, collectively known as Glue proteins, which become packed in SGs. Approximately four hours before the onset of pupariation, concerted exocytosis of mucin-containing SGs, followed by extrusion of the mucins out of the prepupal body are essential for gluing the puparium to the substratum (Borne, Kovalev, Gorb, & Courtier-Orgogozo, 2020). Interestingly, these three events of SG development (biogenesis, maturation and exocytosis) occur sequentially and

only once in each cell of the salivary gland, that will later on be degraded during metamorphosis (Duan et al., 2020; Tracy, Velentzas, & Baehrecke, 2016). The tagging of one of these mucins with fluorophores (Sgs3-GFP or Sgs3-dsRed), (Biyasheva, Do, Lu, Vaskova, & Andres, 2001) combined with the large size of salivary gland cells and their SGs, have allowed high resolution imaging and real time traceability of SG biogenesis, maturation and secretion, leading to the identification and characterization of dozens of factors required along the exocytic pathway (Burgess et al., 2011; Neuman et al., 2022; Reynolds, Zhang, Tran, & Ten Hagen, 2019; Torres, Rosa-Ferreira, & Munro, 2014; Tran, Masedunskas, Weigert, & Ten Hagen, 2015).

The exocyst is a hetero-octameric protein complex identified and initially characterized in the budding yeast, and later found to be conserved across all eukaryotic organisms (Hsu et al., 1996; Novick, Field, & Schekman, 1980; Novick et al., 1995; TerBush, Maurice, Roth, & Novick, 1996). Yeast cells bearing mutations in exocyst subunits display intracellular accumulation of secretory vesicles and defects in exocytosis (Govindan, Bowser, & Novick, 1995; TerBush et al., 1996). Molecularly, the exocyst complex participates in vesicle tethering to the plasma membrane prior to SNARE-mediated fusion (An et al., 2021). Exocyst complex malfunction has been therefore associated with tumor growth and invasion, as well as with development of ciliopathies, among other pathological conditions (Luo, Zhang, Luca, & Guo, 2013; Mavor et al., 2016; Thapa et al., 2012; Whyte & Munro, 2002; B. Wu & Guo, 2015).

In this work, we have utilized the *Drosophila* salivary gland to carry out a methodic analysis of the requirement of each of the eight subunits of the exocyst along the regulated exocytic pathway. By inducing temperature-dependent gradual downregulation of the expression of each of the subunits, we discovered novel functions of the exocyst complex in regulated exocytosis, namely in SG biogenesis, SG maturation and homotypic fusion, as well as in SG fusion with the plasma membrane. We propose that the exocyst complex participates in all these processes as a general tethering factor.

Results

Characterization of secretory granule progression during salivary gland development

Salivary glands of *Drosophila melanogaster* larvae fulfill different functions during larval development. Mostly, they act as exocrine glands producing non-digestive enzymes during the larval feeding period, as well as mucins when the larva is about to pupariate (Costantino et al., 2008; Farkas et al., 2014). More recently, salivary glands have been proposed to behave as endocrine organs as well, secreting a yet unidentified factor that regulates larval growth (Li et al., 2022). Biosynthesis of mucins produced by salivary glands, named Salivary gland secreted proteins (Sgs), begins at the second half of the third larval instar in response to an ecdysone peak (Biyasheva et al., 2001). After being glycosylated at the Endoplasmic Reticulum (ER) and the Golgi Complex (GC), mucins are packed in SGs. Following subsequent developmentally-controlled hormonal stimuli, SGs are massively exocytosed, releasing the mucins to the gland lumen, and finally expelling them outside of the puparium, and gluing it to the substratum (Biyasheva et al., 2001). We used Sgs3-GFP or Sgs3-dsRed transgenic lines to follow this process *in vivo*. In wandering larvae, Sgs3-dsRed can be detected in salivary glands (Figure 1A'), while in prepupae, Sgs3-dsRed has been secreted out from the puparium, and is no longer detectable in salivary glands (Figure 1B'). To have a better temporal and spatial resolution of this process, we dissected and analyzed by confocal microscopy salivary glands expressing Sgs3-GFP at 4 h intervals starting at 96 h after egg laying (AEL). Expression of Sgs3-GFP begins at 96-100 h AEL, and can be detected at the distal region of the gland (Figure 1C). Later on, Sgs3-GFP expression expands to more proximal cells, and at 116 h AEL, the mucin becomes detectable in the whole gland, with the exception of ductal cells which do not express Sgs3 (Figure 1C) (Biyasheva et al., 2001). Thereafter, at 116-120 h AEL, in response to an ecdysone peak, SGs fuse with the apical plasma membrane, and release their content to the gland lumen (Figure 1C).

Detailed observation of distal cells of salivary glands revealed that SGs enlarge from 96 h AEL onwards (Figure 1D), (Ma & Brill, 2021b; Neuman, Lee, Selegue, Cavanagh, & Bashirullah, 2021), a phenomenon that we quantified by measuring SG diameter (Figure 1D and Supplementary Table 1). At 96-100 h AEL nascent SGs are smaller than 1 μm in diameter. Later, and up to 112 h AEL, most SGs are smaller than 3 μm in diameter, and classified them as "Immature SGs". From 112 h AEL onwards most SGs are bigger than 3 μm in diameter and classified as "Mature SGs" (Figure 1D and Supplementary Table 1). The maximal SG diameter that we detected was 7.13 μm at 116-120 AEL, just before exocytosis (Supplementary Table 1).

The eight subunits of the exocyst complex are required for regulated exocytosis of secretory granules

Fluorophore-tagged Sgs3 can also be used to screen for exocytosis mutants in which Sgs3-GFP is retained inside salivary glands at the prepupal stage (de la Riva-Carrasco et al., 2021; Ma et al., 2020). Using this approach, we found that the exocyst complex is apparently required for exocytosis of SGs, since silencing of any of the eight subunits of the complex results in retention of Sgs3-GFP in salivary glands of prepupae (Figure 2 and Supplementary Figure 1B). We used the salivary gland specific driver *forkhead*-Gal4 (*fkh*-Gal4) to induce the expression of RNAis against each of the eight subunits of the exocyst complex in larvae that also expressed Sgs3-GFP. We analyzed Sgs3-GFP distribution in wandering larvae and prepupae (Figure 2A-B), and observed that whereas control prepupae were able to expel Sgs3 outside the puparium (Figure 2A' and C), this process was blocked in most individuals expressing RNAis against any of the exocyst subunits, with Sgs3-GFP being detected inside salivary glands of prepupae (Figure 2B'-C and Supplementary Figure 1B). These observations suggest that all exocyst subunits are required for exocytosis of SGs.

128 Having established that knock-down of each of the exocyst subunits can block secretion of
129 Sgs3, leading to retention of the mucin in the salivary glands (Figure 2), we investigated if exocytosis is
130 actually impaired in these larvae. We dissected salivary glands of control and exocyst knock-down
131 individuals at 116 h AEL, and analyzed them under the confocal microscope. Whereas control salivary
132 gland cells were filled with mature SGs (Figure 3A), a more heterogeneous situation was found in
133 salivary glands cells expressing RNAi against exocyst subunits, with some cells displaying mature SGs,
134 and other, immature SGs, while even some displayed Sgs3-GFP in a mesh or network-like structure
135 (Figure 3B). Therefore, we investigated if this mosaic phenotypic manifestation was due to variations
136 in cell-to-cell Gal4-UAS activation and therefore RNAi expression, being an indication of potentially
137 different functions of the exocyst complex in the secretory pathway of salivary gland cells. We
138 performed RNAi-mediated knock-down of each of the eight exocyst subunits at different temperatures
139 (29, 25, 21 and 19°C), that were accurately controlled in water baths, to obtain different levels of
140 silencing and likely different phenotypic manifestations of exocyst complex downregulation. Whereas
141 expression of a control RNAi resulted in mature SGs irrespectively of the temperature, expression of
142 exocyst subunits RNAis at high temperatures (29°C) resulted, as a general rule, in phenotypes
143 consistent with early arrest of the secretory pathway, since in most cells Sgs3-GFP was retained in a
144 reticular structure or packed in immature SGs (Figure 3C, Supplementary Figure 1A and Supplementary
145 Table 3). By lowering the temperature of RNAi expression, and therefore moderating silencing, the
146 most severe phenotypes (early arrest of the secretory pathway) gradually became less prominent and
147 simultaneously, the proportion of cells displaying immature SGs, and even mature SGs, became more
148 noticeable (Figure 3C and Supplementary Figure 1A and Supplementary Table 3), suggesting that lower
149 expression of RNAis allowed the progression of the secretory pathway. Notably, for each of the RNAis
150 tested there was a temperature at which each of the three phenotypic outcomes could be clearly
151 identified, although this particular temperature could be different for each RNAi, likely due to

152 expression levels of the transgenes (Figure 3C, Supplementary Figure 1A and Supplementary Table 3).
153 RT-qPCR confirmed that different culturing temperatures resulted in different degrees of silencing of
154 exocyst subunit mRNA as shown in Supplementary Figure 2 for *exo70* and *sec3* (Supplementary Figure
155 2A-B). Also, we found that different phenotypic outcomes resulting from expression of different RNAi
156 transgenic lines that target the same subunit (*exo70)* are due to differences in the levels of mRNA
157 downregulation generated by each particular (*exo70* ^{RNAiV} and *exo70*^{RNAiBL}), and that there is a
158 correlation between the level of mRNA downregulation and strength of the phenotype observed
159 (Supplementary Figure 2C).

160 To define more precisely the role of the exocyst, and rule out potential pleiotropic effects due
161 to developmental defects derived from chronic exocyst downregulation, we made use of the Gal80
162 thermosensitive tool (*Gal80*^{ts}) ((Lee & Luo, 1999)). Larva were grown at a restrictive temperature
163 (18°C) until they reached the 3er instar (120 hours). In this manner, the exocyst complex could be
164 functional up until that developmental stage. Then, larvae were transfered to the permissive
165 temperature (29°C) and salivary glands were dissected 36 hours later. We found that temporally-
166 restricted expression of *sec3*^{RNAi} or *sec15*^{RNAi} phenocopied unrestricted expression of the same RNAis at
167 29°C (Supplementary Figure 3), indicating that the phenotypes obtained are not due to pleiotropic
168 effects caused by developmentally unrestricted downregulation of the exocyst. Finally, the MLS
169 phenotype generated by expression of *sec15*^{RNAi} could be rescued by simultaneous expression of GFP-
170 Sec15, supporting the notion that defective biogenesis of SGs was specifically provoked by *sec15* loss
171 of function (Supplementary Figure 4).

172 A comprehensive analysis of cell polarity, as well as a number of general markers of cellular
173 homeostasis (Supplementary Figures 5 and 6), ruled out that defects in SG biogenesis or maturation
174 observed after knock-down of exocyst subunits could stem from potential secondary effects derived
175 from poor cellular health, but rather reflect genuine functions of the exocyst complex in the secretory

176 pathway. Along these lines, a recent report showed that apical polarity defects generated by loss of
177 polarity protein Crumbs, do not affect or interfere with SG exocytosis (Lattner, Leng, Knust,
178 Brankatschk, & Flores-Benitez, 2019), further supporting the notion that there are parallel pathways
179 controlling cell polarity and SG biogenesis, maturation and exocytosis.

180 The fact that the three phenotypic outcomes (1-Sgs3-GFP retained in a mesh; 2-immature SG
181 and 3-mature-not exocytosed SG) could be retrieved with appropriate silencing any of the eight
182 subunits lead us to propose that the holocomplex, and not subcomplexes or individual subunits, could
183 function several times along the secretory pathway, and that each of these activities could require
184 different amounts of exocyst complex. Importantly, irrespectively of the temperature of expression of
185 RNAis, retention of SGs in salivary glands cells was always significantly higher in exocyst knock-down
186 individuals than in controls (Figure 3D and Supplementary Figure 1B), indicating that ultimately, the
187 exocyst is required for SG exocytosis.

188

189 **The exocyst complex is required for secretory granule biogenesis**

190 We decided to characterize each of the three phenotypic manifestations of exocyst loss-of-
191 function in more detail. The early-most manifestation of the requirement of the exocyst in the
192 secretory pathway was the reticular or mesh-like phenotype obtained by strong silencing (29°C) any of
193 the subunits (Figure 4A). This phenotype was reminiscent of mutants in which Sgs3 is retained at
194 endoplasmic reticulum exit sites (ERES) or at ER-Golgi Complex (GC) contact sites (Burgess et al., 2011;
195 Reynolds et al., 2019), suggesting that knock-down of the exocyst may provoke Sgs3 retention at the
196 ER or GC, blocking SG biogenesis . Indeed, we found that RNAi-mediated silencing of *sec15* ,*sec3* or
197 *sec10* provoked Sgs3 retention in the ER since it colocalized with ER markers, as indicated by
198 Pearson´s coefficient , whereas in control larvae Sgs3-GFP was inside SGs, at a comparable
199 developmental stage (Figure 4B-G and Supplementary Figures 7 and 8).

We analyzed in detail GFP-Sec15 subcellular localization, and found that associated closely with the *trans*-Golgi marker RFP-Golgi, but not to the ER marker KDEL-RFP, in salivary glands just prior to SG biogenesis (Figure 5 and Supplementary Movie 1). This association was lost after the onset SG biogenesis, suggesting that the exocyst associates with the GC at the specific developmental stage when Sgs3 transits through that organelle (Figure 5B-E). Three-dimensional reconstruction of Sec15-Golgi *foci* confirmed the spatial association with the exocyst (Figure 5E and Supplementary Movie 2-3). In line with this, we found that exocyst silencing under conditions that block Sgs3-GFP in the ER (29°C), both, *cis* and *trans*-CG structures were severely affected (Figure 6 and Supplementary Figure 9). This suggests that at this stage of salivary gland development the exocyst complex localizes to the GC, where it is required to maintain *cis*- and *trans*-GC morphology and allow the correct transport of Sgs3 from the ER through the GC (Figure 6E-F).

Role of the exocyst in secretory granule maturation: Homotypic fusion

Given that appropriate silencing conditions of any of the exocyst subunits can result in accumulation of immature SGs (Figure 7A), we set out to investigate a potential role of the exocyst in SG maturation. SG maturation is a multifaceted process that involves, among other events, homotypic fusion between immature SGs (Du et al., 2016; Neuman & Bashirullah, 2018). We found that GFP-Sec15 often localized in discrete *foci* in between immature SGs (75% of total GFP-Sec15), but this localization drops dramatically when SGs have undergone maturation (15%) (Figure 7B, C and Supplementary Movie 4-5). This transient localization of the GFP-Sec15 supports the notion of a role of the exocyst in SG homofusion, which was confirmed by live imaging of salivary glands *ex-vivo* (Figure 7D and Supplementary Movie 6). In support of this notion, when GFP-Sec15 was overexpressed at 25 °C, unusually large SGs of up to 20 μm in diameter could be detected, a size never observed in control salivary glands overexpressing GFP alone (Figure 7E-H), indicating that overexpression of the Sec15

subunit alone is sufficient to induce homotypic fusion between SGs, which is in agreement with reports that indicate that Sec15 functions as a seed for exocyst complex assembly (Escrevente, Bento-Lopes, Ramalho, & Barral, 2021; Guo, Roth, Walch-Solimena, & Novick, 1999). Sec15 overexpression is expected to induce the formation of of exocyst holocomplexes, provoking excessive homofusion among SGs. In contrast, overexpression of Sec8, which is not expected to induce the formation of the whole complex, did not have an effect on homotypic fusion of SGs (Figure 7F, H).

The characteristic localization of GFP-Sec15 *foci* in between adjacent immature SGs, the fact that Sec15 overexpression results in oversized SGs, and the observation that downregulation of any subunit of the exocyst complex at appropriate levels results in accumulation of immature SGs, weigh in favor of the notion that the exocyst plays a critical role in SG homotypic fusion.

Role of the exocyst in secretory granule maturation: acquisition of membrane proteins

Besides homotypic fusion, maturation of SGs involves the incorporation of specific proteins that are required for homotypic fusion, apical navigation or fusion with the apical plasma membrane. The mechanisms by which these maturation factors associate with SG are not well understood. One of such proteins is the calcium sensor Synaptotagmin-1 (Syt-1), which localized at the basolateral membrane of salivary gland cells before SG biogenesis (96 h AEL) (Supplementary Figure 10A) and later, became detectable on the membrane of nascent SGs (diameter<1μm), prior to homotypic fusion (Figure 8A and Supplementary Figure 10B). As SGs mature, the presence of Syt-1 on SGs became more prominent, with a sharp increase after SG homofusion (Supplementary Figure 10C-D), suggesting that recruitment of Syt-1 to SGs continued after homotypic fusion had occurred (Figure 8M). Downregulation of the exocyst subunits Sec5 or Sec3 to levels that generate immature SGs, significantly reduced the presence of Syt-1 on their membranes, as compared to immature SGs of control salivary glands (Figure 8A-C and Supplementary Figure 11A-C). Interestingly, weaker knock-

down, which allowed the formation of mature SGs, improved but not completely restored Syt-1 recruitment, compared to control salivary cells (Supplementary Figure 11D-F), indicating that Syt-1 is recruited to mature SGs in an exocyst-dependent manner (Figure 8M).

CD63, the *Drosophila* homolog of mammalian Tsp29Fa, is another protein required for SG maturation. CD63 localizes at the apical plasma membrane before SG formation and reaches the membrane of SGs through endosomal retrograde trafficking (Supplementary Figure 10E), (Ma et al., 2020). We investigated if the exocyst participates in recruitment of CD63 to SGs, and found that CD63 could be readily detected at the membrane of 1μm; 3μm or 5μm SGs (Figure 8D and Supplementary Figure 10F-H), while upon Sec5 or Sec3 downregulation CD63 was significantly reduced on immature SGs (Figure 8D-F and Supplementary Figure 11G-I). Interestingly, milder reduction of Sec3 expression, under conditions that allow the formation of mature SGs, did not affect CD63 recruitment to SGs (Supplementary Figure 11J-L), indicating that CD63 is recruited to SGs before homotypic fusion in an exocyst-dependent manner and that, unlike to Syt-1, recruitment ceases after homotypic fusion has occurred (Figure 8M).

The small GTPases Rab11 and Rab1 were reported to be required for SG maturation. Whereas Rab11 associates to SGs independently of their size, Rab1 was found transiently on immature SGs only (Ma & Brill, 2021a; Neuman et al., 2021), and moreover, Rab1 recruitment to SGs depends on Rab11 (Neuman et al., 2021). Given that Rab11 is a stable component of SGs and Rab1 is not, we reasoned that other players, perhaps the exocyst, might be involved in Rab1 association or dissociation from the SG membrane. In fact, silencing of Sec5 under conditions that allowed the formation of immature SGs, provoked significant reduction of Rab1-YFP on the SG membrane (Figure 8G-I), suggesting that the exocyst participated in Rab1 recruitment (Figure 8M).

Remarkably, immature SGs that resulted from Sec5 or Sec3 knock-down displayed higher-than-normal levels of YFP-Rab11 around them (Figure 8J-L and Supplementary Figure 11M-O), suggesting

272 that the exocyst is a negative regulator of Rab11 recruitment. This observation is in apparent
273 contradiction with previous reports by others and us that indicate that Rab11 is required for SG
274 maturation (de la Riva-Carrasco et al., 2021; Ma & Brill, 2021a; Neuman et al., 2021). Noteworthy,
275 overexpression of a constitutively active form of Rab11 (UAS-YFP-Rab11^{CA}), which was readily recruited
276 to SGs, also provoked an arrest of SG maturation, thereby phenocopying exocyst complex knock-down
277 (Supplementary Figure 12A-C). Thus, during maturation of SGs, the levels of active Rab11 need to be
278 precisely regulated and this is achieved, at least in part, by the exocyst (Figure 8M and Supplementary
279 Figure 12F).
280 Given that the exocyst is an effector of different Rab-GTPases during vesicle exocytosis (Guo et
281 al., 1999; Novick et al., 1995; S. Wu, Mehta, Pichaud, Bellen, & Quiocho, 2005), we next investigated if
282 Rab11 is required for recruiting the exocyst to SGs. Indeed, we found that Sec15 failed to localize on
283 SGs following knock-down of Rab11 (Supplementary Figure 12D-E), indicating a crucial role of Rab11 in
284 recruitment of Sec15, and probably of the whole exocyst to SGs.
285 Overall, the results described in this section suggest that Rab11 recruits Sec15, and perhaps
286 the whole exocyst, to immature SGs to allow homotypic fusion and maturation (Supplementary Figure
287 12D-E) while in turn, the exocyts limits the levels and/or activity of Rab11 on SGs (Figure 8J-L and
288 Supplementary Figure 11M-R), as too much Rab11 is apparently detrimental for SG maturation
289 (Supplementary Figure 12A-C). We propose that a single-negative feedback loop precisely regulates
290 Rab11 and exocyst complex activity/levels, thus controlling recruitment of maturation factors such as
291 Syt-1, CD63 and Rab1, and therefore, the outcome of SG maturation (Supplementary Figure 12F).
292
293 **The exocyst is required for secretory granule fusion with the apical plasma membrane**
294 Under low silencing conditions of exocyst subunits the prevalent phenotype was mature SGs
295 retained in salivary gland cells (Figure 3D, Figure 9A, and Supplementary Figure 1B), suggesting a

function of the complex in SG fusion with the apical plasma membrane. The process of SG-plasma membrane fusion can be assessed by visualizing the incorporation of plasma membrane-specific components to the membrane of SGs (de la Riva-Carrasco et al., 2021; Rousso et al., 2016; Tran et al., 2015). Phosphatidylinositol 4,5-bisphosphate (PI(4,5)P_2) is a lipid of the inner leaflet of the apical plasma membrane, which is absent in endomembranes (Phan et al., 2019). Using a fluorophore-based reporter of PI(4,5)P_2 the SGs that have fused with the plasma membrane can be distinguished from those that have not. Using this approach we found that silencing of Exo70 impaired fusion with the plasma membrane (Figure 9B-D). Consistent with a role of the exocyst in fusion of SGs with the plasma membrane, at this stage of development GFP-Sec15 was no longer detected GFP-Sec15 was detected on SGs at the sites of contact with the plasma membrane (Figure 9E-G and Supplementary Movie 7). These data indicate that during regulated exocytosis, the exocyst complex is required for fusion of SGs to the apical plasma membrane, possibly acting as a tethering complex (Figure 9H-I).

Overall, by utilizing the *Drosophila* larval salivary gland, we have made a comprehensive analysis of the role of the exocyst complex in the pathway of regulated exocytosis. We found that the exocyst is critically required for biogenesis of SGs, for their maturation and homotypic fusion and for mediating fusion between SGs and the plasma membrane.

Discussion

The exocyst was initially identified as crucial for secretion in yeast (Novick et al., 1980; TerBush et al., 1996) and later on, for basolateral trafficking in animal epithelial cells (Grindstaff et al., 1998; Lipschutz et al., 2000); (Langevin et al., 2005), with implications in various cellular processes, including cell migration, cytokinesis, ciliogenesis and autophagy (Bodemann et al., 2011; Park et al., 2010; Rogers et al., 2004; Thapa et al., 2012). Recently, an in-depth study of the mammalian exocyst was performed, showing that each of the eight subunits of the complex are essential for constitutive secretion of

320 soluble proteins (Pereira et al., 2023). However, fewer is known about the function of the exocyst in
321 regulated exocytosis. A recent work indicates that, in cultured pancreatic beta cells, the exocyst
322 mediates tethering of insulin-containing granules to the plasma membrane and to the cortical F-actin
323 network, being required for exocytosis of a subset of these granules (Zhao et al., 2023). Previous
324 studies had implicated specific subunits of the complex in insulin-stimulated exocytosis of the glucose
325 transporter Glut4 in cultured adipocytes (Inoue, Chang, Hwang, Chiang, & Saltiel, 2003), as well as in
326 skeletal muscle cells (Fujimoto et al., 2019). In *Drosophila*, some subunits of the complex (Sec3, Sec5,
327 Sec6, Sec8 and Sec15) were recently suggested to be required for SG development (Ma et al., 2020),
328 although earlier, a role for the Sec10 in salivary gland exocytosis had been disregarded (Andrews,
329 Zhang, Trotta, & Broadie, 2002). Therefore, a role of the exocyst in regulated exocytosis is less clear. In
330 this study, we not only demonstrate that the eight subunits of the complex are required for regulated
331 exocytosis of SGs of *Drosophila* larval salivary gland, but also that the holocomplex participates in
332 multiple steps along the secretory pathway.

333 Most studies of the secretory pathway rely on a bimodal readout: Intracellular retention of SGs
334 *versus* exocytosis of SG content. These approaches set a limit to our understanding of the specific
335 functions that regulators and effectors exert on the exocytic pathway. By using fluorescently labeled
336 versions of a SG cargo protein in *Drosophila* salivary glands, Sgs3, we have shown that knock-down of
337 any of the exocyst subunits can bring about three distinct phenotypic outcomes: 1-Impairment of SG
338 biogenesis, 2-impairment of SG homotypic fusion and maturation, or 3-impairment of SG fusion with
339 the apical plasma membrane. Noteworthy, the frequency at which these defects occurs depends on
340 the extent of exocyst downregulation, implying that each of the three functions depends on different
341 levels of the complex: SG-plasma membrane fusion is highly sensitive to even slight reductions of
342 exocyst subunits levels; SG maturation requires intermediate levels of the complex, and SG biogenesis

343 seems to be the most robust of the three processes, and strong reduction of exocyst levels is required
344 to bring about this defect.

345 Although exocyst subcomplexes or individual subunits have been suggested to play specific
346 roles in cell biology (Mehta et al., 2005), it is generally believed that the functions of the exocyst are
347 carried out by the holocomplex (Ahmed et al., 2018). Studies analyzing the requirement of all eight
348 subunits in a single biological process are not abundant. In *Drosophila*, a study was performed in which
349 the eight subunits were found to be required for developmentally regulated autophagy, during salivary
350 cell death, but not for starvation-induced autophagy in the fat body (Tracy et al., 2016) and also for
351 proper synaptic development at the neuromuscular junction (Kang et al., 2024). However, in other
352 biological settings some subunits of the exocyst (Sec3, Sec5, Sec6, Sec8, and Sec10) but not others
353 (Sec15, Exo70 and Exo84) were shown to be specifically required for general as well as specific
354 autophagy in yeast (Singh et al., 2019). In mammalian cells, Exo84- and Sec5-induced exocyst complex
355 activation have opposing roles on autophagy machinery activation (Bodemann et al., 2011). Our
356 systematic analysis of the requirement of each of the exocyst subunits in biogenesis, maturation and
357 exocytosis of SGs led us to conclude that all three biological processes are carried out by the
358 holocomplex, and not by individual subunits or subcomplexes.

359 Consistent with the three biological functions that the exocyst exerts in the secretory pathway,
360 we found that its subcellular localization during salivary gland development is dynamic. Immediately
361 after the onset of Sgs3 synthesis, the exocyst localized at the Golgi complex; later, when SG biogenesis
362 has begun the exocyst was mostly present at the fusion point between immature SGs, and finally it
363 localized on mature SGs in close proximity to the apical plasma membrane. These different subcellular
364 localizations are coherent with the three phenotypes that we have observed after precise modulation
365 of exocyst levels. Exocyst localization at the trans-Golgi network and at the plasma membrane has
366 been reported before in mammalian cells (Yeaman, Grindstaff, Wright, & Nelson, 2001), and although

367 it was suggested in that study that the exocyst might be required at several steps of the secretory
368 pathway from the TGN to the plasma membrane, the idea was not further explored.
369 By analyzing SG-plasma membrane fusion markers, we have shown that, paralleling the
370 requirement of the exocyst in constitutive exocytosis, the complex participates in SG fusion with the
371 plasma membrane in regulated exocytosis as well. Moreover, we have found that the Sec15 subunit
372 localizes exactly at contact sites between SGs and the plasma membrane, further supporting the
373 notion that the exocyst plays a role in this fusion process. It is accepted that the function exerted by
374 the exocyst in the fusion between SGs and the plasma membrane depends on Ral GTPases (Brymora,
375 Valova, Larsen, Roufogalis, & Robinson, 2001; Wang, Li, & Sugita, 2004). RalA is the only Ral GTPase
376 described so far in *Drosophila*, and we have recently reported that RalA is involved in SG-plasma
377 membrane fusion in the salivary gland (de la Riva-Carrasco et al., 2021). Therefore, it seems likely that,
378 paralleling constitutive exocytosis, the interaction between RalA and the exocyst is critical for tethering
379 SGs to the plasma membrane during regulated exocytosis as well. The molecular components
380 regulating tethering and fusion of SGs to the plasma membrane remain largely unknown. Perhaps, this
381 is because the proteins involved in these processes participate in earlier steps of the secretory
382 pathway as well. Our temperature-dependent manipulation of the expression of exocyst subunits, in
383 combination with differential requirements of the complex in terms of quantity/activity in each of the
384 processes was instrumental for uncovering three different discrete steps in which the exocyst plays a
385 role along the regulated secretory pathway.
386 Proteins that will be secreted are co-translationally translocated to the ER, and then
387 transported into the cis-region of the GC in COPII-coated vesicles that are 60–90 nm in diameter and
388 therefore, sufficient to accommodate most membrane and secreted molecules (Raote & Malhotra,
389 2021). Larger cargos, such as collagen and mucins might use alternative ER-cis-GC communication
390 mechanism that are independent of vesicular carriers. Specifically, direct connections between the ER

391 and cis-GC are formed in a Tango1 and COPII dependent manner (Reynolds et al., 2019)(Yang, Feng, &
392 Pastor-Pareja, 2024). Disruption of these connections not only affects SG formation, but also has
393 profound impact on GC structure (Bard & Malhotra, 2006; Rios-Barrera, Sigurbjornsdottir, Baer, &
394 Leptin, 2017). We found that strong silencing of any of the exocyst subunits results in retention of Sgs3
395 in the ER, abrogation of SG biogenesis, and alteration of normal morphology of the GC. In *Drosophila*,
396 as well as in mammalian cells, Golgi complex is polarized in *cis* and *trans*-cisternae that are held
397 together by tethering complexed of the CATCHR family. Disruption of these connections result in
398 altered Golgi complex morphology, reflected in fragmentation and swelling of *cisternae* and
399 impairment of the secretory pathway (D'Souza, Taher, & Lupashin, 2020; Khakurel & Lupashin, 2023;
400 Liu et al., 2019). The fact that exocyst silencing not only affected SG formation, but also had profound
401 impact on GC structure, together with the observation that Sec15 specifically associated with the Golgi
402 complex but not with the ER before the onset of SG biogenesis, argues in favor of a role of this
403 complex as a tethering complex between cisternae. We propose that the exocyst might be redundant
404 with other CATCHR complexes in this function since only severe downregulation of exocyst subunits
405 expression can manifest this phenotype.
406 Maturation of SGs is a multidimensional process that involves homotypic fusion, acidification,
407 cargo condensation, and acquisition of membrane proteins that will steer SGs to the apical plasma
408 membrane and contribute to the recognition, tethering and fusion (Boda et al., 2023; Ji et al., 2018;
409 Nagy et al., 2022; Syed, Zhang, Tran, Bleck, & Ten Hagen, 2022). Previously, the exocyst was shown to
410 be required for maturation of Weibel-Palade bodies (Sharda et al., 2020). In the current work, we have
411 shown that the exocyst participates in several aspects of SG maturation. One of such processes is
412 homotypic fusion of immature SGs. We found that an adequate extent of downregulation of the
413 expression of any of the exocyst subunits leads to accumulation of immature SGs. Furthermore,
414 consistent with a function of the exocyst in SG homofusion, we found that Sec15 localizes

415 preferentially at the fusion point between adjacent immature SGs. In support of this notion, we found
416 that overexpression of Sec15 results in unusually large granules, likely derived from uncontrolled
417 homotypic fusion. Therefore, our data suggest that the exocyst complex is the tethering factor
418 responsible to bring immature SGs in close proximity to enable fusion.

419 Besides SG growth by homotypic fusion, several factors are recruited to the maturing SG,
420 including the transmembrane proteins CD63 and Syt-1. Our temperature-dependent genetic
421 manipulations revealed that the addition of Syt-1 to SGs occurs immediately after they have emerged
422 from the TGN, and addition of this protein continues after they have attained a mature size. Syt-1
423 localizes at the basolateral membrane of salivary gland cells before SG biogenesis, and it is not known
424 how Syt-1 reaches the maturing SGs. Given that the exocyst is required for loading SGs with Syt-1, one
425 possibility is that a vesicular carrier transports Syt-1 from the basolateral membrane to nascent and
426 maturing SGs, and that the contact between SGs and these vesicles is mediated by the exocyst. CD63,
427 which is also required for SG maturation, localizes instead at the apical plasma membrane before SG
428 biogenesis, and reaches the SGs from the endosomal retrograde pathway through endosomal tubes
429 (Ma et al., 2020). We found that cells in which the exocyst has been knocked-down display reduced
430 levels of CD63 around SGs, suggesting that the exocyst might contribute to the contact between
431 endosomal tubes and SGs as well. Based on our analysis, this maturation event should take place
432 mostly before, and not after, homotypic fusion. Thus, our results support the notion that the exocyst
433 complex might contribute to tethering maturing SGs to different types of membrane-bound carriers
434 that transport maturation factors like Syt-1 and CD63. These observations expand the notion that a
435 crosstalk between the secretory and endosomal pathways occurs (Ma & Brill, 2021a; Ma et al., 2020;
436 Papandreou & Tavernarakis, 2020), and that the exocyst is a critical factor linking the two pathways.

437 Vesicle maturation, either in the endocytic or the exocytic pathways, usually involves changes
438 in vesicle-bound Rab proteins (Ailion et al., 2014; Ma & Brill, 2021a; Thomas, Highland, & Fromme,

2021). The mechanisms that mediate these Rab-switches are not completely understood. Specifically, in *Drosophila* larval salivary glands, Rab1 and Rab11 association to SGs appear to be crucial for SG maturation and timely exocytosis (Neuman et al., 2021). We found that the levels of Rab1 and Rab11 on SGs are respectively positively and negatively regulated by the exocyst, and that additionally, Rab11 is itself required for recruitment of Sec15 to immature SGs. These complex relationships between Rab11, Rab1 and the exocyst can be explained through a single-negative feedback loop that would guarantee adequate levels of Rab11 and the exocyst on maturing SGs. This possibility is supported by previous evidence from *Drosophila* and other systems that indicate that Rab11 and Sec15 interact physically and genetically (Escrevente et al., 2021; Guo et al., 1999; Novick, 2016). In fact, the exocyst is an effector of Rab11 (Sec4p in yeasts), as GTP-bound Rab11 recruits Sec15 to secretory vesicles, which in turn triggers formation of the holocomplex on the vesicle membrane as previously shown in yeast, *Drosophila* and mammalian cells (S. Wu et al., 2005) (Takahashi et al., 2012) (Zhang, Ellis, Sriratana, Mitchell, & Rowe, 2004).

An increasing number of publications reveal the complexity and variety of vesicle trafficking routes that feed into the biogenesis, maturation and exocytosis of SGs. Our study has revealed that the exocyst holocomplex acts at several steps of the pathway of regulated exocytosis: namely, maintaining Golgi complex morphology to allow protein exit from the ER and transit through the early secretory pathway; promoting homotypic fusion of SGs and acquisition of maturation factors; and finally, allowing SG-plasma membrane fusion. We propose that all these events depend on the activity of the exocyst complex as a tethering factor.

Materials and methods

Fly stocks and genetics

462 All fly stocks were kept on standard corn meal/agar medium at 25°C. Crosses were set up in vials
463 containing two males and five females of the required genotypes at 25°C. Crosses were flipped every
464 24 hours to avoid larval overcrowding, and then moved to the desired temperature: 29°, 25°, 21°, 19°
465 or 18°C. The temperature used for each experiment is specified in figure legends. In the experiments of
466 Figures 2, 3, 8 and Supplementary Figures 1 and 11, all crosses were maintained in a bath water to
467 reduce temperature fluctuations. *D. melanogaster* lines used in this work are listed in Supplementary
468 Table 2, and were obtained from the Bloomington Drosophila Stock Center
469 (http://flystocks.bio.indiana.edu) or from the Vienna Drosophila Stock Center
470 (https://stockcenter.vdrc.at); Sgs3-dsRed was generated by A.J. Andres' Lab (University of Nevada,
471 United States).
472
473 **Sgs3-GFP retention phenotype.**
474 Larvae or prepupae of the desired genotype were visualized and photographed inside glass vials under
475 a fluorescence dissection microscope Olympus MVX10. In prepupae, localization of Sgs3-GFP or Sgs3-
476 dsRed inside salivary glands or outside the puparium was determined. Each experiment was repeated
477 at least three times.
478
479 **Developmental staging and SG size.**
480 When larvae were cultured at 25°C, SG maturation progressed according to the timeline shown in Figure
481 1. Roughly, at 29°C larval development was shortened by 24 hours, and extended in 1 ,3 and 4 days when
482 larvae were cultured at 21, 19°C and 18 °C respectively. Precise physiological staging of each salivary
483 gland was carried out according to Neuman and co-workers (Neuman et al., 2021) upon dissection and
484 observation under the confocal microscope. In all experiments, only SGs from the distal-most cells of
485 the salivary glands were imaged to avoid potential variations in SG size due to desynchronization in the

486 synthesis of Sgs3. Data of temperatures and developmental staging from each experiment are
487 synthesized in Supplementary Table 4.
488
489 **RNA extraction and cDNA synthesis**
490 Total RNA was isolated from dissected salivary glands of third-instar larvae using 500 µl of Quick-Zol
491 reagent (Kalium Technologies, RA00201) following the manufacturer's instructions. The concentration
492 and integrity of the RNA were determined using NanoDrop (Thermo Fisher Scientific)
493 spectrophotometry. RNA (1 µg) was reverse-transcribed using M-MLV Reverse Transcriptase (Invitrogen,
494 10338842) using oligo-dT as a primer (https://doi.org/10.1080/15548627.2021.1991191). Control
495 reactions omitting reverse transcriptase were used to assess the absence of contaminating genomic DNA
496 in the RNA samples. An additional control without RNA was included.
497
498 **Real-time PCR**
499 Gene expression was analyzed by quantitative PCR in a CFX96 Touch (Bio-Rad) cycler. The reactions were
500 performed using HOT FIREPol EvaGreen qPCR Mix Plus (without ROX; Solis BioDyne, 08-25-00001), 0.40
501 µM primers, and 12–25 ng of cDNA, in a final volume of 10.4 µl
502 (https://doi.org/10.1080/15548627.2021.1991191). Cycle conditions were initial denaturation at 95°C
503 for 15 min, and 40 cycles of denaturation at 95°C for 20 s, annealing at 60°C for 1 min, and extension
504 and optical reading stage at 72°C for 30 s, followed by a dissociation curve consisting of ramping the
505 temperature from 65 to 95°C while continuously collecting fluorescence data
506 (https://doi.org/10.1080/15548627.2021.1991191). Product purity was confirmed by agarose gel
507 electrophoresis. Relative gene expression levels were calculated according to the comparative cycle
508 threshold (CT) method (https://doi.org/10.1080/15548627.2021.1991191). Normalized target gene
509 expression relative to rpl29 was obtained by calculating the difference in CT values, the relative change

510 in target transcripts being computed as 2−ΔCT. The efficiencies of each target and housekeeping gene
511 amplification were measured and shown to be approximately equal. Oligonucleotides were obtained
512 from Macrogen (Seoul, Korea), and their sequences were the following: exo70: Fw 5'-
513 GAAGTGGTTCTCCGATCGCT-3', Rv 5'-ACGAGCGGAGGTTGTCTTTT-3'; sec3: Fw 5'-
514 GAAGACGCAACACATGGACG-3', Rv 5'-CTTTGCATATTGGCCCCATCC-3'; sec5: Fw 5'-
515 GTCAATGAGACTGCCAAGAACT-3', Rv 5'-CCTGCAGTGGAATGTGCCTA-3'; rpl29: Fw 5'-
516 GAACAAGAAGGCCCATCGTA-3', Rv 5'-AGTAAACAGGCTTTGGCTTGC-3'. Rpl29 was used as housekeeping
517 gene. Specificity and quality of oligonucleotide sequences for exo70, sec3, sec5, and rpl29 were checked
518 using Primer Blast Resource of the NCBI (http://www.ncbi.nlm.nih.gov/tools/primer-blast/).
519
520 **Quantification of the penetrance of phenotypes upon knockdown of exocyst subunits.**
521 Sgs3-GFP intracellular distribution was analyzed in salivary gland cells, and one of three phenotypic
522 categories was defined for each cell: 1) "mesh-like structure" when Sgs3-GFP was distributed in a
523 network-like compartment; 2) "Immature SGs" when Sgs3-GFP was in SGs with a median diameter
524 smaller than 3 μm; and 3) "Mature SGs" when Sgs3-GFP was in SGs with a median diameter equal or
525 larger than 3 μm. The penetrance of each of the three phenotypes was calculated for each genotype of
526 interest at the four different temperatures analyzed.
527
528 **Salivary gland imaging.**
529 Salivary glands of the desired stage were dissected in cold PBS (137 mM NaCl, 2.7 mM KCl, 4.3 mM
530 Na_2HPO_4, 1.47 mM KH_2PO_4, [pH 8]), and then imaged directly under the confocal microscope without
531 fixation for no more than five minutes. In the experiment of Figure 9G and Supplementary Figure 6E,
532 salivary glands were fixed for 2 hours in 4% PFA (Paraformaldehyde, Sigma) at room temperature, and
533 then washed three times for 15 minutes with PBS- 0.1% Triton X-100. For filamentous actin staining,

534 salivary glands were incubated for 1 hour with Alexa Fluor 647 Phalloidin (ThermoFisher Scientific 1:400)
535 in PBS- 0.1% Triton X-100; stained tissues were mounted in gelvatol mounting medium (Sigma) and
536 imaged at a confocal microscope Carl Zeiss LSM 710 with a Plan-Apochromat 63X/1.4NA oil objective,
537 or Carl Zeiss LSM 880 with a Plan-Apochromat 20X/0.8 NA air objective or a Plan-Apochromat 63X/1.4NA
538 oil objective.
539 For live imaging, salivary glands were dissected in PBS, and then mounted in a 15 mm diameter plastic
540 chamber with a glass bottom made of a cover slip, containing 40 µl of HL3.1 medium (70 mM NaCl, 5
541 mM KCl, 1.5 mM CaCl2, 2 mM MgCl2, 5 mM HEPES, 115 mM sucrose, 5 mM trehalose, and pH 7.2 with
542 NaHCO3). The medium was removed allowing the tissue to adhere to the bottom of the chamber, and
543 then a Biopore membrane hydrophilic PTFE with a pore size of 0.4 µm (Millipore, Sigma) was placed over
544 the sample, and HL3.1 medium was added on top covering the membrane. Images were captured under
545 an inverted Carl Zeiss LSM 880 confocal microscope with a Plan-Apochromat 20X/0.8 NA air objective or
546 a Plan-Apochromat 63X/1.4NA oil objective. For Supplementary Movie 1, frames were obtained every
547 2.25 seconds, while for Supplementary Movie 6 and 7, frames were captured every 0.78 and 0.67
548 seconds respectively.
549
550 **Image processing and analysis.**
551 Image deconvolution was performed using the Parallel Spectral Deconvolution plugin of the ImageJ
552 software (NIH, Bethesda, MD) with standard pre-sets (Schneider, Rasband, & Eliceiri, 2012). Image
553 analyses were made with ImageJ (Schneider et al., 2012), and graphs were generated with the R Studio
554 software (Team, 2020). For SG quantification, a region of interest (ROI) from each cell was used. In each
555 ROI, the area of SGs was assessed, and SG diameter was calculated assuming that SGs are circular, using
556 the formula $((Area/\pi)^{1/2})*2$ = Diameter. In experiments of Figure 4B, D, F, H and Supplementary Figure
557 7A, C, E, G, I two-dimensional lines scans were generated with the ImageJ plot profile. Fluorescence

558 intensity was determined related to maximal intensity of each marker, always within a linear range. For
559 quantification of fluorescence intensity of Syt1, CD63, Rab1 and Rab11 (Figure 8 and Supplementary
560 Figure 11), the mean intensity of three different ROIs of 5 μm^2 from each cell was measured. 17-35 cells
561 from 4-11 salivary glands were used in the analysis. Association analyses in Figure 5B, E were performed
562 considering structures as associated when the fluorescence spikes, of each fluorophore, had a distance
563 minor or equal to ~0.6 μm. In the experiment of Figure 7C, GFP-Sec15 *foci* between granules were
564 measured over total foci in four different ROIs of 225 μm^2 from each cell. For nucleus quantification
565 (Supplementary Figure 5E) the area from each one, was measured using Image J freehand section.
566 In polarity experiments, the mean fluorescence intensity of apical markers (Supplementary Figure 6A, B)
567 was obtained by drawing a plotted line, of ~2 μm wide, over the apical membrane. In the case of $PI(4,5)P_2$
568 and F-actine (Supplementary Figure 6 D, E), localized in both compartments particularly enriched in
569 apical membrane, a perpendicular line, of ~9 μm wide, was draw from the basolateral region to the
570 apical and the coefficient between the maximum fluorescence intensity of both regions was calculated.
571 Pearson's coefficient was obtained with JACoP plugging of Image J (Bolte & Cordelieres, 2006). The Golgi
572 defect, upon exocyst knock down (Supplementary Figure 9), was measured as the number of cells with
573 aberrant *cis*-Golgi or with swollen *trans*-Golgi vesicles over total cells within each salivary gland.
574
575 **Statistical analyses.**
576 Statistical significance was calculated using one-way analysis of variance (ANOVA), a Likelihood Ratio
577 test or a Wald Test, and followed by a Tuckey's test with a 95% confidence interval ($p < 0.05$) when
578 comparing multiple factors.
579
580
581 **Acknowledgements**

We are grateful to Dr. Andrew Andres, Dr. Gabor Juhasz, the Bloomington Stock Centre and the Vienna Drosophila Resource Centre for fly strains. Dr. Andrés Rossi and Dr Esteban Miglietta, from FIL microscopy facility, for technical support with confocal microscopy; Andrés Liceri for fly food preparation; the FIL personnel for assistance and members of the Wappner lab for fruitful discussions.

Competing interests

The authors declare no competing or financial interests.

Additional information

Funding

This work was supported by grants from Agencia Nacional de Promoción de Científica y Tecnológica: PICT-2018-1501 and PICT-2021-I-A-00240 to PW and PICT-2021-GRF-TII00418 to MM. SSF and SPP were supported with fellowships of the Consejo Nacional de Investigaciones Científicas y Técnicas.

Author contributions

SSF, Conceptualization, Data curation, Formal analysis, Validation, Investigation, Methodology, Writing – review and editing; SPP, Investigation, Methodology; SF, Investigation, Writing – review and editing; PW, Conceptualization, Funding acquisition, Project administration, Writing – review and editing; MM, Conceptualization, Supervision, Funding acquisition, Methodology, Writing – original draft, Project administration, Writing – review and editing

References

Aggarwal, A., Jennings, C. L., Manning, E., & Cameron, S. J. (2023). Platelets at the Vessel Wall in Non-Thrombotic Disease. *Circ Res, 132*(6), 775-790. doi:10.1161/CIRCRESAHA.122.321566

Ahmed, S. M., Nishida-Fukuda, H., Li, Y., McDonald, W. H., Gradinaru, C. C., & Macara, I. G. (2018). Exocyst dynamics during vesicle tethering and fusion. *Nat Commun, 9*(1), 5140. doi:10.1038/s41467-018-07467-5

Ailion, M., Hannemann, M., Dalton, S., Pappas, A., Watanabe, S., Hegermann, J., . . . Jorgensen, E. M. (2014). Two Rab2 interactors regulate dense-core vesicle maturation. *Neuron, 82*(1), 167-180. doi:10.1016/j.neuron.2014.02.017

An, S. J., Rivera-Molina, F., Anneken, A., Xi, Z., McNellis, B., Polejaev, V. I., & Toomre, D. (2021). An active tethering mechanism controls the fate of vesicles. *Nat Commun, 12*(1), 5434. doi:10.1038/s41467-021-25465-y

Andrews, H. K., Zhang, Y. Q., Trotta, N., & Broadie, K. (2002). Drosophila sec10 is required for hormone secretion but not general exocytosis or neurotransmission. *Traffic, 3*(12), 906-921. doi:10.1034/j.1600-0854.2002.31206.x

Biyasheva, A., Do, T. V., Lu, Y., Vaskova, M., & Andres, A. J. (2001). Glue secretion in the Drosophila salivary gland: a model for steroid-regulated exocytosis. *Dev Biol, 231*(1), 234-251. doi:10.1006/dbio.2000.0126

Boda, A., Varga, L. P., Nagy, A., Szenci, G., Csizmadia, T., Lorincz, P., & Juhasz, G. (2023). Rab26 controls secretory granule maturation and breakdown in Drosophila. *Cell Mol Life Sci, 80*(1), 24. doi:10.1007/s00018-022-04674-8

Bodemann, B. O., Orvedahl, A., Cheng, T., Ram, R. R., Ou, Y. H., Formstecher, E., . . . White, M. A. (2011). RalB and the exocyst mediate the cellular starvation response by direct activation of autophagosome assembly. *Cell, 144*(2), 253-267. doi:10.1016/j.cell.2010.12.018

Bolte, S., & Cordelieres, F. P. (2006). A guided tour into subcellular colocalization analysis in light microscopy. *J Microsc, 224*(Pt 3), 213-232. doi:10.1111/j.1365-2818.2006.01706.x

Borne, F., Kovalev, A., Gorb, S., & Courtier-Orgogozo, V. (2020). The glue produced by Drosophila melanogaster for pupa adhesion is universal. *J Exp Biol, 223*(Pt 8). doi:10.1242/jeb.220608

Brymora, A., Valova, V. A., Larsen, M. R., Roufogalis, B. D., & Robinson, P. J. (2001). The brain exocyst complex interacts with RalA in a GTP-dependent manner: identification of a novel mammalian Sec3 gene and a second Sec15 gene. *J Biol Chem, 276*(32), 29792-29797. doi:10.1074/jbc.C100320200

Burgess, J., Del Bel, L. M., Ma, C. I., Barylko, B., Polevoy, G., Rollins, J., . . . Brill, J. A. (2012). Type II phosphatidylinositol 4-kinase regulates trafficking of secretory granule proteins in Drosophila. *Development, 139*(16), 3040-3050. doi:10.1242/dev.077644

Burgess, J., Jauregui, M., Tan, J., Rollins, J., Lallet, S., Leventis, P. A., . . . Brill, J. A. (2011). AP-1 and clathrin are essential for secretory granule biogenesis in Drosophila. *Mol Biol Cell, 22*(12), 2094-2105. doi:10.1091/mbc.E11-01-0054

Costantino, B. F., Bricker, D. K., Alexandre, K., Shen, K., Merriam, J. R., Antoniewski, C., . . . Andres, A. J. (2008). A novel ecdysone receptor mediates steroid-regulated developmental events during the mid-third instar of Drosophila. *PLoS Genet, 4*(6), e1000102. doi:10.1371/journal.pgen.1000102

D'Souza, Z., Taher, F. S., & Lupashin, V. V. (2020). Golgi inCOGnito: From vesicle tethering to human disease. *Biochim Biophys Acta Gen Subj, 1864*(11), 129694. doi:10.1016/j.bbagen.2020.129694

de la Riva-Carrasco, R., Perez-Pandolfo, S., Suarez Freire, S., Romero, N. M., Bhujabal, Z., Johansen, T., . . . Melani, M. (2021). The immunophilin Zonda controls regulated exocytosis in endocrine and exocrine tissues. *Traffic, 22*(4), 111-122. doi:10.1111/tra.12777

Du, W., Zhou, M., Zhao, W., Cheng, D., Wang, L., Lu, J., . . . Xu, T. (2016). HID-1 is required for homotypic fusion of immature secretory granules during maturation. *Elife, 5*. doi:10.7554/eLife.18134

Duan, J., Zhao, Y., Li, H., Habernig, L., Gordon, M. D., Miao, X., . . . Buttner, S. (2020). Bab2 Functions as an Ecdysone-Responsive Transcriptional Repressor during Drosophila Development. *Cell Rep, 32*(4), 107972. doi:10.1016/j.celrep.2020.107972

Escrevente, C., Bento-Lopes, L., Ramalho, J. S., & Barral, D. C. (2021). Rab11 is required for lysosome exocytosis through the interaction with Rab3a, Sec15 and GRAB. *J Cell Sci, 134*(11). doi:10.1242/jcs.246694

Farkas, R., Datkova, Z., Mentelova, L., Low, P., Benova-Liszekova, D., Beno, M., . . . Mechler, B. M. (2014). Apocrine secretion in Drosophila salivary glands: subcellular origin, dynamics, and identification of secretory proteins. *PLoS One, 9*(4), e94383. doi:10.1371/journal.pone.0094383

Fujimoto, B. A., Young, M., Carter, L., Pang, A. P. S., Corley, M. J., Fogelgren, B., & Polgar, N. (2019). The exocyst complex regulates insulin-stimulated glucose uptake of skeletal muscle cells. *Am J Physiol Endocrinol Metab, 317*(6), E957-E972. doi:10.1152/ajpendo.00109.2019

Govindan, B., Bowser, R., & Novick, P. (1995). The role of Myo2, a yeast class V myosin, in vesicular transport. *J Cell Biol, 128*(6), 1055-1068. doi:10.1083/jcb.128.6.1055

Grindstaff, K. K., Yeaman, C., Anandasabapathy, N., Hsu, S. C., Rodriguez-Boulan, E., Scheller, R. H., & Nelson, W. J. (1998). Sec6/8 complex is recruited to cell-cell contacts and specifies transport vesicle delivery to the basal-lateral membrane in epithelial cells. *Cell, 93*(5), 731-740. doi:10.1016/s0092-8674(00)81435-x

Guo, W., Roth, D., Walch-Solimena, C., & Novick, P. (1999). The exocyst is an effector for Sec4p, targeting secretory vesicles to sites of exocytosis. *EMBO J, 18*(4), 1071-1080. doi:10.1093/emboj/18.4.1071

Hsu, S. C., Ting, A. E., Hazuka, C. D., Davanger, S., Kenny, J. W., Kee, Y., & Scheller, R. H. (1996). The mammalian brain rsec6/8 complex. *Neuron, 17*(6), 1209-1219. doi:10.1016/s0896-6273(00)80251-2

Inoue, M., Chang, L., Hwang, J., Chiang, S. H., & Saltiel, A. R. (2003). The exocyst complex is required for targeting of Glut4 to the plasma membrane by insulin. *Nature, 422*(6932), 629-633. doi:10.1038/nature01533

Ji, S., Samara, N. L., Revoredo, L., Zhang, L., Tran, D. T., Muirhead, K., . . . Ten Hagen, K. G. (2018). A molecular switch orchestrates enzyme specificity and secretory granule morphology. *Nat Commun, 9*(1), 3508. doi:10.1038/s41467-018-05978-9

Kang, C. J., Guzman-Clavel, L. E., Lei, K., Koo, M., To, S., & Roche, J. P. (2024). The exocyst subunit Sec15 is critical for proper synaptic development and function at the Drosophila NMJ. *Mol Cell Neurosci, 128*, 103914. doi:10.1016/j.mcn.2023.103914

Khakurel, A., & Lupashin, V. V. (2023). Role of GARP Vesicle Tethering Complex in Golgi Physiology. *Int J Mol Sci, 24*(7). doi:10.3390/ijms24076069

Kogel, T., & Gerdes, H. H. (2010). Maturation of secretory granules. *Results Probl Cell Differ, 50*, 1-20. doi:10.1007/400_2009_31

Langevin, J., Morgan, M. J., Sibarita, J. B., Aresta, S., Murthy, M., Schwarz, T., . . . Bellaiche, Y. (2005). Drosophila exocyst components Sec5, Sec6, and Sec15 regulate DE-Cadherin trafficking from recycling endosomes to the plasma membrane. *Dev Cell, 9*(3), 365-376. doi:10.1016/j.devcel.2005.07.013

Lattner, J., Leng, W., Knust, E., Brankatschk, M., & Flores-Benitez, D. (2019). Crumbs organizes the transport machinery by regulating apical levels of PI(4,5)P(2) in Drosophila. *Elife, 8*. doi:10.7554/eLife.50900

Lee, T., & Luo, L. (1999). Mosaic analysis with a repressible cell marker for studies of gene function in neuronal morphogenesis. *Neuron, 22*(3), 451-461. doi:10.1016/s0896-6273(00)80701-1

Ley, K., Hoffman, H. M., Kubes, P., Cassatella, M. A., Zychlinsky, A., Hedrick, C. C., & Catz, S. D. (2018). Neutrophils: New insights and open questions. *Sci Immunol, 3*(30). doi:10.1126/sciimmunol.aat4579

Li, Z., Qian, W., Song, W., Zhao, T., Yang, Y., Wang, W., . . . Cheng, D. (2022). A salivary gland-secreted peptide regulates insect systemic growth. *Cell Rep, 38*(8), 110397. doi:10.1016/j.celrep.2022.110397

Lipschutz, J. H., Guo, W., O'Brien, L. E., Nguyen, Y. H., Novick, P., & Mostov, K. E. (2000). Exocyst is involved in cystogenesis and tubulogenesis and acts by modulating synthesis and delivery of basolateral plasma membrane and secretory proteins. *Mol Biol Cell, 11*(12), 4259-4275. doi:10.1091/mbc.11.12.4259

Liu, S., Majeed, W., Grigaitis, P., Betts, M. J., Climer, L. K., Starkuviene, V., & Storrie, B. (2019). Epistatic Analysis of the Contribution of Rabs and Kifs to CATCHR Family Dependent Golgi Organization. *Front Cell Dev Biol, 7*, 126. doi:10.3389/fcell.2019.00126

Luo, G., Zhang, J., Luca, F. C., & Guo, W. (2013). Mitotic phosphorylation of Exo84 disrupts exocyst assembly and arrests cell growth. *J Cell Biol, 202*(1), 97-111. doi:10.1083/jcb.201211093

Ma, C. J., & Brill, J. A. (2021a). Endosomal Rab GTPases regulate secretory granule maturation in Drosophila larval salivary glands. *Commun Integr Biol, 14*(1), 15-20. doi:10.1080/19420889.2021.1874663

Ma, C. J., & Brill, J. A. (2021b). Quantitation of Secretory Granule Size in Drosophila Larval Salivary Glands. *Bio Protoc, 11*(11), e4039. doi:10.21769/BioProtoc.4039

Ma, C. J., Yang, Y., Kim, T., Chen, C. H., Polevoy, G., Vissa, M., . . . Brill, J. A. (2020). An early endosome-derived retrograde trafficking pathway promotes secretory granule maturation. *J Cell Biol, 219*(3). doi:10.1083/jcb.201808017

Mavor, L. M., Miao, H., Zuo, Z., Holly, R. M., Xie, Y., Loerke, D., & Blankenship, J. T. (2016). Rab8 directs furrow ingression and membrane addition during epithelial formation in Drosophila melanogaster. *Development, 143*(5), 892-903. doi:10.1242/dev.128876

Mehta, S. Q., Hiesinger, P. R., Beronja, S., Zhai, R. G., Schulze, K. L., Verstreken, P., . . . Bellen, H. J. (2005). Mutations in Drosophila sec15 reveal a function in neuronal targeting for a subset of exocyst components. *Neuron, 46*(2), 219-232. doi:10.1016/j.neuron.2005.02.029

Morgan, A. (1995). Exocytosis. *Essays Biochem, 30*, 77-95.

Nagy, A., Szenci, G., Boda, A., Al-Lami, M., Csizmadia, T., Lorincz, P., . . . Low, P. (2022). Ecdysone receptor isoform specific regulation of secretory granule acidification in the larval Drosophila salivary gland. *Eur J Cell Biol, 101*(4), 151279. doi:10.1016/j.ejcb.2022.151279

Neuman, S. D., & Bashirullah, A. (2018). Hobbit regulates intracellular trafficking to drive insulin-dependent growth during Drosophila development. *Development, 145*(11). doi:10.1242/dev.161356

Neuman, S. D., Jorgensen, J. R., Cavanagh, A. T., Smyth, J. T., Selegue, J. E., Emr, S. D., & Bashirullah, A. (2022). The Hob proteins are novel and conserved lipid-binding proteins at ER-PM contact sites. *J Cell Sci, 135*(5). doi:10.1242/jcs.259086

Neuman, S. D., Lee, A. R., Selegue, J. E., Cavanagh, A. T., & Bashirullah, A. (2021). A novel function for Rab1 and Rab11 during secretory granule maturation. *J Cell Sci, 134*(15). doi:10.1242/jcs.259037

Novick, P. (2016). Regulation of membrane traffic by Rab GEF and GAP cascades. *Small GTPases, 7*(4), 252-256. doi:10.1080/21541248.2016.1213781

Novick, P., Field, C., & Schekman, R. (1980). Identification of 23 complementation groups required for post-translational events in the yeast secretory pathway. *Cell, 21*(1), 205-215. doi:10.1016/0092-8674(80)90128-2

Novick, P., Garrett, M. D., Brennwald, P., Lauring, A., Finger, F. P., Collins, R., & TerBush, D. R. (1995). Control of exocytosis in yeast. *Cold Spring Harb Symp Quant Biol, 60*, 171-177. doi:10.1101/sqb.1995.060.01.020

Omar-Hmeadi, M., & Idevall-Hagren, O. (2021). Insulin granule biogenesis and exocytosis. *Cell Mol Life Sci, 78*(5), 1957-1970. doi:10.1007/s00018-020-03688-4

Papandreou, M. E., & Tavernarakis, N. (2020). Crosstalk between Endo/Exocytosis and Autophagy in Health and Disease. *Biotechnol J, 15*(8), e1900267. doi:10.1002/biot.201900267

Park, K. M., Fogelgren, B., Zuo, X., Kim, J., Chung, D. C., & Lipschutz, J. H. (2010). Exocyst Sec10 protects epithelial barrier integrity and enhances recovery following oxidative stress, by activation of the MAPK pathway. *Am J Physiol Renal Physiol, 298*(3), F818-826. doi:10.1152/ajprenal.00596.2009

Pereira, C., Stalder, D., Anderson, G. S. F., Shun-Shion, A. S., Houghton, J., Antrobus, R., . . . Gershlick, D. C. (2023). The exocyst complex is an essential component of the mammalian constitutive secretory pathway. *J Cell Biol, 222*(5). doi:10.1083/jcb.202205137

Phan, T. K., Williams, S. A., Bindra, G. K., Lay, F. T., Poon, I. K. H., & Hulett, M. D. (2019). Phosphoinositides: multipurpose cellular lipids with emerging roles in cell death. *Cell Death Differ, 26*(5), 781-793. doi:10.1038/s41418-018-0269-2

Reynolds, H. M., Zhang, L., Tran, D. T., & Ten Hagen, K. G. (2019). Tango1 coordinates the formation of endoplasmic reticulum/Golgi docking sites to mediate secretory granule formation. *J Biol Chem, 294*(51), 19498-19510. doi:10.1074/jbc.RA119.011063

Rogers, K. K., Wilson, P. D., Snyder, R. W., Zhang, X., Guo, W., Burrow, C. R., & Lipschutz, J. H. (2004). The exocyst localizes to the primary cilium in MDCK cells. *Biochem Biophys Res Commun, 319*(1), 138-143. doi:10.1016/j.bbrc.2004.04.165

Rousso, T., Schejter, E. D., & Shilo, B. Z. (2016). Orchestrated content release from Drosophila glue-protein vesicles by a contractile actomyosin network. *Nat Cell Biol, 18*(2), 181-190. doi:10.1038/ncb3288

Schneider, C. A., Rasband, W. S., & Eliceiri, K. W. (2012). NIH Image to ImageJ: 25 years of image analysis. *Nat Methods, 9*(7), 671-675. doi:10.1038/nmeth.2089

Sharda, A. V., Barr, A. M., Harrison, J. A., Wilkie, A. R., Fang, C., Mendez, L. M., . . . Flaumenhaft, R. (2020). VWF maturation and release are controlled by 2 regulators of Weibel-Palade body biogenesis: exocyst and BLOC-2. *Blood, 136*(24), 2824-2837. doi:10.1182/blood.2020005300

Singh, S., Kumari, R., Chinchwadkar, S., Aher, A., Matheshwaran, S., & Manjithaya, R. (2019). Exocyst Subcomplex Functions in Autophagosome Biogenesis by Regulating Atg9 Trafficking. *J Mol Biol, 431*(15), 2821-2834. doi:10.1016/j.jmb.2019.04.048

Sugita, S. (2008). Mechanisms of exocytosis. *Acta Physiol (Oxf), 192*(2), 185-193. doi:10.1111/j.1748-1716.2007.01803.x

Syed, Z. A., Zhang, L., Tran, D. T., Bleck, C. K. E., & Ten Hagen, K. G. (2022). Regulated Restructuring of Mucins During Secretory Granule Maturation In Vivo. *Proc Natl Acad Sci U S A, 119*(43), e2209750119. doi:10.1073/pnas.2209750119

Takahashi, S., Kubo, K., Waguri, S., Yabashi, A., Shin, H. W., Katoh, Y., & Nakayama, K. (2012). Rab11 regulates exocytosis of recycling vesicles at the plasma membrane. *J Cell Sci, 125*(Pt 17), 4049-4057. doi:10.1242/jcs.102913

Team, R. (2020). RStudio: Integrated Development Environment for R. Retrieved from http://www.rstudio.com/

TerBush, D. R., Maurice, T., Roth, D., & Novick, P. (1996). The Exocyst is a multiprotein complex required for exocytosis in Saccharomyces cerevisiae. *EMBO J, 15*(23), 6483-6494.

Thapa, N., Sun, Y., Schramp, M., Choi, S., Ling, K., & Anderson, R. A. (2012). Phosphoinositide signaling regulates the exocyst complex and polarized integrin trafficking in directionally migrating cells. *Dev Cell, 22*(1), 116-130. doi:10.1016/j.devcel.2011.10.030

Thomas, L. L., Highland, C. M., & Fromme, J. C. (2021). Arf1 orchestrates Rab GTPase conversion at the trans-Golgi network. *Mol Biol Cell, 32*(11), 1104-1120. doi:10.1091/mbc.E20-10-0664

Torres, I. L., Rosa-Ferreira, C., & Munro, S. (2014). The Arf family G protein Arl1 is required for secretory granule biogenesis in Drosophila. *J Cell Sci, 127*(Pt 10), 2151-2160. doi:10.1242/jcs.122028

Tracy, K., Velentzas, P. D., & Baehrecke, E. H. (2016). Ral GTPase and the exocyst regulate autophagy in a tissue-specific manner. *EMBO Rep, 17*(1), 110-121. doi:10.15252/embr.201541283

Tran, D. T., Masedunskas, A., Weigert, R., & Ten Hagen, K. G. (2015). Arp2/3-mediated F-actin formation controls regulated exocytosis in vivo. *Nat Commun, 6*, 10098. doi:10.1038/ncomms10098

Wang, L., Li, G., & Sugita, S. (2004). RalA-exocyst interaction mediates GTP-dependent exocytosis. *J Biol Chem, 279*(19), 19875-19881. doi:10.1074/jbc.M400522200

Whyte, J. R., & Munro, S. (2002). Vesicle tethering complexes in membrane traffic. *J Cell Sci, 115*(Pt 13), 2627-2637. doi:10.1242/jcs.115.13.2627

Wu, B., & Guo, W. (2015). The Exocyst at a Glance. *J Cell Sci, 128*(16), 2957-2964. doi:10.1242/jcs.156398

Wu, S., Mehta, S. Q., Pichaud, F., Bellen, H. J., & Quiocho, F. A. (2005). Sec15 interacts with Rab11 via a novel domain and affects Rab11 localization in vivo. *Nat Struct Mol Biol, 12*(10), 879-885. doi:10.1038/nsmb987

Yang, K., Feng, Z., & Pastor-Pareja, J. C. (2024). p24-Tango1 interactions ensure ER-Golgi interface stability and efficient transport. *J Cell Biol, 223*(5). doi:10.1083/jcb.202309045

Yeaman, C., Grindstaff, K. K., Wright, J. R., & Nelson, W. J. (2001). Sec6/8 complexes on trans-Golgi network and plasma membrane regulate late stages of exocytosis in mammalian cells. *J Cell Biol, 155*(4), 593-604. doi:10.1083/jcb.200107088

Zhang, X. M., Ellis, S., Sriratana, A., Mitchell, C. A., & Rowe, T. (2004). Sec15 is an effector for the Rab11 GTPase in mammalian cells. *J Biol Chem, 279*(41), 43027-43034. doi:10.1074/jbc.M402264200

Zhao, K., Matsunaga, K., Mizuno, K., Wang, H., Okunishi, K., & Izumi, T. (2023). Functional hierarchy among different Rab27 effectors involved in secretory granule exocytosis. *Elife, 12*. doi:10.7554/eLife.82821

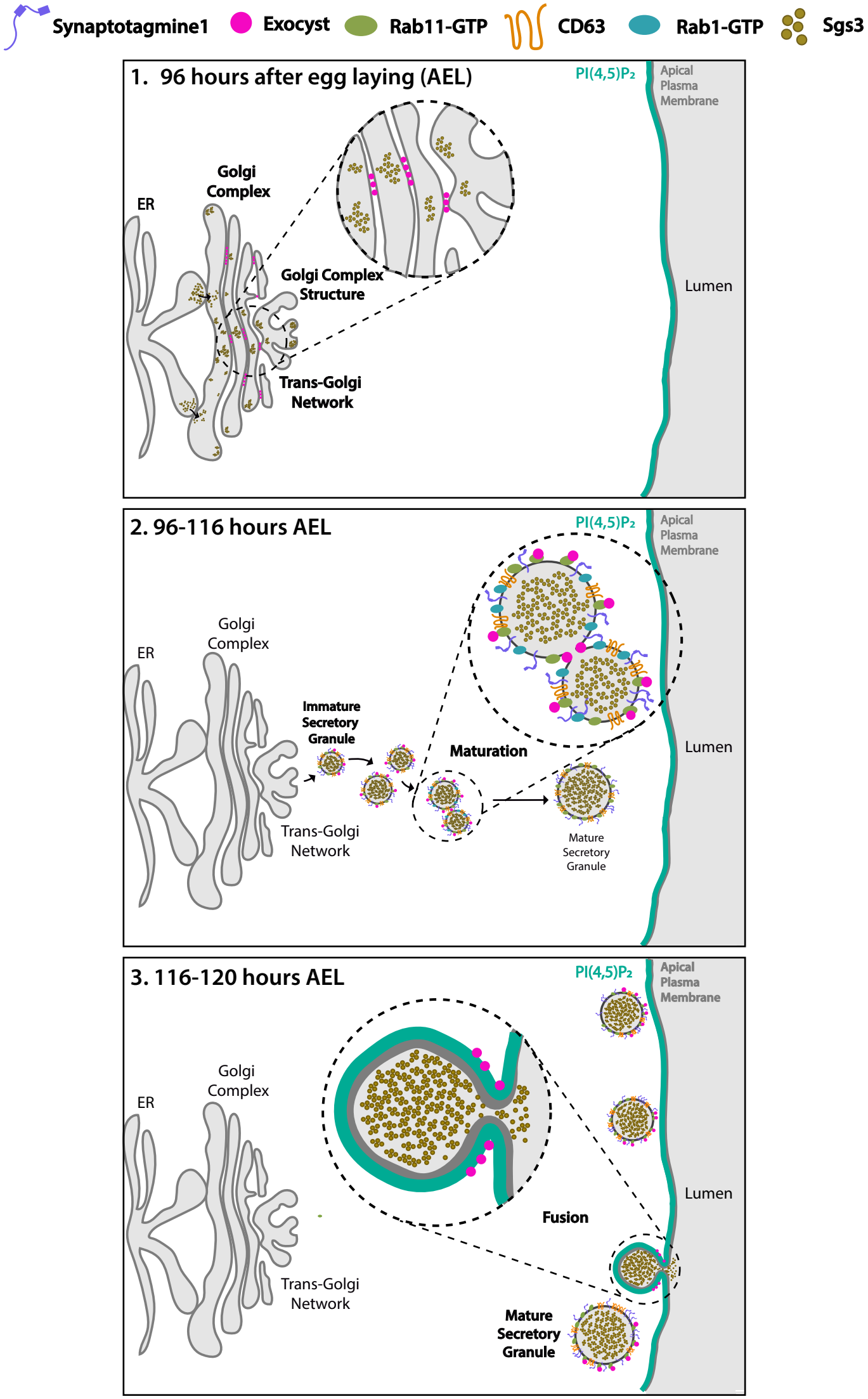
Synaptotagmine1
Exocyst
Rab11-GTP
CD63
Rab1-GTP
Sgs3
1. 96 hours after egg laying (AEL)
PI(4,5)P2
Apical Plasma Membrane
Golgi Complex
ER
Golgi Complex Structure
Trans-Golgi Network
Lumen
2. 96-116 hours AEL
PI(4,5)P2
Apical Plasma Membrane
Golgi Complex
ER
Immature Secretory Granule
Maturation
Trans-Golgi Network
Mature Secretory Granule
Lumen
3. 116-120 hours AEL
PI(4,5)P2
Apical Plasma Membrane
Golgi Complex
ER
Fusion
Trans-Golgi Network
Mature Secretory Granule
Lumen

Graphical abstract. Proposed model of the action of the exocyst in maintenance of normal Golgi complex structure, maturation and exocytosis of secretory granules in *Drosophila* larval salivary gland cells. 1-Before secretory granule (SG) biogenesis (<96 hours AEL), the exocyst (pink dots) localizes at the Golgi complex, where it is required to maintain the normal Golgi structure. The mucine Sgs3 (brown dots) moves through the secretory pathway from the endoplasmic reticulum (ER) to the Golgi complex, from where immature SGs containing the mucine sprout out. 2-After sprouting, SGs undergo maturation (96-116 hours AEL). During maturation, the exocyst localizes in between immature SGs, where it is required for homotypic fusion. The exocyst is also required for incorporation of maturation factors to the membrane of SGs. These maturation factors include Syt-1 (purple line), DC63 (orange line), Rab11 (green oval) and Rab1 (light blue oval). At this stage, the exocyst no longer localizes at the Golgi complex. 3- When maturation has been completed SGs fuse with the apical plasma membrane and exocytosis takes place. During exocytosis (116-120 hours AEL), the exocyst localizes at mature SGs, in contact with the apical plasma membrane, where it is required for tethering and subsequent fusion, prior to release of the SG content to the salivary gland lumen.

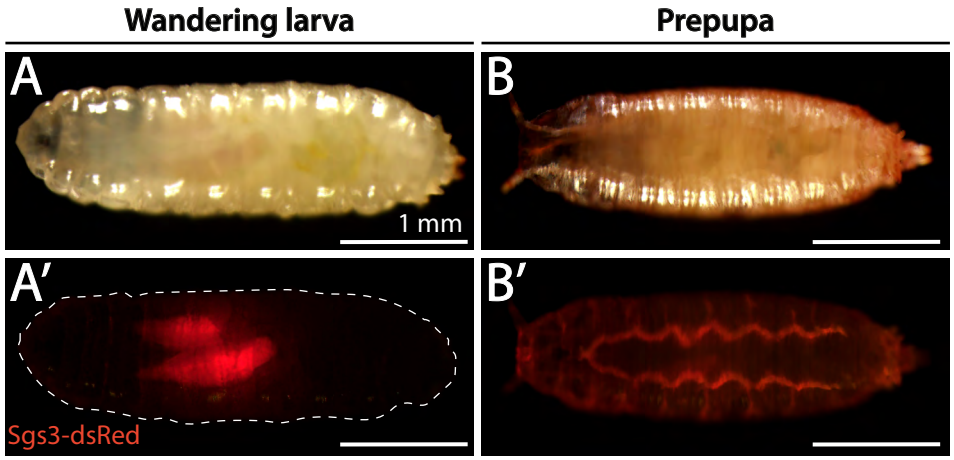
Wandering larva
Prepupa
A
B
1 mm
A′
B′
Sgs3-dsRed

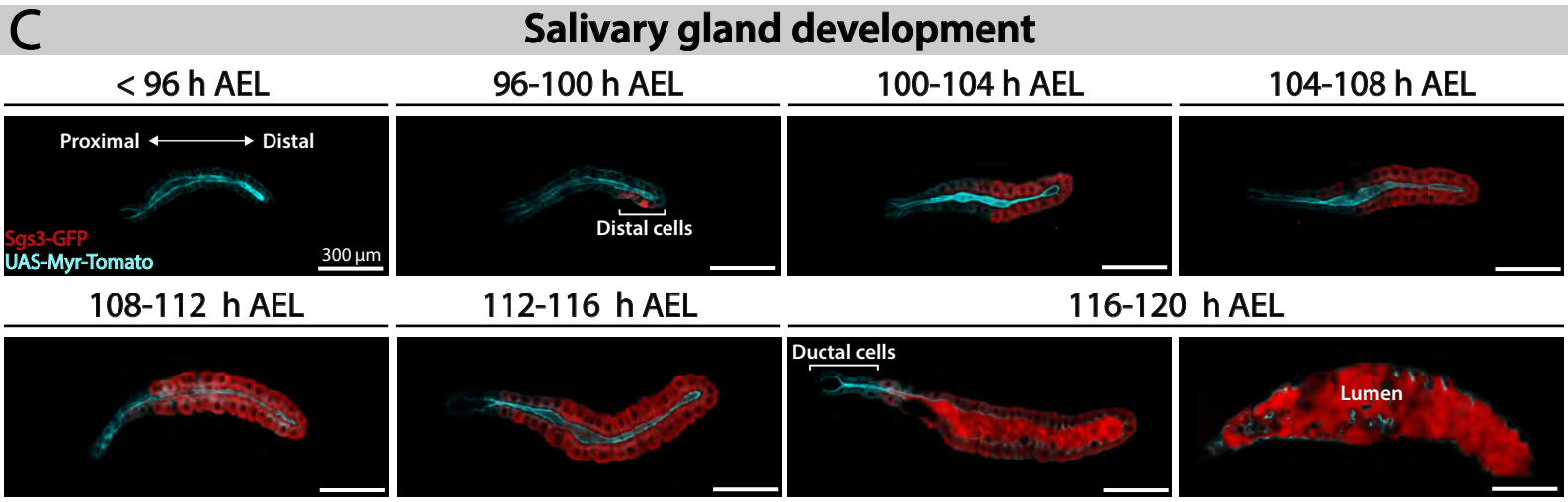
C
Salivary gland development
< 96 h AEL
96-100 h AEL
100-104 h AEL
104-108 h AEL
Proximal
Distal
Sgs3-GFP
UAS-Myr-Tomato
300 µm
Distal cells
108-112 h AEL
112-116 h AEL
116-120 h AEL
Ductal cells
Lumen

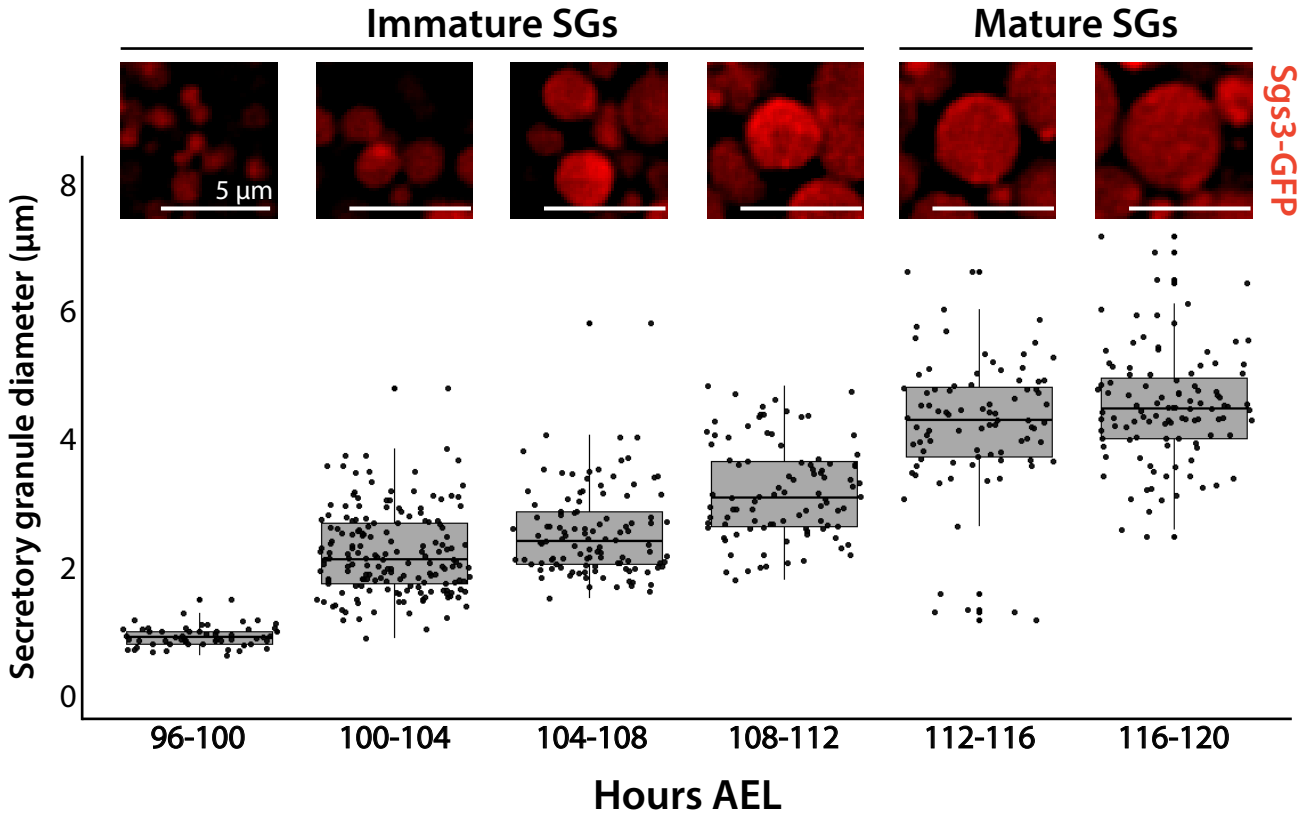
D
Secretory granules progression
Immature SGs
Mature SGs
Sgs3-GFP
5 µm
Secretory granule diameter (µm)
0
2
4
6
8
96-100
100-104
104-108
108-112
112-116
116-120
Hours AEL

Figure 1. Larval salivary gland as a model for regulated exocytosis. Images of a wandering larva (A-A') and a prepupa (B-B') expressing Sgs3-dsRed and visualized under white light (A and B) or by epiflourescence (A'-B'). Sgs3-dsRed localized in salivary glands of wandering larvae (A') and outside the puparium in prepupae (B'). Scale bar 1 mm. (C) Confocal images of unfixed salivary glands dissected from larvae at the indicated time intervals (h AEL= hours after egg laying). Sgs3-GFP is shown in red and the plasma membrane labelled with myr-Tomato (*sgs3-GFP, fkh-Gal4/ UAS-myr-Tomato*) is shown in cyan. At 96 h AEL, Sgs3 synthesis could be detected in the distal cells of the gland. Thereafter, Sgs3 expression gradually expanded proximally, and at 116 h AEL all salivary gland cells expressed Sgs3, with the exception of ductal cells. Exocytosis of SGs began by this time point, and Sgs3 could be detected in the gland lumen. At 120 h AEL concerted exocytosis of SGs has ended. Scale bar 300 μm. (D) Confocal images of SGs labelled with Sgs3-GFP; SG diameter distribution at each time interval is displayed below. Based on its diameter, SGs are classified as immature (diameter < 3 μm) or mature (diameter ≥ 3μm). Only SGs from distal cells were used for diameter determination. Data points for this graph are shown in Supplementary Table 1. For all time intervals analyzed n = 3, except for the 108-112 h AEL interval for which n = 4. "n" represents the number of salivary glands analyzed. Scale bar 5 μm.

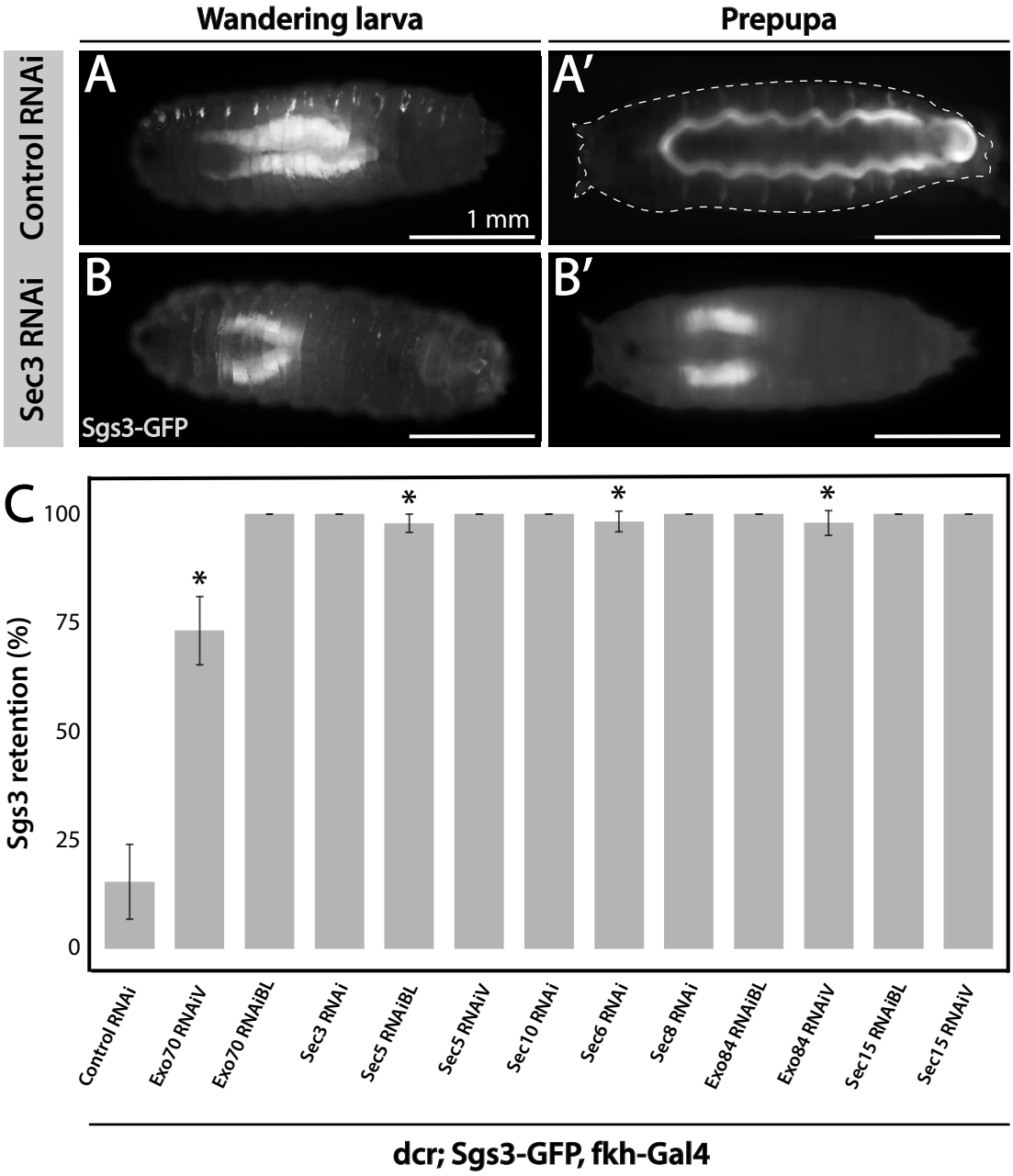
Wandering larva
Prepupa
Control RNAi
Sec3 RNAi
A
A′
B
B′
1 mm
Sgs3-GFP
C
Sgs3 retention (%)
100
75
50
25
0
*
Control RNAi
Exo70 RNAiV
Exo70 RNAiBL
Sec3 RNAi
Sec5 RNAiBL
Sec5 RNAiV
Sec10 RNAi
Sec6 RNAi
Sec8 RNAi
Exo84 RNAiBL
Exo84 RNAiV
Sec15 RNAiBL
Sec15 RNAiV
dcr; Sgs3-GFP, fkh-Gal4

Figure 2. The exocyst is required for Sgs3 secretion. (A-B) Images of a larva and a prepupa expressing Sgs3-GFP, and visualized with epifluorescence. Sgs3-GFP was inside the salivary glands in control wandering larvae (A), and outside the puparium (A') in control prepupae (*sgs3-GFP*, *fkh-Gal4/UAS-cherry*^{RNAi}). Expression of *sec3* ^{RNAi} in salivary glands (*UAS-sec3*^{RNAi}; *sgs3-GFP, fkh-Gal4)* did not affect expression of Sgs3-GFP in larvae (B), but blocked Sgs3-GFP release outside the puparium, so the protein was retained inside the salivary glands (B'). This phenotypic manifestation is referred as "retention phenotype". Scale bar 1 mm. (C) Quantification of the penetrance of the retention phenotype in prepupae expressing the indicated RNAis. RNAis were expressed using *fkh-Gal4* and larvae were cultured at 29°C. All RNAis tested against exocyst complex subunits displayed a retention phenotype, with a penetrance significantly different from the control RNAi (*UAS-cherry*^{RNAi}) according to Likelihood ratio test followed by Tuckey´s test (p-value< 0.05). *cherry*^{RNAi} n= 7; *exo70*^{RNAiV} n= 11; *exo70*^{RNAiBL} n= 8; *sec3*^{RNAi} n= 6; *sec5*^{RNAiBL} n= 17; *sec5*^{RNAiV} n= 6; *sec10*^{RNAi} n= 9; *sec6*^{RNAi} n= 11; *sec8*^{RNAi} n= 5; *exo84*^{RNAiBL} n=5 ; *exo84*^{RNAiV}, n=6; *sec15*^{RNAiBL} n=3 ; *sec15*^{RNAiV} n=4. "n" represents the number of vials containing 20 to 30 prepupae per vial. For exocyst subunits with more than one RNAi line available, "BL" indicates a Bloomington Stock Center allele and "V" a Vienna Stock Center allele (see Supplementary Table 2 for stock numbers).

Sgs3-GFP, fkh-GAL4

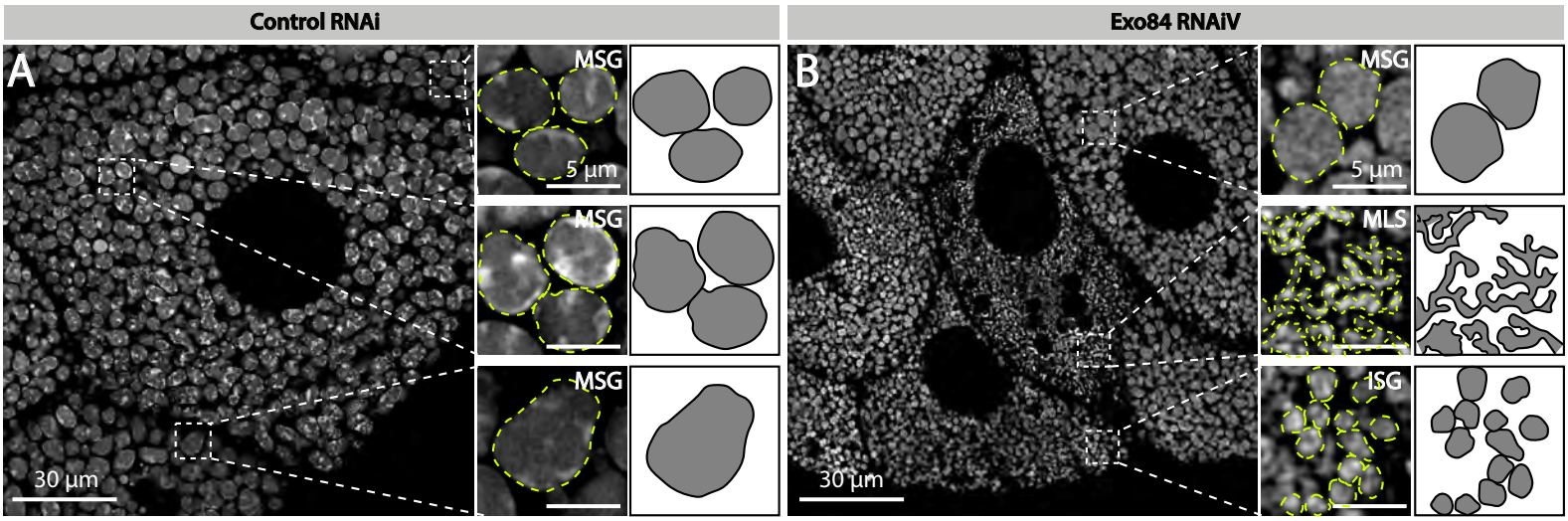

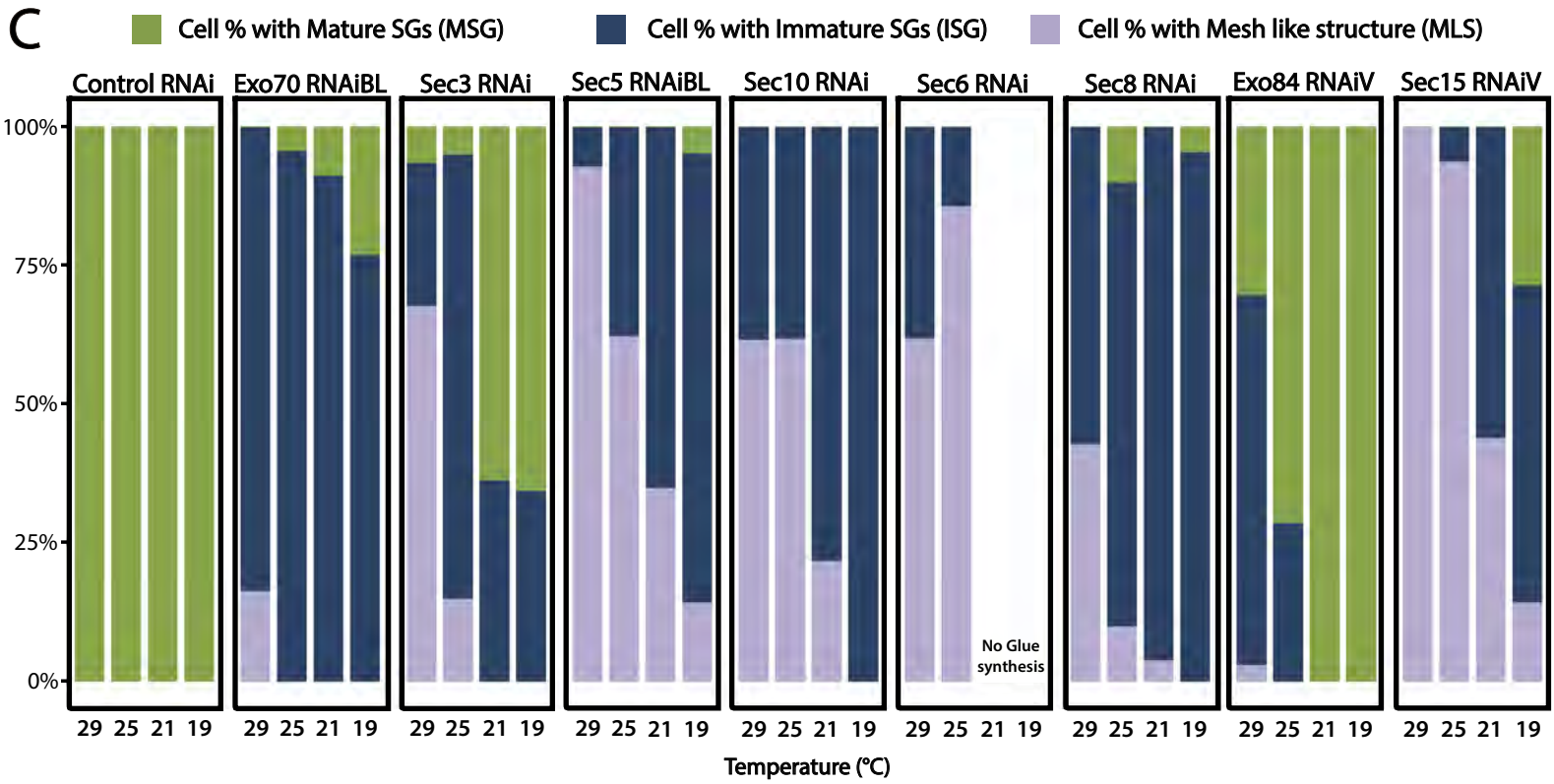

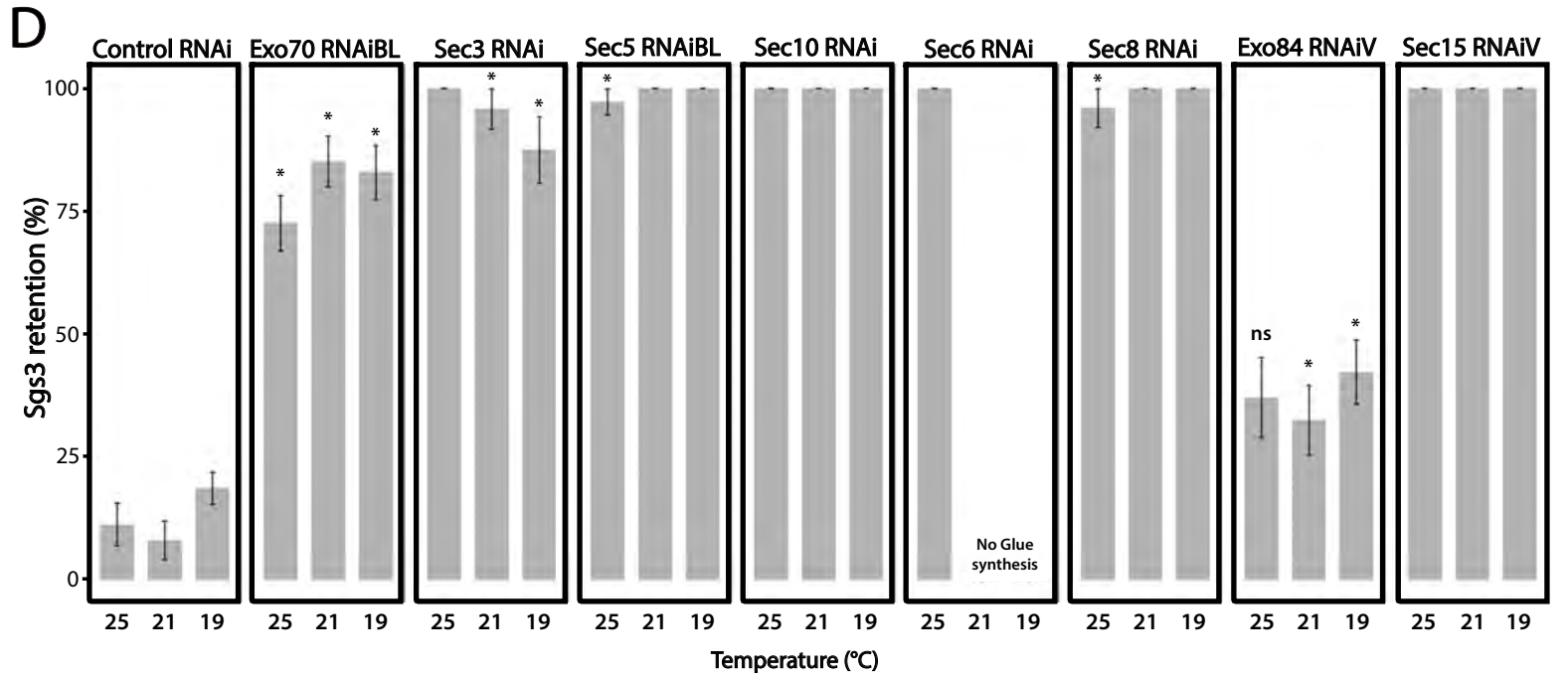

Figure 3. **Phenotypic manifestations of exocyst subunits silencing.** At the end of larval development (116-120 h AEL) salivary gland cells of control individuals (*sgs3-GFP*, *fkh-Gal4/ UAS-cherry*^{RNAi}) (A) were filled with mature SGs (insets). In cells expressing *exo84*^{RNAiV} (*UAS-exo84*^{RNAiV}*; sgs3-GFP*, *fkh-Gal4*) (B), three different phenotypes could be visualized in a single salivary gland: cells with mature SGs (MSG), cells with immature SGs (ISG) and cells with no SG, in which Sgs3 was retained in a mesh (MLS). Scale bar 30 μm in main panels, and 5 μm in insets. For didactic purposes, MSG, ISG and MLS were drawn on the right, next to the corresponding inset (C) Quantification of the penetrance of each of the three phenotypes observed upon downregulation of each of the exocyst subunits. Larvae were grown at four different temperatures (29, 25, 21 or 19°C) to achieve different levels of RNAi expression. "n" = Number of salivary glands analyzed; *control*^{RNAi} (*cherry*^{RNAi}) n = 4 (29 °C), n = 5 (25, 21 and 19 °C); *exo70*^{RNAiBL} n = 11 (29 °C), n = 7 (25, 21 °C), n = 6 (19 °C); *sec3*^{RNAi} n = 7 (29, 25 °C), n = 4 (21 °C), n = 9 (19 °C); *sec5*^{RNAiBL} n = 4 (29 °C), n = 12 (25 °C), n = 9 (21 °C), n = 6 (19 °C) ; *sec10*^{RNAi} n = 8 (29 °C), n = 6 (25, 19 °C), n = 7 (21 °C); *sec6*^{RNAi} n = 9 (29 °C), n = 4 (25 °C); *sec8*^{RNAi} n = 8 (29 °C), n = 6 (25, 19 °C), n = 7 (21°C); *exo84*^{RNAiV} n = 8 (29 °C), n = 4 (25, 19 °C), n = 5 (21 °C) ; *sec15*^{RNAiV} n = 4 (29, 25 °C), n = 6 (21 °C), n = 5 (19 °C). Raw data use to generate this graph is shown in Supplementary Table 3. (D) Quantification of the penetrance of the Sgs3-GFP retention phenotype in salivary glands of prepupae of the indicated genotypes. Only a few control individuals (*sgs3-GFP*, *fkh-Gal4/ UAS-cherry*^{RNAi}) displayed the retention phenotype. Downregulation of exocyst subunits provoked significant retention of Sgs3 inside the salivary glands irrespective to the temperature (25, 21 or 19 °C). Expression of *sec6*^{RNAi} at 21 or 19 °C resulted in no synthesis of Sgs3-GFP or Sgs3-dsRed, so the distribution of phenotypes was not assessed for this genotype at these temperatures. RNAis were expressed with *fkh*-Gal4. "n" = Number of vials with 20-30 larvae. *control*^{RNAi} (*cherry*^{RNAi}) n = 7 (25 °C), n = 9 (21 °C), n = 19 (19 °C); *exo70*^{RNAiBL} n = 13 (25 °C), n = 9 (21°C), n = 22 (19 °C); *sec3*^{RNAi} n = 9 (25 °C), n =6 (21, 19 °C); *sec5*^{RNAiBL} n = 9 (25 °C), n = 7 (21 °C), n = 12 (19 °C); *sec10*^{RNAi} n = 10 (25 °C), n = 5 (21 °C), n = 4 (19 °C); *sec6*^{RNAi} n = 10 (25 °C); *sec8*^{RNAi} n = 5 (25 °C), n = 8 (21 °C), n = 22 (19 °C); *exo84*^{RNAiV} n = 8 (25, 19 °C), n = 6 (21 °C) ; *sec15*^{RNAiV} n = 5 (25 °C), n = 9 (21 °C), n = 8 (19 °C). Statistical analysis was performed using a Likelihood ratio test followed by Tuckey´s test ("*"=p-value< 0.05). For those genotypes with 100% penetrance no statistical analysis was performed due to the lack of standard error. "ns"= not significant. Comparisons were made between RNAis for each of the temperatures analyzed.

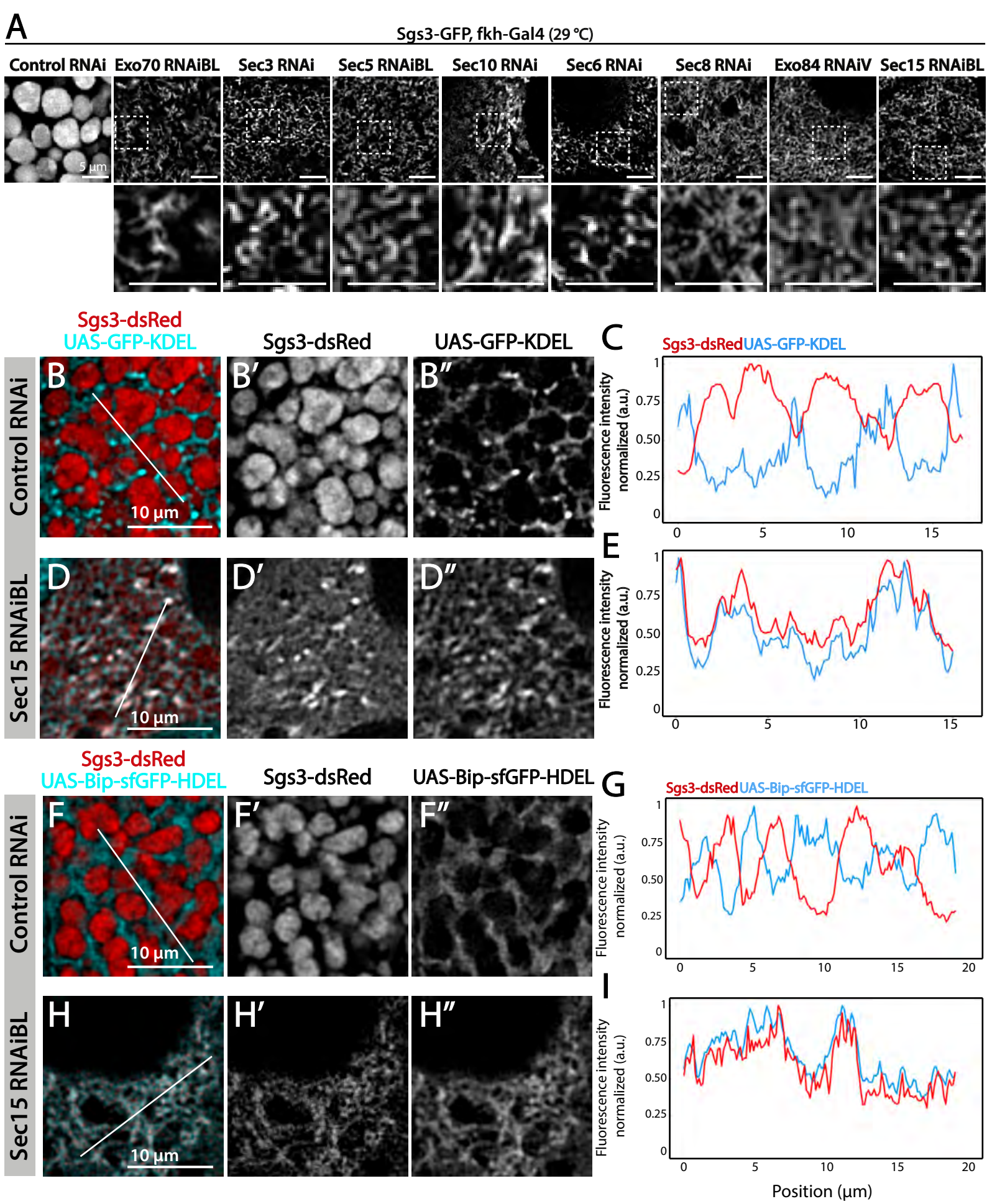
A
Sgs3-GFP, fkh-Gal4 (29 °C)
Control RNAi
Exo70 RNAiBL
Sec3 RNAi
Sec5 RNAiBL
Sec10 RNAi
Sec6 RNAi
Sec8 RNAi
Exo84 RNAiV
Sec15 RNAiBL
5 µm
Sgs3-dsRed
UAS-GFP-KDEL
Sgs3-dsRed
UAS-GFP-KDEL
Control RNAi
Sec15 RNAiBL
B
B′
B″
D
D′
D″
10 µm
C
E
Fluorescence intensity normalized (a.u.)
Sgs3-dsRed
UAS-GFP-KDEL
Sgs3-dsRed
UAS-Bip-sfGFP-HDEL
Sgs3-dsRed
UAS-Bip-sfGFP-HDEL
F
F′
F″
H
H′
H″
G
I
Position (µm)

Figure 4. The exocyst is required for Sgs3-GFP exit from ER and SG biogenesis. Confocal images of unfixed salivary glands of the indicated genotypes. Larvae were grown at 29 °C to achieve maximal activation of the Gal4-UAS system, and maximal downregulation of exocyst subunits. (A) In control salivary glands (*sgs3-GFP*, *fkh-Gal4/ UAS-cherry*^{RNAi}) 116-120 AEL, Sgs3-GFP was packed in mature SGs. Salivary glands expressing RNAis against each of the exocyst subunits, where Sgs3-GFP exhibited a reticular distribution are shown. SGs were not formed in these cells. Scale bar 5 μm. The ER, labeled with GFP-KDEL (*UAS-GFP-KDEL*), (B and D) or Bip-sfGFP-HDEL (*UAS-Bip-sfGFP-HDEL*), (F and H) distributed in between SGs in control salivary glands (B and F); in sec15^{RNAi} salivary glands (*fkh-Gal4/ UAS-sec15*^{RNAiBL}) SGs did not form and the Sgs3-dsRed signal overlapped with the ER markers (D and H). (C, E, G and I) Two-dimensional line scans of fluorescence intensity across the white lines in panels B, D, F and H of Sgs3-dsRed and the ER markers. In all cases transgenes were expressed using *fkh*-Gal4. Scale bar 10 μm.

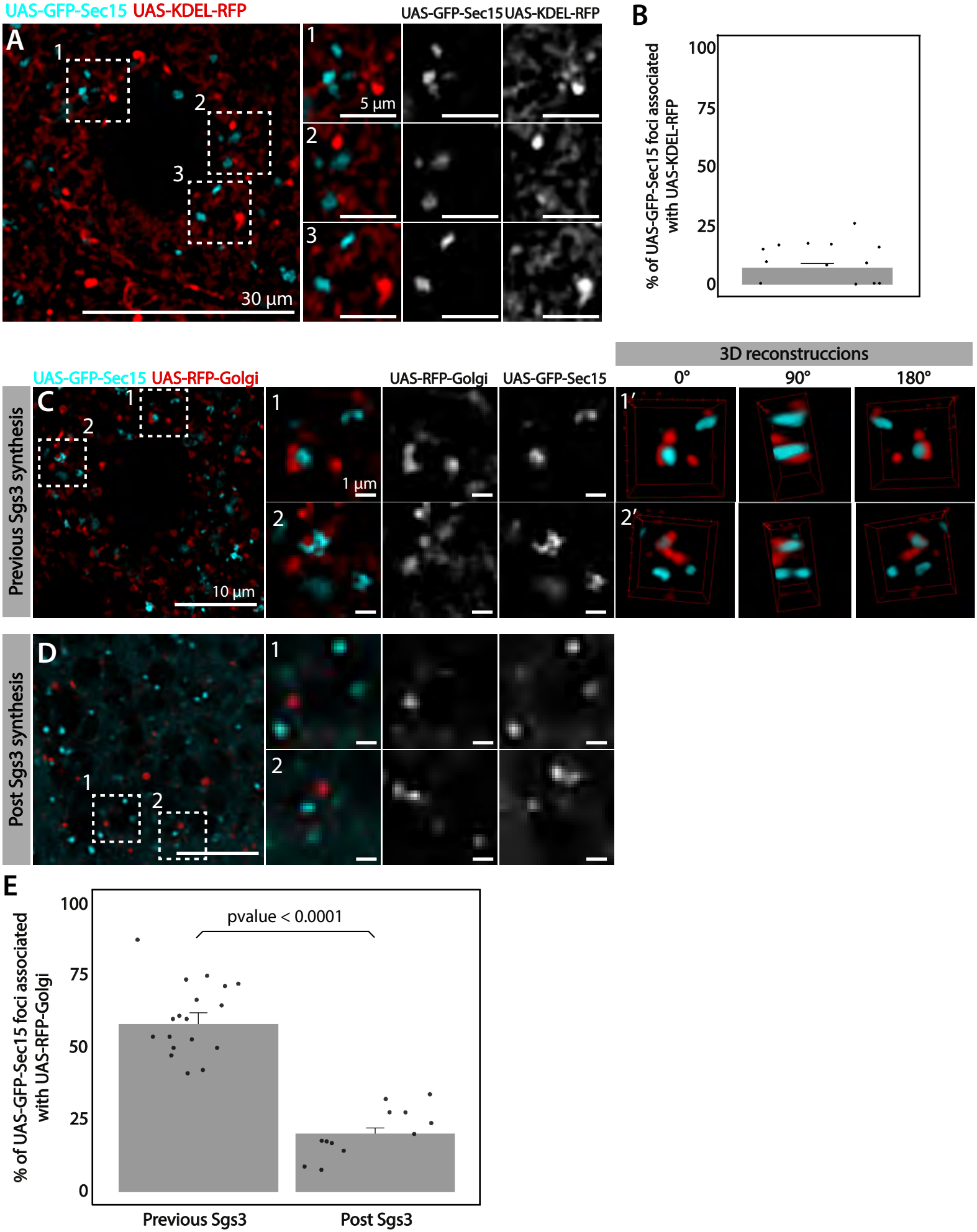
UAS-GFP-Sec15 UAS-KDEL-RFP
A
1
2
3
30 µm
UAS-GFP-Sec15 UAS-KDEL-RFP
5 µm
B
% of UAS-GFP-Sec15 foci associated with UAS-KDEL-RFP
100
75
50
25
0
3D reconstruccions
UAS-GFP-Sec15 UAS-RFP-Golgi
UAS-RFP-Golgi
UAS-GFP-Sec15
0°
90°
180°
Previous Sgs3 synthesis
C
1 µm
10 µm
1′
2′
Post Sgs3 synthesis
D
E
pvalue < 0.0001
% of UAS-GFP-Sec15 foci associated with UAS-RFP-Golgi
Previous Sgs3
Post Sgs3

Figure 5. The exocyst localizes at the Golgi complex before Sgs3 synthesis. Confocal images of unfixed salivary glands expressing GFP-Sec15 and (A) the ER marker KDEL-RFP or (C) the trans-Golgi marker RFP-Golgi. Sec15 foci did not localize at or associate with the ER (A-B). (C) Sec15 foci were found in close association with trans-Golgi complex cisternae. Examples of association events are shown in insets 1 and 2, including different angles of three-dimensional reconstruction stacks. (D) Sec15 foci and trans-Golgi complex association was lost after Sgs3 synthesis has begun. (E) Quantification of Sec15 foci-Golgi complex association events before and after the onset of Sgs3 synthesis. (Wald Test, p-value < 0.05). "n" represents the number of salivary glands analyzed, n=4.

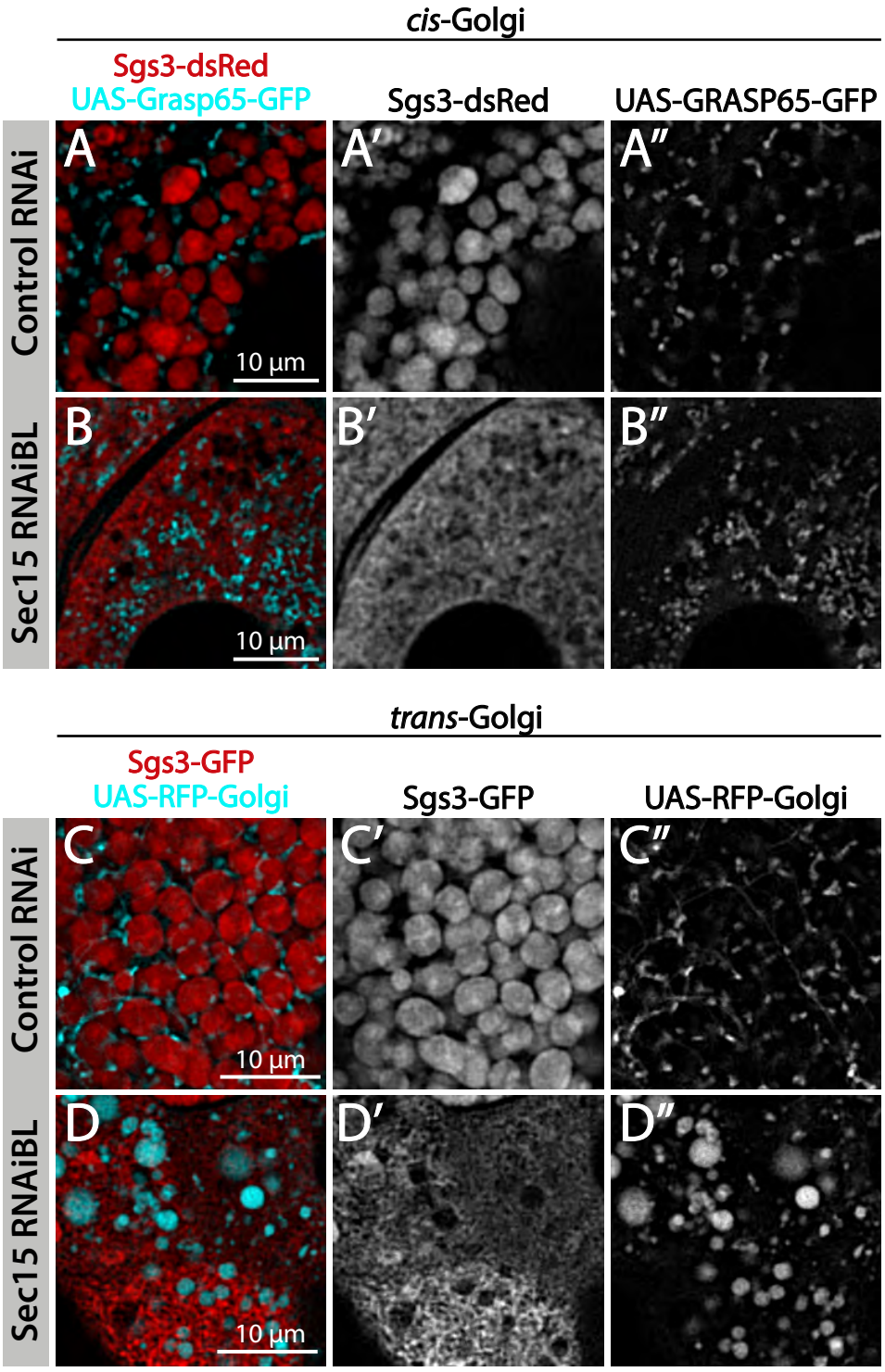
cis-Golgi
Sgs3-dsRed
UAS-Grasp65-GFP
Sgs3-dsRed
UAS-GRASP65-GFP
Control RNAi
Sec15 RNAiBL
A
A′
A″
B
B′
B″
10 µm
10 µm
trans-Golgi
Sgs3-GFP
UAS-RFP-Golgi
Sgs3-GFP
UAS-RFP-Golgi
C
C′
C″
D
D′
D″
10 µm
10 µm

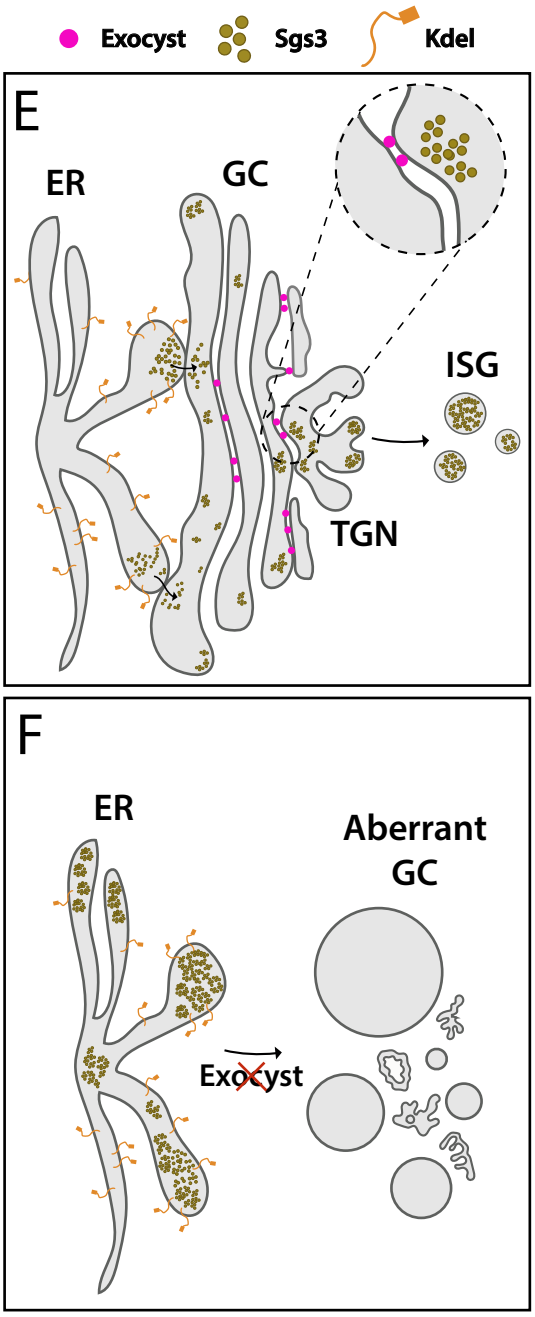
Exocyst
Sgs3
Kdel
E
ER
GC
ISG
TGN
F
ER
Aberrant
GC
Exocyst

Figure 6. The exocyst is required to maintain normal Golgi complex morphology. Confocal images of unfixed salivary glands of the indicated genotypes. Larvae were grown at 29 °C to achieve maximal activation of the Gal4-UAS system and maximal downregulation of exocyst subunits. In control larvae (*fkh-Gal4/ UAS-white*^{RNAi}), Sgs3-dsRed (A) or Sgs3-GFP (C) were in mature SGs. In sec15^{RNAi} salivary glands (*fkh-Gal4/ UAS-sec15*^{RNAiBL}) Sgs3 was retained in a mesh-like structure (B and D), also shown in Figure 4. (A, B) The *cis*-Golgi complex was labelled with Grasp65-GFP (*UAS-Grasp65-GFP*), (and the *trans*-Golgi with RFP-Golgi (*UAS-RFP-Golgi*), (C, D). The morphology of the *cis*- and *trans*-Golgi complexes changed dramatically in sec15-knockdown cells (B", D"), in comparison to controls (A", C"). Transgenes were expressed with *fkh-Gal4*. Scale bar 10 μm. (E) Model of Sgs3 transit from the ER through the *cis*- and trans-Golgi complex to sprouting SGs from the *trans*-Golgi complex. (F) The exocyst is needed for tethering the Golgi complex cisternae and to support Golgi complex structure. In the absence of the exocyst Golgi cisternae disconnect, *cis*- and trans-Golgi become dysfunctional, resulting in Sgs3 retention at the ER.

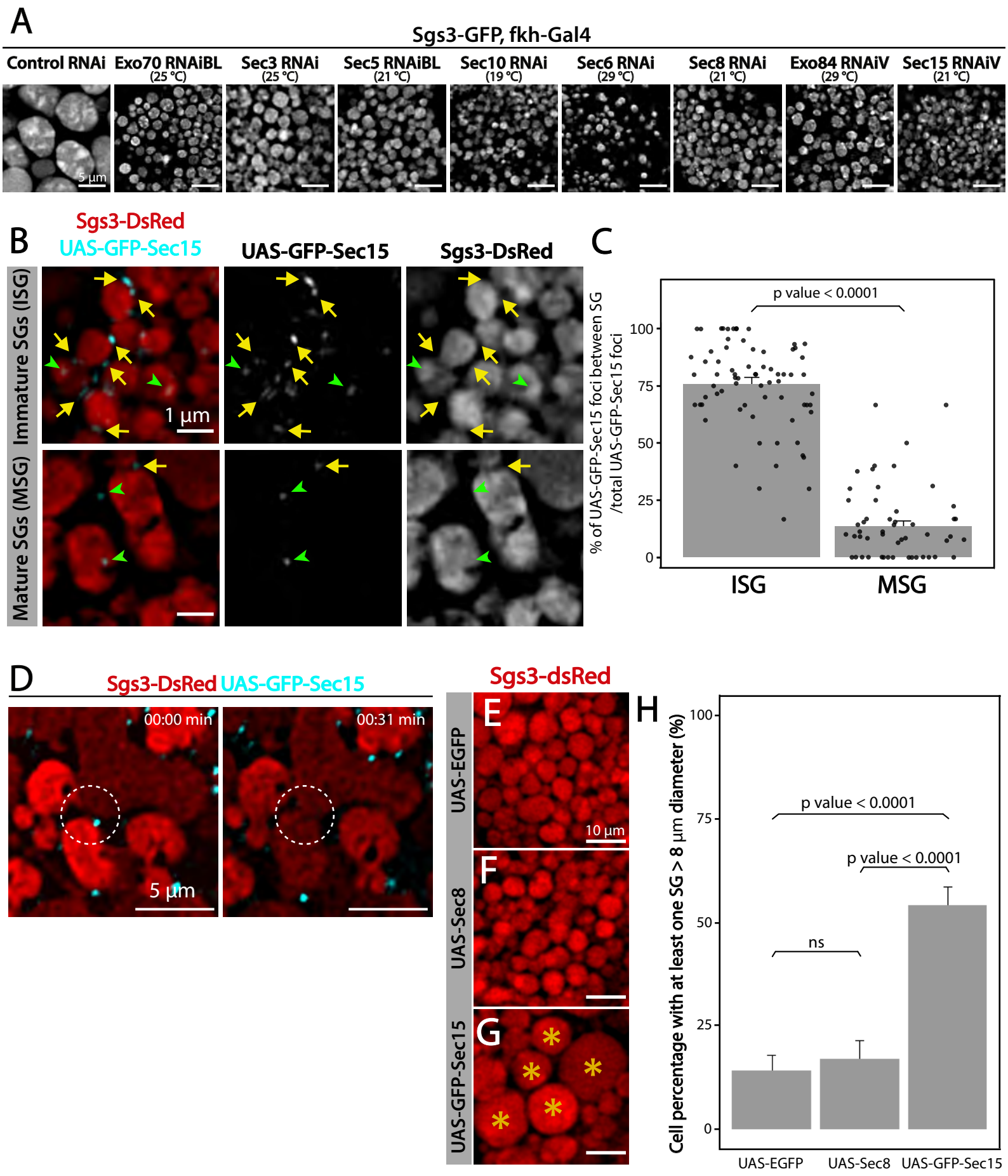
A
Sgs3-GFP, fkh-Gal4
Control RNAi
Exo70 RNAiBL (25 °C)
Sec3 RNAi (25 °C)
Sec5 RNAiBL (21 °C)
Sec10 RNAi (19 °C)
Sec6 RNAi (29 °C)
Sec8 RNAi (21 °C)
Exo84 RNAiV (29 °C)
Sec15 RNAiV (21 °C)
5 µm
B
Sgs3-DsRed
UAS-GFP-Sec15
UAS-GFP-Sec15
Sgs3-DsRed
Immature SGs (ISG)
Mature SGs (MSG)
1 µm
C
% of UAS-GFP-Sec15 foci between SG /total UAS-GFP-Sec15 foci
p value < 0.0001
100
75
50
25
0
ISG
MSG
D
Sgs3-DsRed UAS-GFP-Sec15
00:00 min
00:31 min
5 µm
Sgs3-dsRed
UAS-EGFP
UAS-Sec8
UAS-GFP-Sec15
E
F
G
10 µm
H
Cell percentage with at least one SG > 8 µm diameter (%)
p value < 0.0001
p value < 0.0001
ns
100
75
50
25
0
UAS-EGFP
UAS-Sec8
UAS-GFP-Sec15

Figure 7. The exocyst is required for secretory granule homotypic fusion. (A) Confocal images of unfixed salivary glands of the indicated genotypes. In control salivary glands (*sgs3-GFP*, *fkh-Gal4/ UAS-cherry*^{RNAi}), Sgs3-GFP was packed in mature SGs. RNAis targeting any of the subunits of the exocyst were expressed at the indicated temperatures, giving rise to salivary cells with immature granules. Scale bar 5 μm. (B) GFP-Sec15 (cyan) and Sgs3-dsRed (red) were expressed in salivary glands (*sgs3-dsRed/ UAS-GFP-sec15; fkh-Gal4*) at 18 °C. GFP-Sec15 foci were mostly found in between SGs (yellow arrows) in cells bearing immature SGs (upper panel) and not in cells with mature SGs (lower panel), in which most foci did not localize in between SGs (green arrowheads). Scale bar 1 μm. (C) Quantification of Sec15 foci in between SGs relative to the total number of Sec15 foci (%) (Wald Test, p-value < 0.05). Eight salivary glands with ISGs and 5 salivary glands with MSGs were analyzed. (D) Still panels of two different frames of Supplementary movie 6 showing that during a homotypic fusion event, GFP-Sec15 accumulated precisely at the contact site between two neighboring SGs (dotted circle); scale bar 5 μm. (E-G) Expression of EGFP (*sgs3-dsRed; UAS-EGFP, fkh-Gal4*) (E) or Sec8 (*sgs3-dsRed/ UAS-Sec8; fkh-Gal4*) (F) did not affect SG size (red). Expression of GFP-Sec15 (G) (*sgs3-dsRed/ UAS -GFP-sec15; fkh-Gal4*) generated giant SGs (asterisks). Scale bar 10 μm. (H) Quantification of the percentage of salivary gland cells with at least one SG larger than 8 μm diameter; (Likelihood ratio test followed by Tuckey´s test, p-value < 0.05). "n" represents the number of salivary glands analyzed. UAS-EGFP n=7; UAS-Sec8 n=5; UAS-GFP-Sec15 n=5. Transgenes were expressed using *fkh-Gal4.* "ns"= not significant.

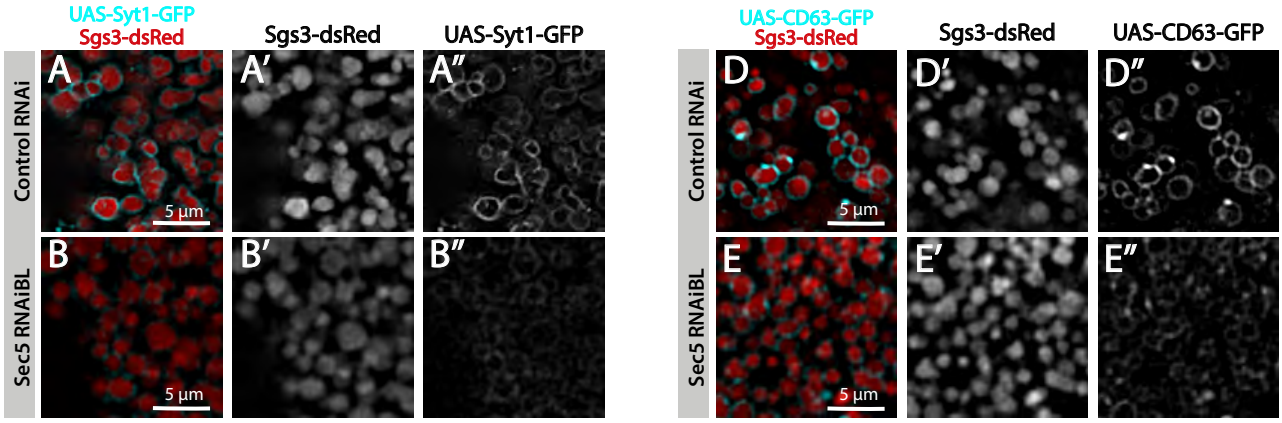
UAS-Syt1-GFP
Sgs3-dsRed
Sgs3-dsRed
UAS-Syt1-GFP
Control RNAi
Sec5 RNAiBL
A
A′
A″
B
B′
B″
5 µm
UAS-CD63-GFP
Sgs3-dsRed
Sgs3-dsRed
UAS-CD63-GFP
D
D′
D″
E
E′
E″

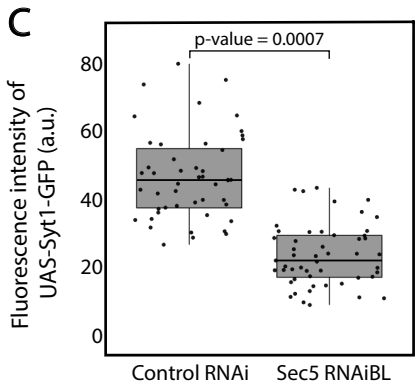
C
p-value = 0.0007
Fluorescence intensity of UAS-Syt1-GFP (a.u.)
0
20
40
60
80
Control RNAi
Sec5 RNAiBL

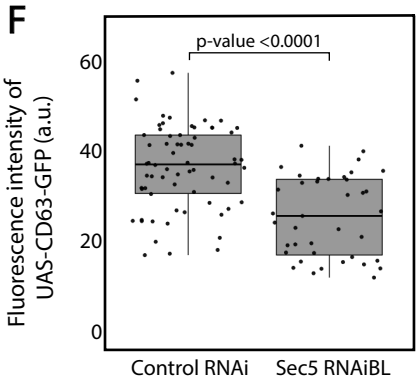
F
p-value <0.0001
Fluorescence intensity of UAS-CD63-GFP (a.u.)
0
20
40
60
Control RNAi
Sec5 RNAiBL

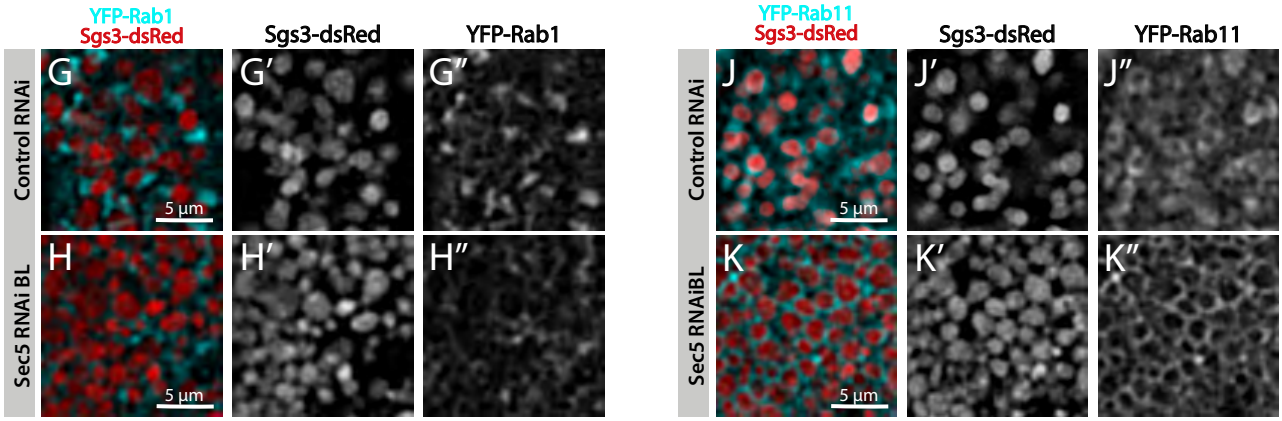
YFP-Rab1
Sgs3-dsRed
Sgs3-dsRed
YFP-Rab1
Control RNAi
Sec5 RNAi BL
G
G′
G″
H
H′
H″
5 µm
YFP-Rab11
Sgs3-dsRed
Sgs3-dsRed
YFP-Rab11
J
J′
J″
K
K′
K″

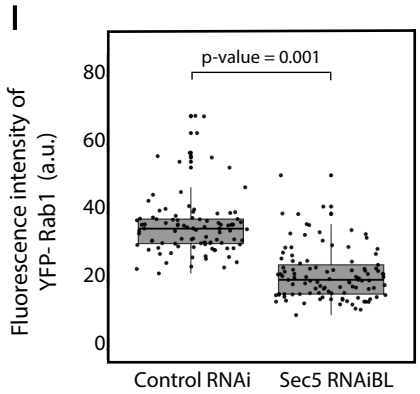
I
p-value = 0.001
Fluorescence intensity of YFP- Rab1 (a.u.)
0
20
40
60
80
Control RNAi
Sec5 RNAiBL

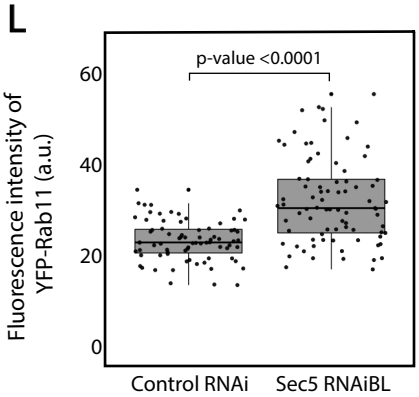
L
p-value <0.0001
Fluorescence intensity of YFP-Rab11 (a.u.)
0
20
40
60
Control RNAi
Sec5 RNAiBL

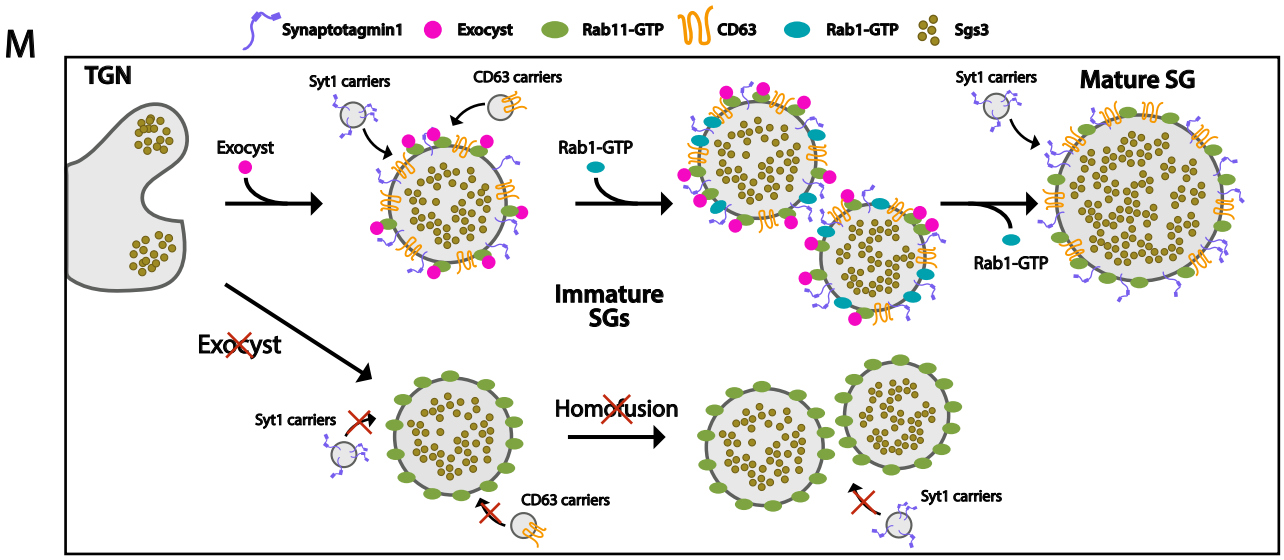
M
Synaptotagmin1
Exocyst
Rab11-GTP
CD63
Rab1-GTP
Sgs3
TGN
Syt1 carriers
CD63 carriers
Exocyst
Rab1-GTP
Syt1 carriers
Mature SG
Rab1-GTP
Immature SGs
Exocyst
Syt1 carriers
Homotusion
CD63 carriers
Syt1 carriers

Figure 8. The exocyst mediates the acquisition of secretory granule maturation factors. Confocal images of unfixed salivary glands of the indicated genotypes. Larvae were grown at 21 °C to reduce the activity of the Gal4-UAS system, and to generate a maximal proportion of cells with immature SGs. (A-B) Recruitment of Syt1-GFP (*UAS-Syt1-GFP*); of (D-E) CD63-GFP (*UAS-CD63-GFP*); of (G-H) YFP-Rab1 and of (J-K) YFP-Rab11 was analyzed in control salivary glands expressing *white*^{RNAi} (*fkh-Gal4/ UAS-white*^{RNAi}) and in salivary glands expressing *sec5*^{RNAiBL} (*fkh-Gal4/ UAS-sec5*^{RNAiBL}). Fluorescent intensity around SGs of each of the analyzed maturation factors was quantified using the ImageJ software and plotted (C, F, I and L). Comparison of fluorescent intensity among genotypes and statistical analysis was performed using one-way analysis of variance (ANOVA). "n" represents the number of salivary glands: (C) *control RNAi* n= 4, *sec5*^{RNAiBL} n= 5; (F) *control RNAi* n= 5, *sec5*^{RNAiBL} n=4; (I) *control RNAi* n= 6, *sec5*^{RNAiBL} n= 9; (L) *control RNAi* n= 11, *sec5*^{RNAiBL} n= 8. Transgenes were expressed using *fkh-Gal4*. Scale bar 5 μm. (M) Proposed model of exocyst-dependent SG homotypic fusion and maturation. The exocyst complex is required for homotypic fusion between immature SGs. Immature SGs incorporate Syt-1, CD63 and Rab1 in an exocyst-dependent manner. Syt-1 continues to be recruited to SGs after homotypic fusion. The exocyst complex also inhibits the incorporation of an excess of Rab11 around SGs.

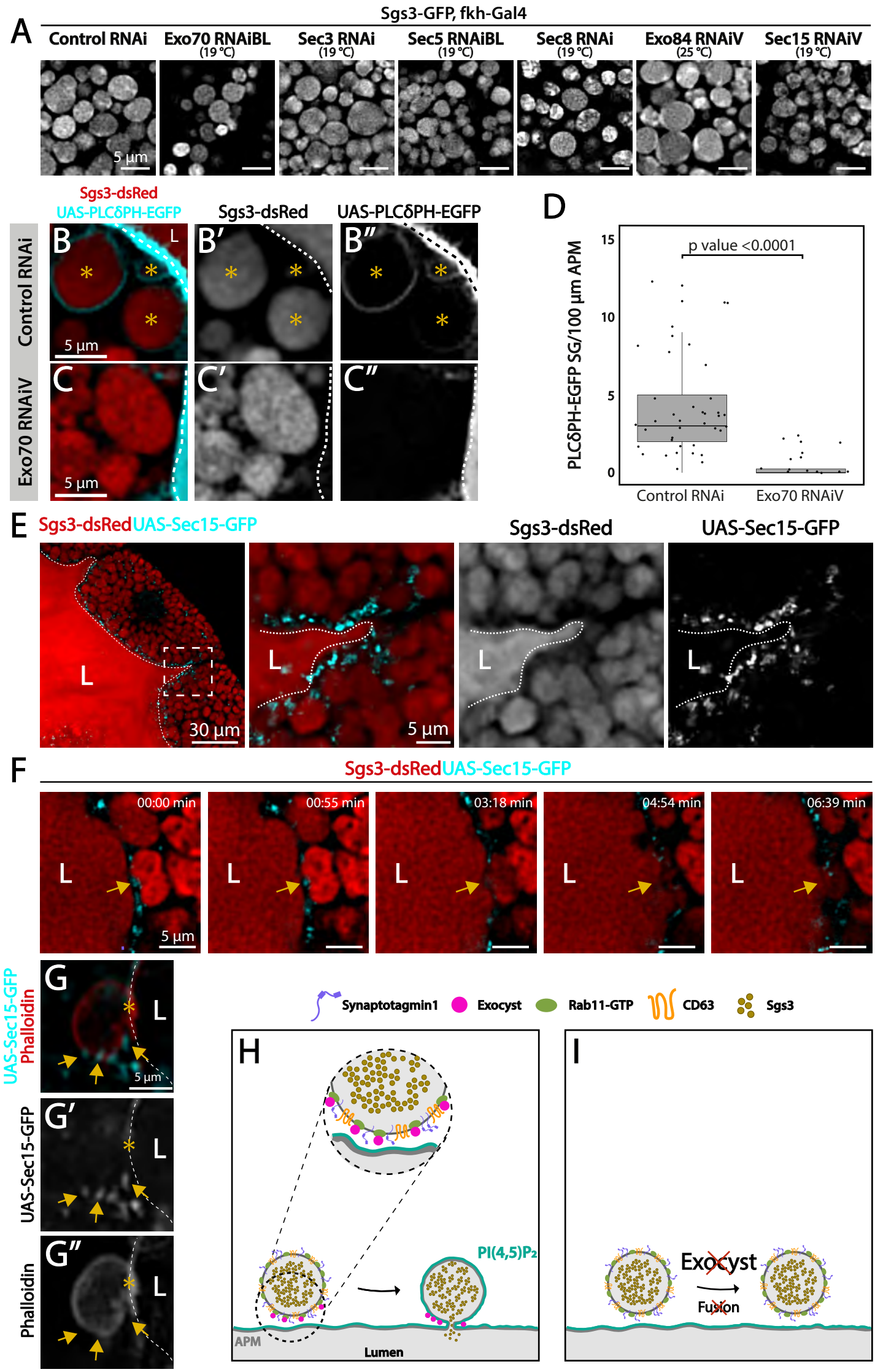
A
Sgs3-GFP, fkh-Gal4
Control RNAi
Exo70 RNAiBL (19 °C)
Sec3 RNAi (19 °C)
Sec5 RNAiBL (19 °C)
Sec8 RNAi (19 °C)
Exo84 RNAiV (25 °C)
Sec15 RNAiV (19 °C)
5 µm
Sgs3-dsRed
UAS-PLCδPH-EGFP
Sgs3-dsRed
UAS-PLCδPH-EGFP
Control RNAi
Exo70 RNAiV
B
B′
B″
C
C′
C″
L
5 µm
D
p value <0.0001
PLCδPH-EGFP SG/100 µm APM
15
10
5
0
Control RNAi
Exo70 RNAiV
E
Sgs3-dsRedUAS-Sec15-GFP
Sgs3-dsRed
UAS-Sec15-GFP
L
30 µm
5 µm
F
Sgs3-dsRedUAS-Sec15-GFP
00:00 min
00:55 min
03:18 min
04:54 min
06:39 min
5 µm
UAS-Sec15-GFP
Phalloidin
G
G′
G″
UAS-Sec15-GFP
Phalloidin
Synaptotagmin1
Exocyst
Rab11-GTP
CD63
Sgs3
H
PI(4,5)P2
APM
Lumen
I
Exocyst
Fusion

Figure 9. The exocyst is required for secretory granule fusion with the plasma membrane during regulated exocytosis. Confocal images of unfixed salivary glands of the indicated genotypes. Larvae were grown at the indicated temperatures to attain levels of RNAi-mediated silencing that bring about maximal proportion of cells with mature, exocytosis incompetent SGs. (A) Sgs3-GFP localized within SGs. Control SGs (*sgs3-GFP*, *fkh-Gal4/ UAS-cherry*^{RNAi}) were indistinguishable from SGs of salivary cells in which a subunit of the exocyst has been knocked-down. Scale bar 5 μm. (B) In control salivary glands (*fkh-Gal4/ UAS-white*^{RNAi}), the PI(4,5)P_2 reporter *UAS-PLCγ-PH-GFP* labels the plasma membrane (dotted line) and also the SGs that have already fused with the plasma membrane (asterisks). (C) SGs of cells expressing *exo70*^{RNAiV} (*UAS-exo70*^{RNAiV}*; fkh-Gal4*) were not labeled with the reporter, indicating that these SGs failed to fuse with the plasma membrane. Scale bar 5 μm. (D) The number of mature SGs positive for PLCγ-PH-EGFP per 100 μm of linear plasma membrane was quantified in the indicated genotypes; Exo70 knock-down reduced SG-plasma membrane fusion (Wald test (p value<0.05); 7 salivary glands per genotype were analyzed. (E) During SG exocytosis the exocyst complex, labelled with GFP-Sec15 (cyan) localized as dots in contact sites between SGs and the apical plasma membrane (dotted line) (*sgs3-dsRed/ UAS-GFP-sec15; fkh-Gal4*). (F) Still panels of Supplementary movie 2 showing a fusion event between a mature SG and the plasma membrane (arrow); a dot of GFP-Sec15 indicating the position of the exocyst (arrow) was positioned just at the site where fusion was taking place. Scale bar 5 μm. (G) Confocal image of a fixed salivary gland. A mature SG that has fused with the plasma membrane (dotted line), and thus became labelled with phalloidin, displayed dots of GFP-Sec15 on its side (arrow), just next to the fusion point (asterisk). Transgenes were expressed with *fkh-Gal4*. The salivary gland lumen is indicated with "L". Scale bar 5 μm. (H) Model of the role of the exocyst complex during SG-plasma membrane fusion during regulated exocytosis. The exocyst sits on the membrane of the SG, and tethers the granule to the plasma membrane, favoring the action of fusion molecules. (I) Upon loss of the exocyst complex, mature SGs cannot contact the plasma membrane and fusion does not occur.

Supplementary Table 1. Quantification of SG diameter at the indicated time intervals after egg laying. SGs from salivary gland distal-most cells were analyzed. Columns display: Hours AEL: hours after egg laying; n: number of salivary glands analyzed; number of cells analyzed; number of SGs measured; mean diameter; median diameter; minimum diameter and maximum diameter.

Hours AEL	n	Cells quantified	SG quantified	Mean (μm)	Median (μm)	Minimum (μm)	Maximum (μm)
96-100	3	7	57	0.92	0.91	0.62	1.49
100-104	3	18	173	2.22	2.11	0.89	4.76
104-108	3	12	112	2.53	2.53	1.50	5.78
108-112	4	13	96	3.18	3.18	1.78	4.81
112-116	3	10	86	4.22	4.22	1.16	6.59
116-120	3	15	107	4.48	4.45	2.47	7.13

Supplementary Table 2. List of the *Drosophila* lines utilized in this work. Stock number and repository center from where each line was obtained are indicated.

Line	Number	Stock Center
Sgs3-GFP	5885	Bloomington
Sgs3-dsRed	-	A.J. Andres' Lab
YFP-Rab11	62549	Bloomington
YFP-Rab1	62539	Bloomington
UAS-dicer2	24650	Bloomington
UAS-White-RNAi	33613	Bloomington
UAS-Cherry-RNAi	35785	Bloomington
UAS-Rab11-RNAi	27730	Bloomington
UAS-Sec3-RNAi	35806	Vienna
UAS-Sec5-RNAi	27526	Bloomington
UAS-Sec5-RNAi	28873	Vienna
UAS-Sec6-RNAi	27314	Bloomington
UAS-Sec8-RNAi	45032	Vienna
UAS-Sec10-RNAi	27483	Bloomington
UAS-Sec15-RNAi	27499	Bloomington
UAS-Sec15-RNAi	35161	Vienna
UAS-Exo84-RNAi	108650	Vienna
UAS-Exo84-RNAi	28712	Bloomington
UAS-Exo70-RNAi	27867	Vienna
UAS-Exo70-RNAi	28041	Bloomington
UAS-PLCγ-PH-EGFP	58362	Bloomington
UAS-Synaptotagmin1-GFP	6925	Bloomington

UAS-Sec8	9556	Bloomington
UAS-CD63-GFP	91390	Bloomington
UAS-Myr-Tomato	32221	Bloomington
UAS-GFP-KDEL	9898	Bloomington
UAS-Bip-SfGFP-HDEL	64749	Bloomington
UAS-RFP-Golgi	30908	Bloomington
UAS-GRASP65-GFP	8508	Bloomington
UAS-EGFP	5430	Bloomington
UAS-GFP-Sec15	39685	Bloomington
UAS-YFP-Rab11^{CA}	9791	Bloomington
tubP-GAL80[ts]	7017	Bloomington
UAS-mCD8-mCherry	27391	Bloomington
UAS-mito-GFP	8443	Bloomington
UASp-GFP-mCherry-Atg8a	37749	Bloomington

Supplementary Table3. Raw data for experiments of Figure 3C and Supplementary Figure 1A.

Data Figure 3C						
Genotype	**Temperature**	**Number of Glands Analyzed**	**Number of Distal Cells Analyzed**	**Phenotype**	**% of Phenotype**	**Standard Deviation**
Control RNAi	29	4	12	Mesh Like Structure	0	0
				SG immature	0	0
				SG mature	100	0
	25	5	13	Mesh Like Structure	0	0
				SG immature	0	0
				SG mature	100	0
	21	5	17	Mesh Like Structure	0	0
				SG immature	0	0
				SG mature	100	0
	19	5	15	Mesh Like Structure	0	0
				SG immature	0	0
				SG mature	100	0
Exo70 RNAi BL	29	11	43	Mesh Like Structure	12.73	28.67
				SG immature	87.27	28.67
				SG mature	0	0
	25	5	23	Mesh Like Structure	0	0
				SG immature	95.24	12.6
				SG mature	4.76	12.6
	21	7	23	Mesh Like Structure	0	0
				SG immature	90.48	25.2
				SG mature	9.52	25.2
	19	4	15	Mesh Like Structure	0	0
				SG immature	0	0
				SG mature	100	0
Sec3 RNAi	29	7	31	Mesh Like Structure	69.52	42.84
				SG immature	24.05	32.37
				SG mature	6.43	11.07
	25	7	20	Mesh Like Structure	16.67	28.87
				SG immature	78.57	28.41
				SG mature	4.76	12.6
	21	4	11	Mesh Like Structure	0	0
				SG immature	27.08	35.6
				SG mature	72.92	35.6
	19	9	32	Mesh Like Structure	0	0
				SG immature	33.52	33.75
				SG mature	66.48	33.75
Sec5 RNAi BL	29	4	14	Mesh Like Structure	96.43	7.14
				SG immature	3.57	7.14
				SG mature	0	0
	25	12	45	Mesh Like Structure	62.5	38.35
				SG immature	37.5	38.35
				SG mature	0	0
	21	9	20	Mesh Like Structure	27.78	44.1
				SG immature	72.22	44.1
				SG mature	0	0
	19	6	21	Mesh Like Structure	12.22	19.05
				SG immature	84.44	18.22
				SG mature	3.33	8.16
Sec10 RNAi	29	9	26	Mesh Like Structure	77.78	44.1
				SG immature	22.22	44.1
				SG mature	0	0
	25	6	34	Mesh Like Structure	59.17	46.95
				SG immature	40.83	46.95
				SG mature	0	0
	21	7	23	Mesh Like Structure	20.24	34.65
				SG immature	79.76	34.65
				SG mature	0	0
	19	6	20	Mesh Like Structure	0	0
				SG immature	100	0
				SG mature	0	0
Sec6 RNAi	29	9	34	Mesh Like Structure	66.67	50
				SG immature	33.33	50
				SG mature	0	0
	25	4	7	Mesh Like Structure	75	50
				SG immature	25	50
				SG mature	0	0
Sec8 RNAi	29	8	37	Mesh Like Structure	41.16	35.88
				SG immature	58.84	35.88
				SG mature	0	0
	25	6	20	Mesh Like Structure	8.33	20.41
				SG immature	80.56	30.58
				SG mature	11.11	27.22
	21	7	26	Mesh Like Structure	3.57	9.45
				SG immature	96.43	9.45
				SG mature	0	0
	19	6	22	Mesh Like Structure	0	0
				SG immature	96.67	8.16
				SG mature	3.33	8.16
Exo84 RNAi V	29	8	33	Mesh Like Structure	2.08	5.89
				SG immature	60.42	32.49
				SG mature	37.5	33.46
	25	4	14	Mesh Like Structure	0	0
				SG immature	27.92	28
				SG mature	72.08	28
	21	5	15	Mesh Like Structure	0	0
				SG immature	0	0
				SG mature	100	0
	19	4	8	Mesh Like Structure	0	0
				SG immature	0	0
				SG mature	100	0
Sec15 RNAi V	29	4	17	Mesh Like Structure	100	0
				SG immature	0	0
				SG mature	0	0
	25	4	16	Mesh Like Structure	87.5	25
				SG immature	12.5	25
				SG mature	0	0
	21	6	25	Mesh Like Structure	43.33	46.33
				SG immature	56.67	46.33
				SG mature	0	0
	19	5	14	Mesh Like Structure	16.67	23.57
				SG immature	53.33	36.13
				SG mature	30	44.72

Data Supplementary Figure 1A						
Genotype	**Temperature**	**Number of Glands Analyzed**	**Number of Distal Cells Analyzed**	**Phenotype**	**% of Phenotype**	**Standard Deviation**
Control RNAi	29	4	12	Mesh Like Structure	0	0
				SG immature	0	0
				SG mature	100	0
	25	5	13	Mesh Like Structure	0	0
				SG immature	0	0
				SG mature	100	0
	21	5	17	Mesh Like Structure	0	0
				SG immature	0	0
				SG mature	100	0
	19	5	15	Mesh Like Structure	0	0
				SG immature	0	0
				SG mature	100	0
Exo70 RNAi V	29	5	17	Mesh Like Structure	0	0
				SG immature	39.43	42.11
				SG mature	60.57	42.11
	25	6	15	Mesh Like Structure	0	0
				SG immature	8.33	20.41
				SG mature	91.67	20.41
	21	6	17	Mesh Like Structure	0	0
				SG immature	0	0
				SG mature	100	0
	19	4	15	Mesh Like Structure	0	0
				SG immature	0	0
				SG mature	100	0
Sec5 RNAi V	29	5	25	Mesh Like Structure	53.33	50.55
				SG immature	46.67	50.55
				SG mature	0	0
	25	5	12	Mesh Like Structure	20	27.39
				SG immature	70	27.39
				SG mature	10	22.36
	21	6	21	Mesh Like Structure	8.33	20.41
				SG immature	87.5	20.92
				SG mature	4.17	10.21
	19	6	27	Mesh Like Structure	5.56	13.61
				SG immature	91.11	14.4
				SG mature	3.33	8.16
Exo84 RNAi BL	29	7	38	Mesh Like Structure	93.2	12.85
				SG immature	6.8	12.85
				SG mature	0	0
	25	5	22	Mesh Like Structure	90	22.36
				SG immature	10	22.36
				SG mature	0	0
	21	6	27	Mesh Like Structure	95.83	10.21
				SG immature	4.17	10.21
				SG mature	0	0
	19	5	21	Mesh Like Structure	66.43	41.31
				SG immature	33.57	41.31
				SG mature	0	0
Sec15 RNAi BL	29	5	25	Mesh Like Structure	100	0
				SG immature	0	0
				SG mature	0	0
	25	6	26	Mesh Like Structure	94.44	13.61
				SG immature	5.56	13.61
				SG mature	0	0
	21	5	14	Mesh Like Structure	100	0
				SG immature	0	0
				SG mature	0	0
	19	5	20	Mesh Like Structure	100	0
				SG immature	0	0
				SG mature	0	0

Supplementary Table 4. Salivary gland developmental staging. Salivary glands analyzed in experiments of the indicated figures. Columns display: Experimental temperature, larval hours of development after egg laying (AEL), equivalent hours of development at 25°C (based on SG phenotype and salivary gland general appearance), presence or absence of Sgs3 in salivary glands, at the developmental time studied, and expected stage of SGs (Mature or Immature).

	Experimental temperature (°C)	Hours of development at the experimental temperature (hours AEL)	Equivalent hours of development at 25°C (hours AEL)	Presence of Sgs3	Expected developmental stage of SGs in wild type
Figure 2	29	~96	116-120	Yes	Mature
Figure 3	19, 21, 25, 29	~216, ~144, ~120, ~96	116-120	Yes	Mature
Figure 4	29	~96	116-120	Yes	Mature
Figure 5	18	~120-168	72-96	No	-
Figure 6	29	~96	116-120	Yes	Mature
Figure 7 A, E-H	29	~96	116-120	Yes	Mature
Figure 8 A, D, G, J	21	~108	96-104	Yes	Immature
Figure 8 B, E, H, K	21	~144	116-120	Yes	Mature
Figure 9 A-D	29	~96	116-120	Yes	Mature
Figure 9 E-G	18	~240	116-120	Yes	Mature
Supplementary Figure 1	29	~96	116-120	Yes	Mature
Supplementary Figure 2	19,25 or 29	~216, ~120, ~96	112-120	Yes	Mature
Supplementary Figure 3 A, D, G	29	~96	116-120	Yes	Mature
Supplementary Figure 3 B, E, H	120 hs at 18 °C and 36 hs at 29 °C	~156	116-120	Yes	Mature
Supplementary Figure 4	18	~240	116-120	Yes	Mature
Supplementary Figure 5 A-F	25	~72	~72	No	-
Supplementary Figure 6 A, E	25 or 29	~72 or ~50	~72	No	-
Supplementary Figure 6 B-D	25	~72	~72	No	-
Supplementary Figure 7	29	~96	116-120	Yes	Mature
Supplementary Figure 8	29	~96	116-120	Yes	Mature
Supplementary Figure 9	29	~96	116-120	Yes	Mature

Supplementary Figure 10 A, E	25	72-96	72-96	No	-
Supplementary Figure 10 B, F	25	100-104	100-104	Yes	Immature
Supplementary Figure 10 C, G	25	108-112	108-112	Yes	Mature
Supplementary Figure 10 D, H	25	116-120	116-120	Yes	Mature
Supplementary Figure 11 A, G, M	25 or 21	96-104 or ~108	96-104	Yes	Immature
Supplementary Figure 11 B, H, N	25 or 21	116-120 or ~144	116-120	Yes	Mature
Supplementary Figure 11 D, E, J, K, P, Q	25 or 21	116-120 or ~144	116-120	Yes	Mature
Supplementary Figure 12 A, B, E	29	~96	116-120	Yes	Mature
Supplementary Figure 12 D	29	~72	96-104	Yes	Immature

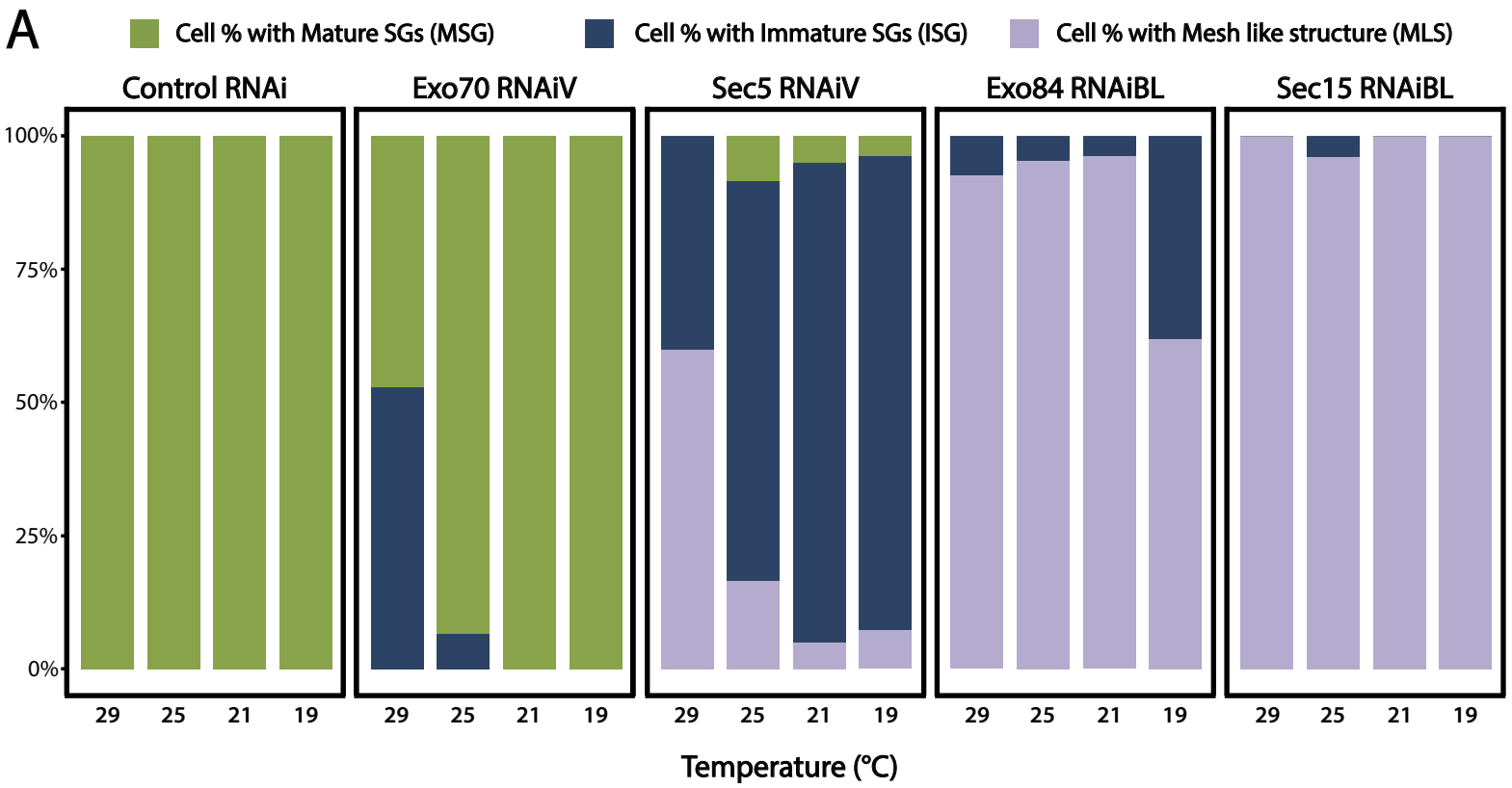
A
Cell % with Mature SGs (MSG)
Cell % with Immature SGs (ISG)
Cell % with Mesh like structure (MLS)
Control RNAi
Exo70 RNAiV
Sec5 RNAiV
Exo84 RNAiBL
Sec15 RNAiBL
100%
75%
50%
25%
0%
29
25
21
19
Temperature (°C)

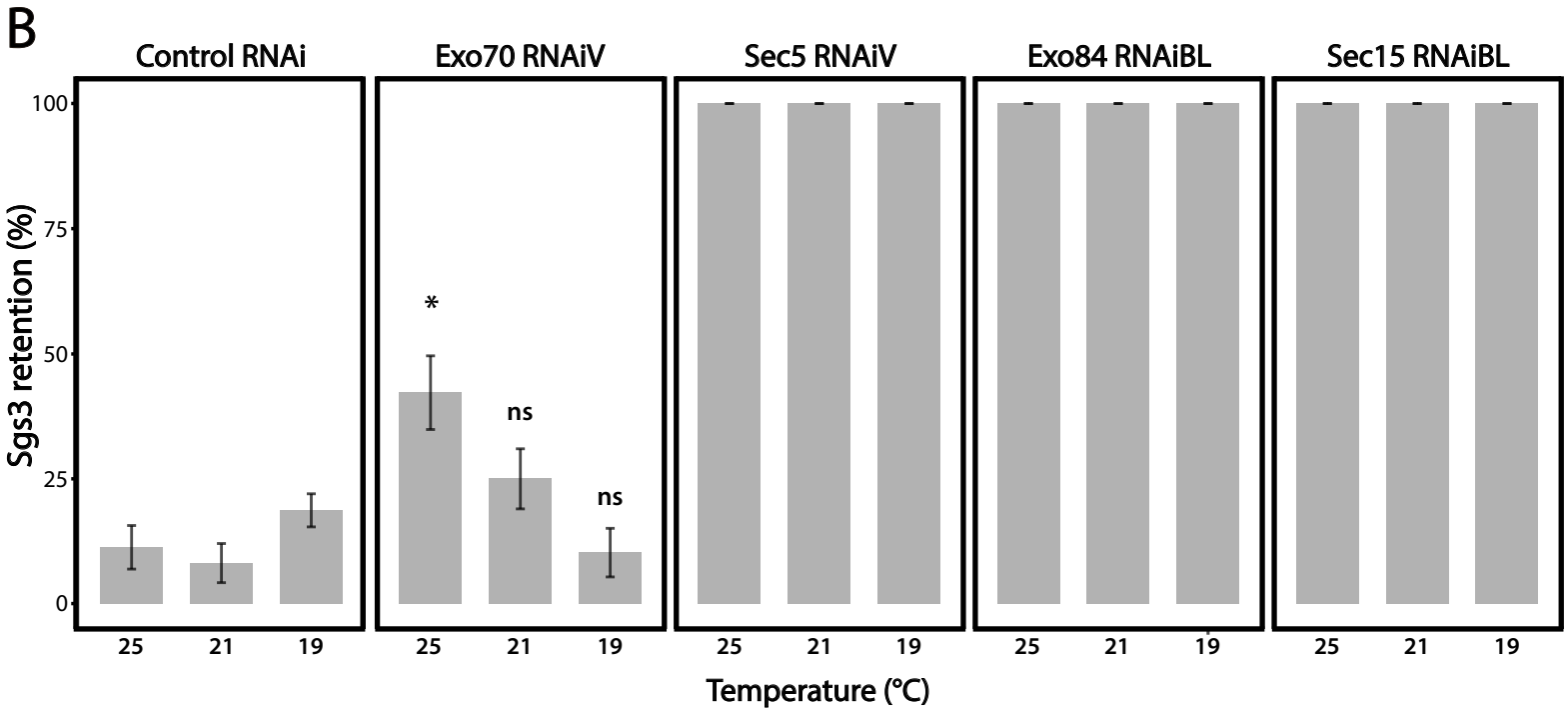
B
Control RNAi
Exo70 RNAiV
Sec5 RNAiV
Exo84 RNAiBL
Sec15 RNAiBL
Sgs3 retention (%)
100
75
50
25
0
*
ns
ns
25
21
19
Temperature (°C)

Supplementary Figure 1. Penetrance of phenotypes observed after silencing subunits of the exocyst. Additional RNA lines targeting exocyst subunits utilized to assess reduction-of-function phenotypes in the pathway of regulated exocytosis. (A) Quantification of the penetrance of each of the three phenotypes observed upon downregulation of each of the exocyst subunits. Larvae were grown at four different temperatures to achieve different levels of RNAi expression of exocyst subunits. "n" = Number of salivary glands analyzed. *control*^{RNAi} (*cherry*^{RNAi}) n = 4 (29 °C), n = 5 (25, 21 and 19 °C); *exo70*^{RNAiV} n = 5 (29 °C), n = 6 (25 °C), n = 6 (21 °C), n = 4 (19 °C); *sec15*^{RNAiBL} n = 5 (29 °C), n = 6 (25 °C), n = 5 (21 °C), n = 5 (19 °C); *exo84*^{RNAiBL} n = 7 (29 °C), n = 5 (25 °C), n = 6 (21 °C), n = 5 (19 °C); *sec5*^{RNAiV} n = 5 (29 °C), n = 5 (25 °C), n = 6 (21 °C), n = 6 (19 °C); (B) Quantification of the penetrance of the Sgs3-GFP retention phenotype in salivary glands of prepupae with the indicated RNAis at different temperatures. "n" = Number of vials containing 20-30 larvae each. *control*^{RNAi} (*cherry*^{RNAi}) n = 7 (25 °C), n = 9 (21 °C), n = 19 (19 °C); *exo70*^{RNAiV} n = 6 (25 °C), n = 8 (21 °C), n = 6 (19 °C); *sec5*^{RNAiV}, n = 4 (25 °C), n = 6 (21 °C), n = 5 (19 °C); *sec15*^{RNAiBL} n = 7 (25 °C), n = 8 (21 °C), n = 7 (19 °C); *exo84*^{RNAiBL} n = 5 (25 °C), n = 4 (21 °C), n = 8 (19 °C). RNAis were expressed using *fkh*-Gal4. Comparisons of the retention phenotype were carried out between genotypes at each different temperature, and statistical analysis was performed using a Likelihood ratio test followed by Tuckey´s test ("*" = p value < 0.05). For those RNAis with 100% penetrance no statistical analysis was performed. "ns" = not significant. This figure represents an extension of the experiments of Figure 3C-D; all RNAis were expressed with controls at the same time, and therefore the controls are identical to those of Figure 3.

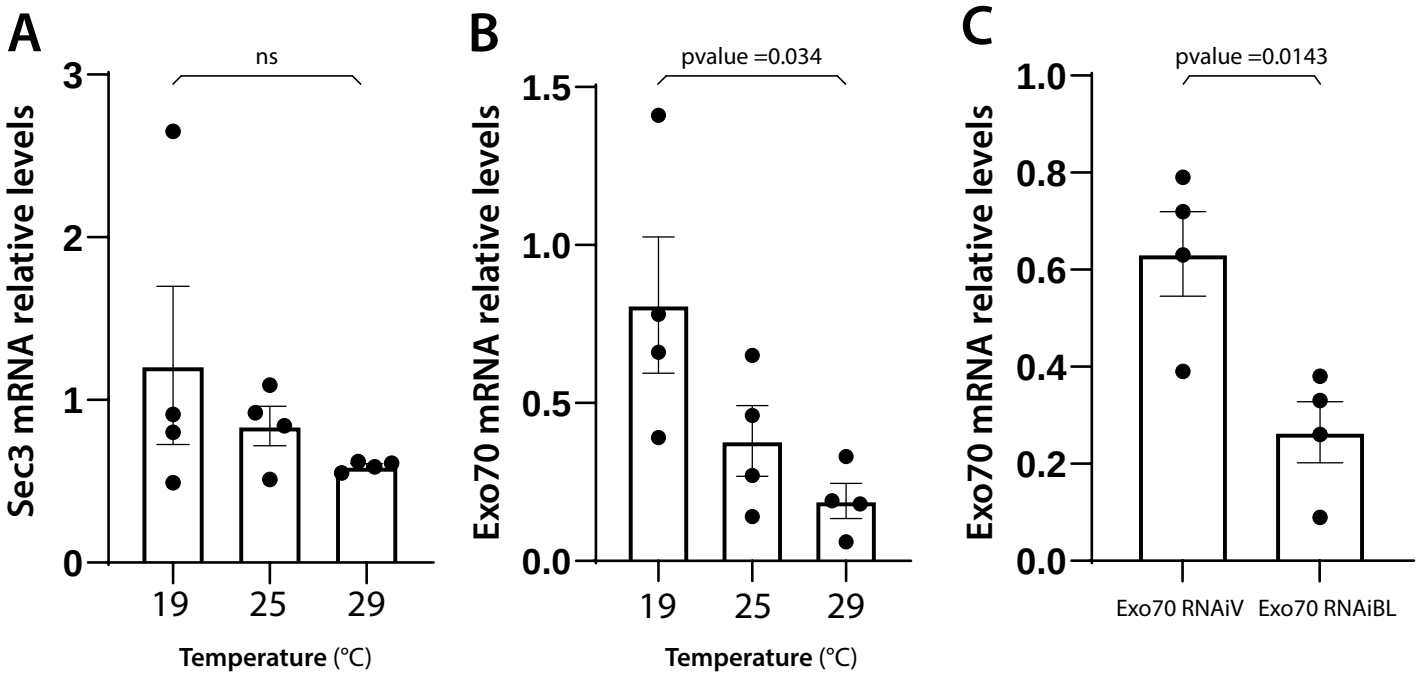
A
ns
Sec3 mRNA relative levels
3
2
1
0
19
25
29
Temperature (°C)
B
pvalue =0.034
Exo70 mRNA relative levels
1.5
1.0
0.5
0.0
19
25
29
Temperature (°C)
C
pvalue =0.0143
Exo70 mRNA relative levels
1.0
0.8
0.6
0.4
0.2
0.0
Exo70 RNAiV
Exo70 RNAiBL

Supplementary Figure 2. Remaining mRNA levels after RNAi-mediated knock-down of exocyst subunits correlate with the observed phenotypes. mRNA levels of the indicated genes were measured by qRT-PCR in homogenates from salivary glands. *sec3* (A) or *exo70* (B) mRNA levels from larva grown at the indicated temperatures were determined in salivary glands expressing *sec3*^{RNAi} (*sgs3-GFP*, *fkh-Gal4/ UAS-sec3*^{RNAi} (A) or *exo70*^{RNAiBL} (*sgs3-GFP*, *fkh-Gal4/ UAS-exo70*^{RNAiBL}) (B) relative to salivary glands expressing *cherry*^{RNAi} (*sgs3-GFP*, *fkh-Gal4/ UAS-cherry*^{RNAi}) from larvae grown at the same temperatures. (C) *exo70* mRNA levels from larva grown at 29 °C were determined in salivary glands expressing *exo70*^{RNAiV} (*sgs3-GFP*, *fkh-Gal4/ UAS-exo70*^{RNAiV}) or *exo70*^{RNAiBL} (*sgs3-GFP*, *fkh-Gal4/ UAS-exo70*^{RNAiBL}) relative to salivary glands expressing *cherry*^{RNAi} (*sgs3-GFP*, *fkh-Gal4/ UAS-cherry*^{RNAi}). n = 4 for all genotypes and conditions. Statistical analysis was performed by one-way ANOVA followed by Tukey's test with a confidence interval higher than 95% ($p < 0.05$). "ns"= not significant.

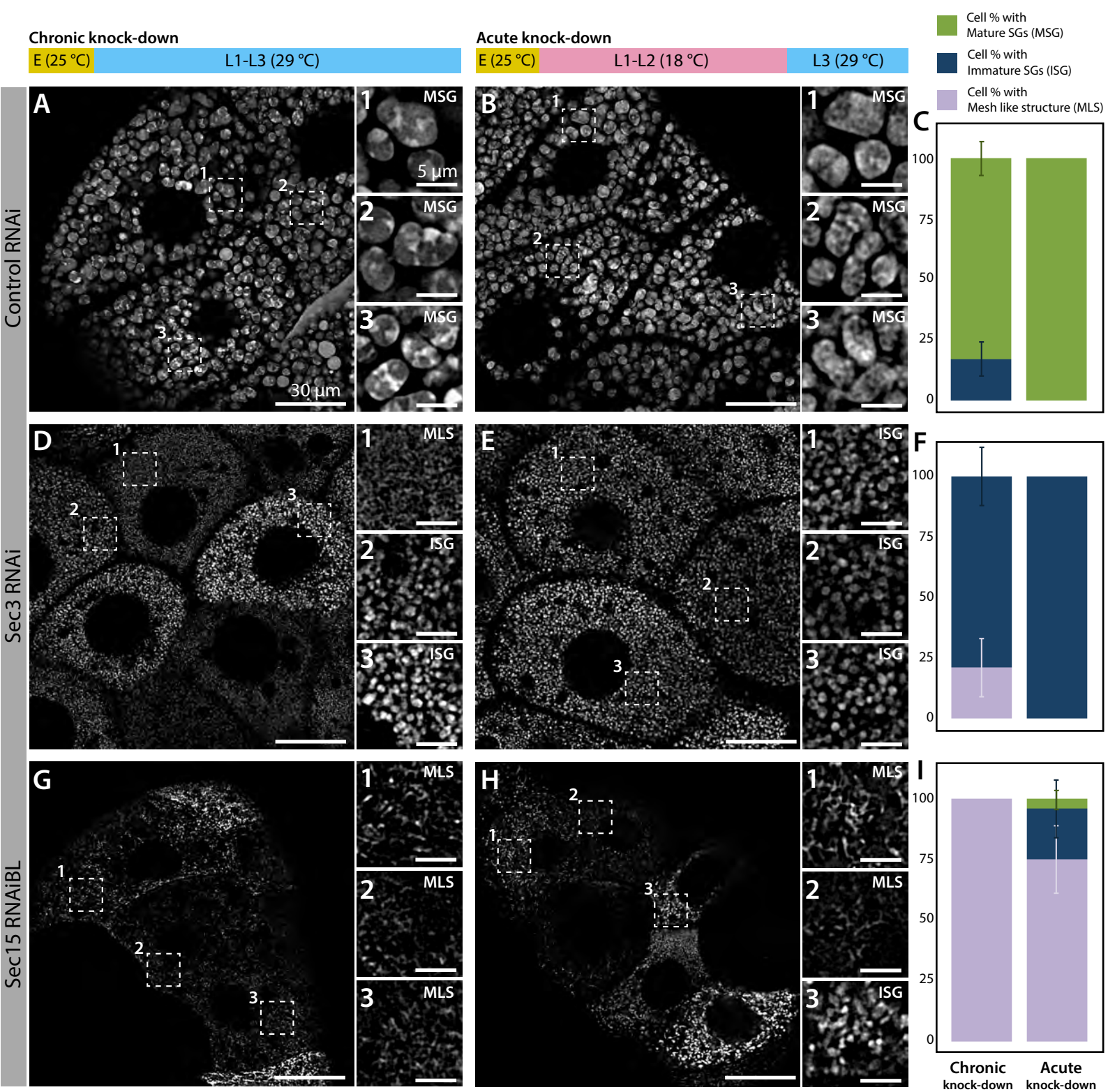
Chronic knock-down
E (25 °C)
L1-L3 (29 °C)
Acute knock-down
E (25 °C)
L1-L2 (18 °C)
L3 (29 °C)
Cell % with Mature SGs (MSG)
Cell % with Immature SGs (ISG)
Cell % with Mesh like structure (MLS)
Control RNAi
Sec3 RNAi
Sec15 RNAiBL
A
B
C
D
E
F
G
H
I
MSG
ISG
MLS
5 µm
30 µm
100
75
50
25
0
Chronic knock-down
Acute knock-down

Supplementary Figure 3. Chronic or Acute knock-down of exocyst subunits generate comparable phenotypes. *Phenotypes of control* (*white*^{RNAi}) (A-C), *sec3*^{RNAi} (D-F) or *sec15*^{RNAiBL} (G-I) salivary glands. The thermo-sensitive Gal80 system (*Gal80*^{ts}) was utilized to compare salivary glands after silencing the indicated genes throughout larval development (chronic silencing: A, D, G) or at the 3rd larval instar only (acute silencing: B, E, H). Chronic RNAi expression was achieved by growing larvae at the restrictive temperature (29 °C) from larval eclosion onwards (A, D and G). Acute RNAi expression was achieved by growing larvae at the permissive temperature (18 °C) from larval eclosion until early L3 (larval 3rd instar), (B, E and H) and then shifting larvae to the restrictive temperature (29 °C) until analyzed. E: embryogenesis; L1: larval 1st instar; L2: 2nd instar; and L3: 3rd instar. The penetrance of each phenotype observed (Mature Secretory Granules, Immature Secretory Granules or Mesh-Like Structure) was quantified for each genotype and experimental condition (C, F and I). No substantial differences were detected between chronic and acute silencing of exocyst subunits. "n" represents the total number of salivary glands analyzed. *control*^{RNAi} (*white*^{RNAi}) (A) n=5, (B) n= 3; *sec3*^{RNAi} (D) n=6, (E)n=7; *sec15*^{RNAiBL} (G, H) n= 4.

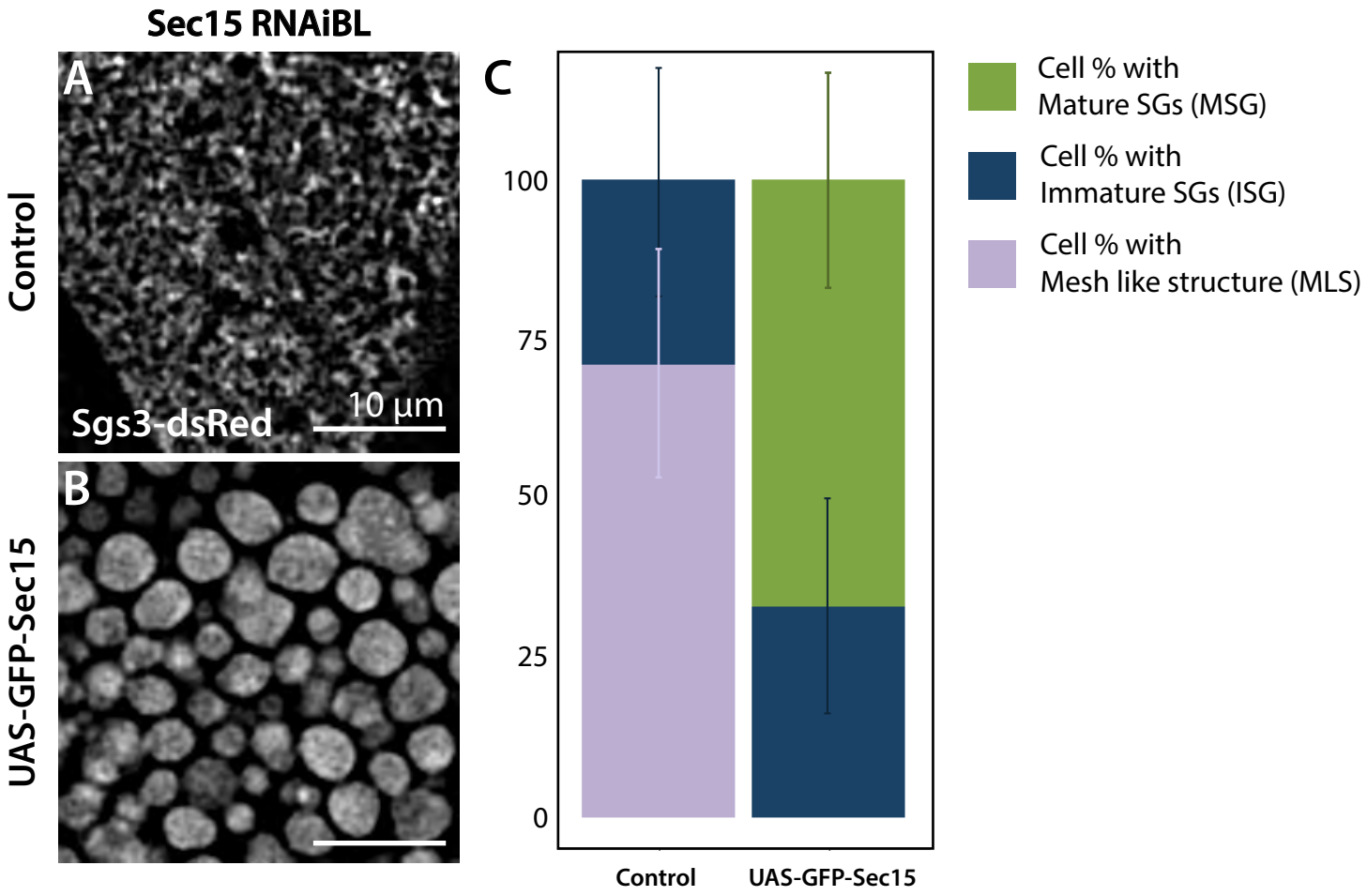
Sec15 RNAiBL
A
Control
Sgs3-dsRed
10 µm
B
UAS-GFP-Sec15
C
100
75
50
25
0
Control
UAS-GFP-Sec15
Cell % with
Mature SGs (MSG)
Cell % with
Immature SGs (ISG)
Cell % with
Mesh like structure (MLS)

Supplementary Figure 4. Expression of GFP-Sec15 can rescue SG maturation after sec15 knock-down. Expression of *sec15*^{RNAiBL} at 18 °C (*sgs3-dsRed; UAS-PLCγPH-GFP, fkh-Gal4/UAS-sec15*^{RNAiBL}*)* (A) generates salivary glands that do not form mature SGs (MSG) in any of the cells analyzed. Simultaneous expression of GFP-Sec15 (*UAS-GFP-sec15/ Sgs3-dsRed*; *UAS-sec15*^{RNAiBL}*/ fkh-Gal4)* (B) generates salivary glands with MSGs in 67% of the cells. (C) Quantification of each of the three possible phenotypes Mature SGs (MSG), Immature SGs (ISG) or Mesh-like structure (MLS) in control larvae (*sgs3-dsRed; UAS-PLCγPH-GFP, fkh-Gal4/UAS-sec15*^{RNAiBL}*)* or after expression of the rescue construct (*UAS-GFP-sec15/ sgs3-dsRed*; *UAS-sec15*^{RNAiBL}*/ fkh-Gal4).* "n" represents the total number of salivary glands analyzed. Control genotype (*UAS-PLCγPH-GFP*) n=7; Rescue genotype (*UAS-GFP-sec15*) n=5.

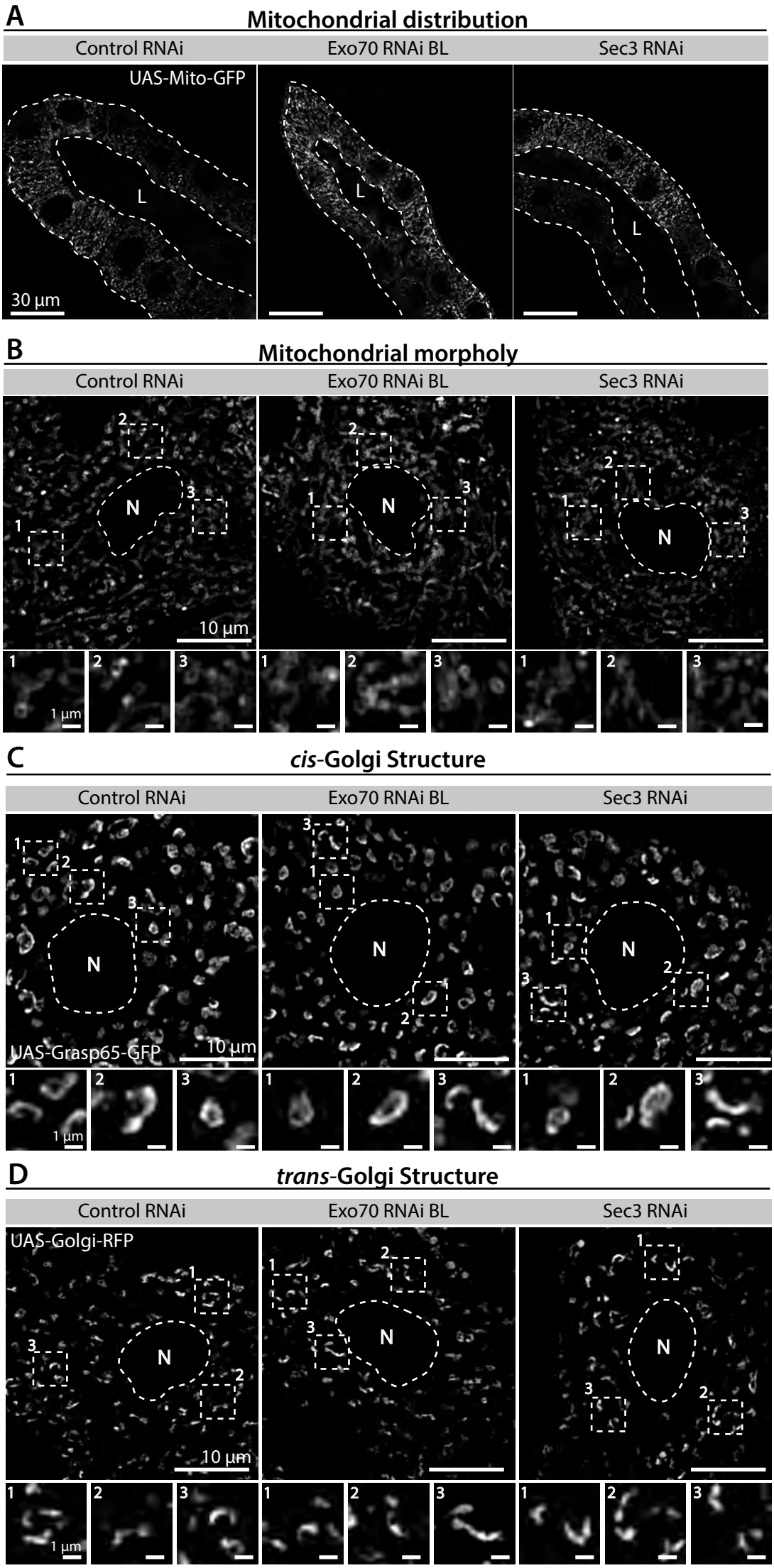
A
Mitochondrial distribution
Control RNAi
Exo70 RNAi BL
Sec3 RNAi
UAS-Mito-GFP
L
30 µm
B
Mitochondrial morpholy
Control RNAi
Exo70 RNAi BL
Sec3 RNAi
N
1
2
3
10 µm
1 µm
C
cis-Golgi Structure
Control RNAi
Exo70 RNAi BL
Sec3 RNAi
N
UAS-Grasp65-GFP
10 µm
1 µm
D
trans-Golgi Structure
Control RNAi
Exo70 RNAi BL
Sec3 RNAi
UAS-Golgi-RFP
N
10 µm
1 µm

E Nucleus

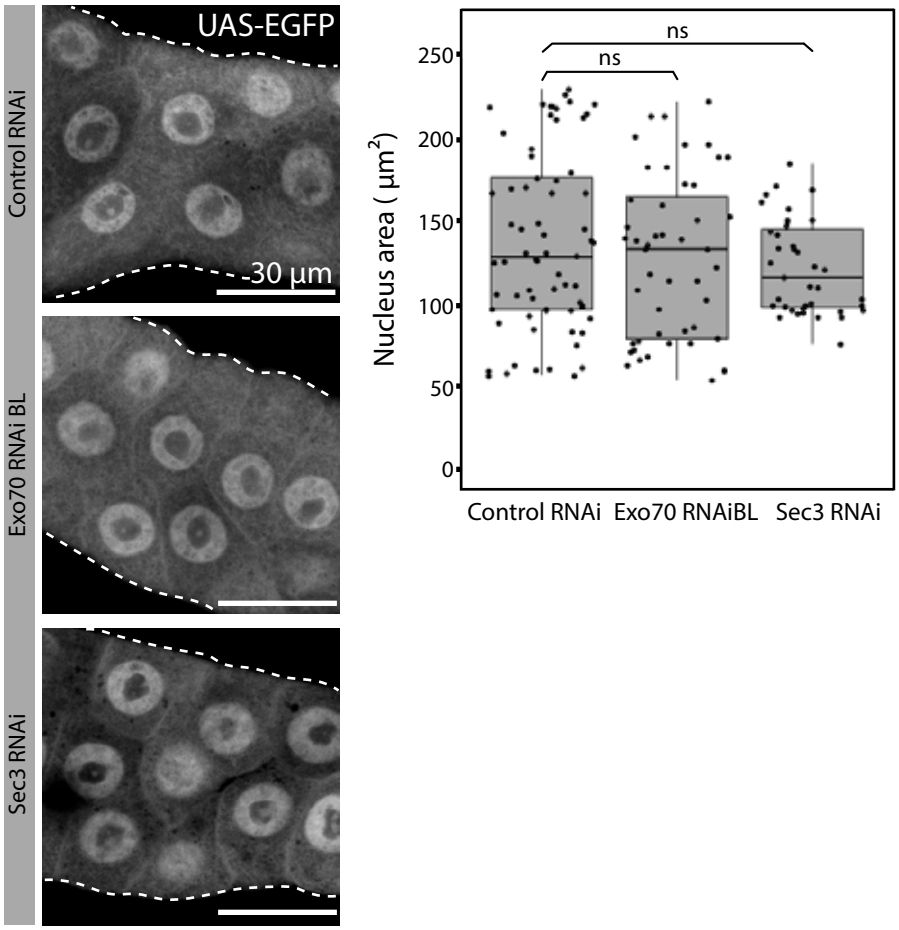

F Autophagy (UAS-GFP-mCherry-ATG8)

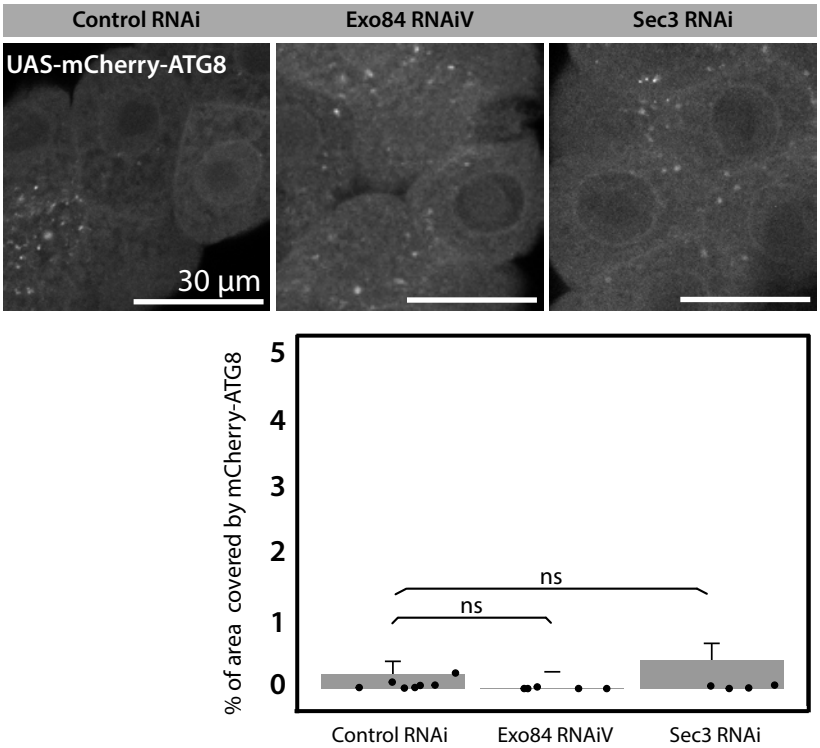

Supplementary Figure 5. Exocyst down-regulation does not affect general cellular health or homeostasis. Mitochondrial distribution and morphology (A-B), *cis*- and *trans*-Golgi complex distribution and morphology (C-D), nuclear size (E), and autophagy (F) were analyzed in salivary glands of control (*UAS-white*^{RNAi}) and exocyst knock-down salivary glands. Mitochondria were labelled with mito-GFP (*UAS-mito-GFP*), *cis*-Golgi with GRASP65 (*UAS-GRASP65-GFP), trans*-Golgi with RFP-Golgi (*UAS-RFP-Golgi*), nuclei with EGFP (*UAS-EGFP*), and autophagy with mChAtg8 (*UAS-GFP-mCh-atg8*). Larvae were grown at 25 °C to achieve a condition at which knock-down of the exocyst subunits mostly generate cells with immature SGs. RNAis were expressed using *fkh-Gal4*. (E) Quantification of nuclear area in the indicated genotypes was performed using image J. (F) Quantification of the area coved by mCh-Atg8 *foci* over the total area of salivary gland analyzed (%) was performed using image J. Statistical analysis was carried-out using one-way analysis of variance (ANOVA) "n" represents the total number of salivary glands analyzed. (E) *control*^{RNAi} (*white*^{RNAi}) n= 8; *exo70*^{RNAiBL} n=5; *sec3*^{RNAi} n=4. (F) starved *control*^{RNAi} (*white*^{RNAi}) n= 5; fed *control*^{RNAi} (*white*^{RNAi}) n= 8; fed *exo84*^{RNAiV} n=5; fed *sec3*^{RNAi} n=5.

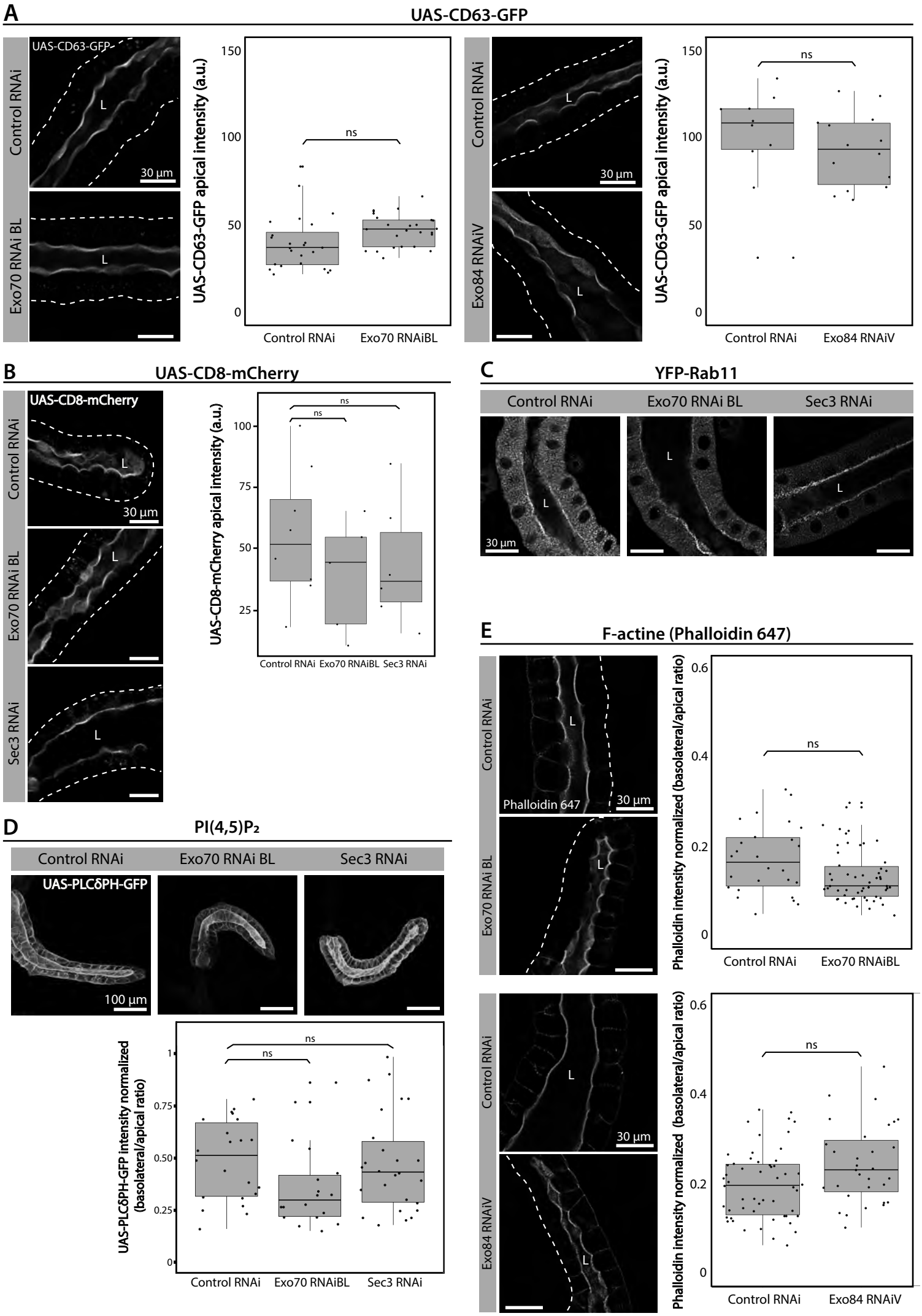
A
UAS-CD63-GFP
Control RNAi
Exo70 RNAi BL
UAS-CD63-GFP
L
30 µm
UAS-CD63-GFP apical intensity (a.u.)
150
100
50
0
ns
Control RNAi
Exo70 RNAiBL
Control RNAi
Exo84 RNAiV
ns
Exo84 RNAiV
B
UAS-CD8-mCherry
Sec3 RNAi
UAS-CD8-mCherry apical intensity (a.u.)
100
75
50
25
Control RNAi Exo70 RNAiBL Sec3 RNAi
C
YFP-Rab11
Control RNAi
Exo70 RNAi BL
Sec3 RNAi
D
PI(4,5)P2
UAS-PLCδPH-GFP
100 µm
UAS-PLCδPH-GFP intensity normalized (basolateral/apical ratio)
1
0.75
0.50
0.25
0
E
F-actine (Phalloidin 647)
Phalloidin 647
Phalloidin intensity normalized (basolateral/apical ratio)
0.6
0.4
0.2

Supplementary Figure 6. Exocyst down-regulation does not affect apical polarity markers. (A) CD63 (*UAS-CD63-GFP*), (B) CD8 (*UAS-CD8-mCherry*), (C) Rab11 (*YFP-Rab11*), (D) PI(4,5)P_2 (*UAS-PLCγ-PH-GFP)* and (E) filamentous actin (phalloidine-647) distribution were analyzed in salivary glands of control (*UAS-white*^{RNAi}) or exocyst knock-down salivary glands (*UAS-exo70*^{RNAiBL}*, UAS-sec3*^{RNAi} or *UAS-exo84*^{RNAiV}). Larvae were grown at 25 °C (*UAS-exo70*^{RNAiBL} *or UAS-sec3*^{RNAi}) or at 29°C (*UAS-exo84*^{RNAiV}) to achieve a condition at which exocyst downregulation generate mostly cells with immature SGs. Note that in (A) and (E), for accurate comparisons, the control genotype (*UAS-white*^{RNAi}) was also assayed at different temperatures. Transgenes were expressed with *fkh-Gal4*. Statistical analysis was performed using (A-B) one-way analysis of variance (ANOVA), (D) Likelihood ratio test followed by Tuckey´s test or (E) Wald Test (p value < 0.05, "ns"=not significant). "n" represents the total number of salivary glands analyzed. (A) *control*^{RNAi} (*white*^{RNAi}) n= 6; *exo70*^{RNAiBL} n=5; *control*^{RNAi} (*white*^{RNAi}) n=3; *exo84*^{RNAiV} n=3. (B) *control*^{RNAi} (*white*^{RNAi}) n= 8; *exo70*^{RNAiBL} n=5; *sec3*^{RNAi} n=6. (D) n=4. (E) *control*^{RNAi} (*white*^{RNAi}) n= 4; *exo70*^{RNAiBL} n=10; *control*^{RNAi} (*white*^{RNAi}) n=6; *exo84*^{RNAiV} n=4.

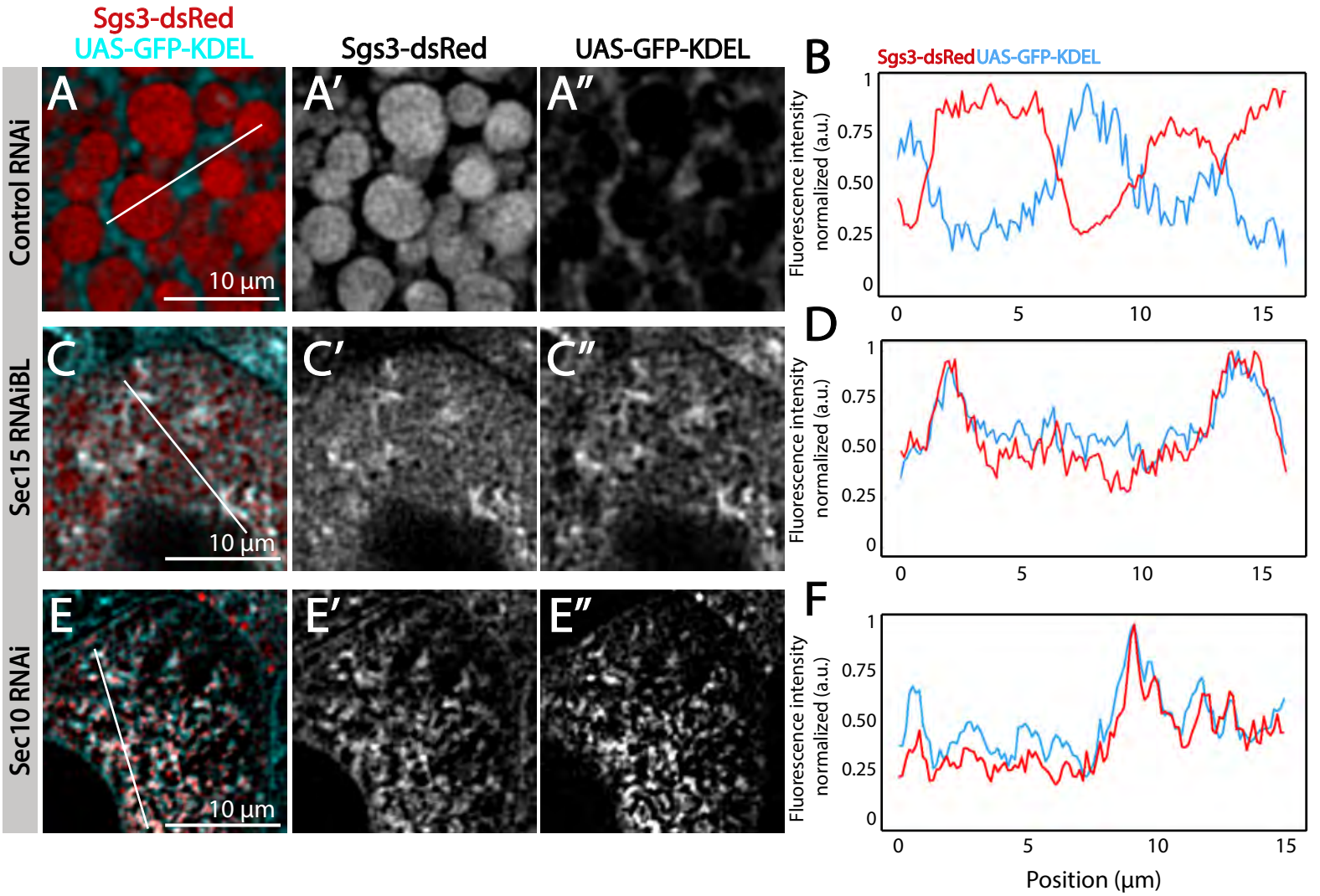
Sgs3-dsRed
UAS-GFP-KDEL
Sgs3-dsRed
UAS-GFP-KDEL
Control RNAi
Sec15 RNAiBL
Sec10 RNAi
A
A′
A″
B
C
C′
C″
D
E
E′
E″
F
10 µm
Fluorescence intensity normalized (a.u.)
Position (µm)

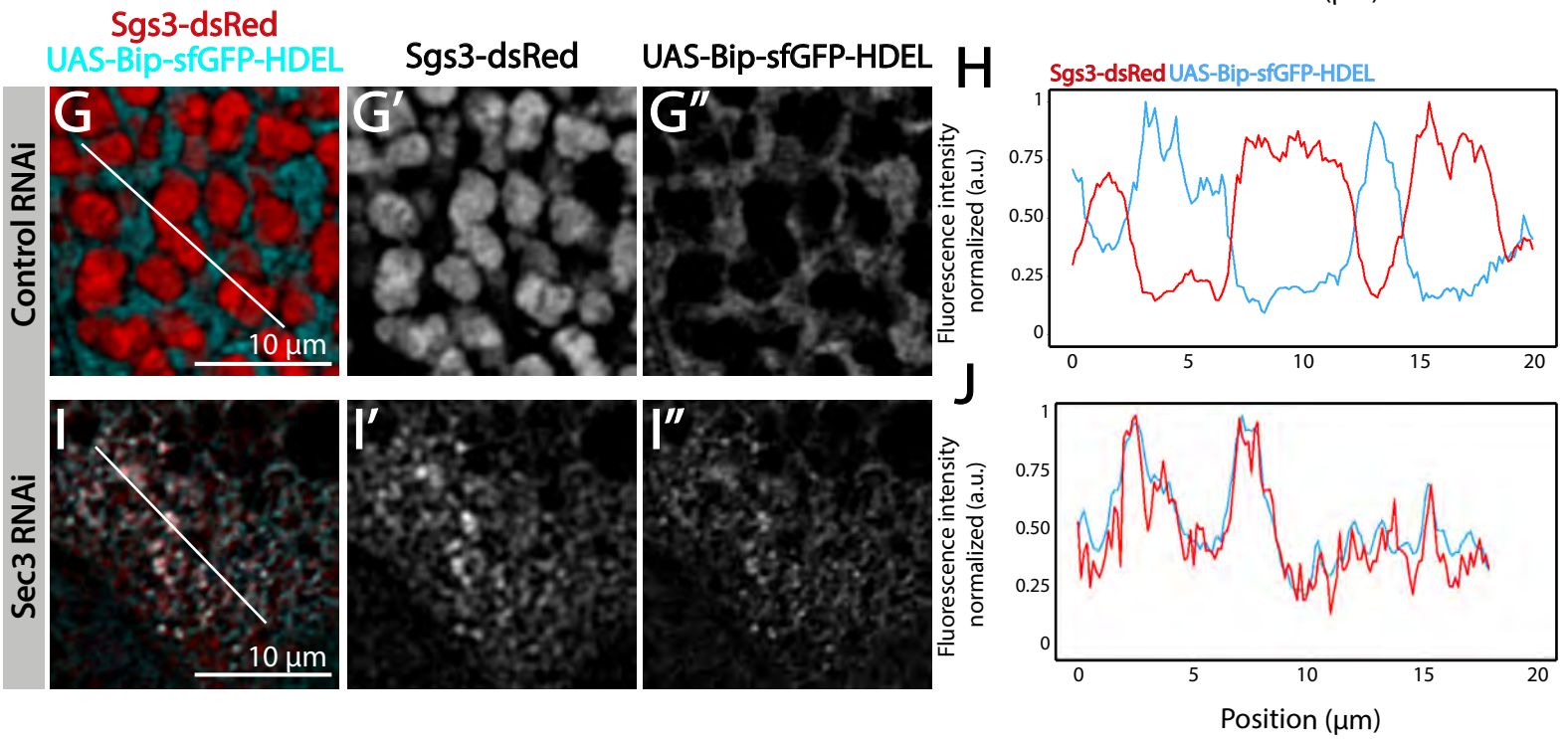
Sgs3-dsRed
UAS-Bip-sfGFP-HDEL
Sgs3-dsRed
UAS-Bip-sfGFP-HDEL
Control RNAi
Sec3 RNAi
G
G′
G″
H
I
I′
I″
J
10 µm
Fluorescence intensity normalized (a.u.)
Position (µm)

Supplementary Figure 7. The exocyst is required for Sgs3-GFP exit from ER and SG biogenesis. Confocal images of unfixed salivary glands of the indicated genotypes. Larvae were grown at 29 °C to achieve maximal activation of the Gal4-UAS system, and maximal downregulation of exocyst complex subunits. The ER was labeled with GFP-KDEL (*UAS-GFP-KDEL*), (A, C and E) or with Bip-sfGFP-HDEL (*UAS-Bip-sfGFP-HDEL*) (G and I). In control salivary glands (*fkh-Gal4/UAS-white*^{RNAi}) (A and G), the ER displayed a network-like appearance localized in between mature SGs that contain Sgs3-dsRed, and thus no colocalization between the ER marker and Sgs3-dsRed was detected (B and H). Upon expression of *sec15*^{RNAi} (*fkh-Gal4/UAS-sec15*^{RNAiBL}) (C), sec10^{RNAi} (*UAS-sec10*^{RNAi}*/ fkh-Gal4*) (E) or *sec3*^{RNAi} (*UAS-sec3*^{RNAi}*; fkh-Gal4*) SGs did not form, and Sgs3-dsRed was retained in the ER, as demonstrated by colocalization of both markers in the two-dimensional line scan analysis (D, F and J). RNAis were expressed using *fkh*-Gal4. Scale bar 10 μm.

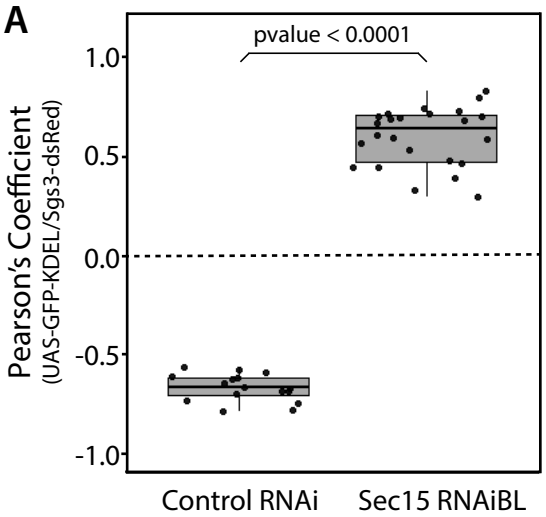
A
pvalue < 0.0001
1.0
0.5
0.0
-0.5
-1.0
Pearson's Coefficient
(UAS-GFP-KDEL/Sgs3-dsRed)
Control RNAi
Sec15 RNAiBL

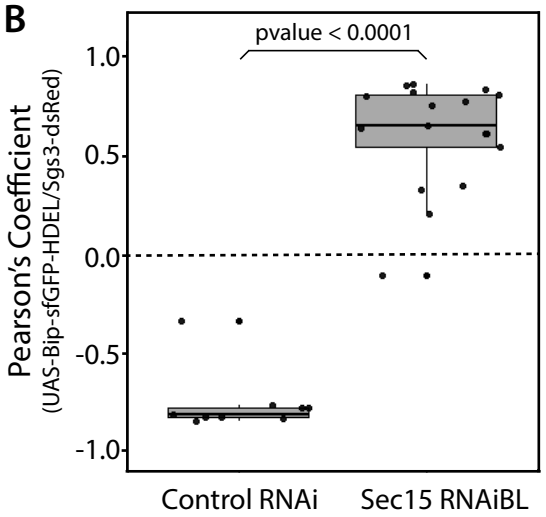
B
pvalue < 0.0001
1.0
0.5
0.0
-0.5
-1.0
Pearson's Coefficient
(UAS-Bip-sfGFP-HDEL/Sgs3-dsRed)
Control RNAi
Sec15 RNAiBL

Supplementary Figure 8. Quantification of colocalization between ER markers and Sgs3. Pearson´s coefficient to evaluate colocalization between the ER markers *UAS-GFP-KDEL* (A) or *UAS-Bip-sfGFP-HDEL* (B) and Sgs3-dsRed in control salivary glands (*UAS-white*^{RNAi}) or after exocyst knock-down (*UAS-sec15*^{RNAiBL}). Larvae were grown at 29 °C. Statistical analysis was performed using one-way analysis of variance (ANOVA). Analysis corresponds to data shown in Figure 4. "n" represents the total number of salivary glands analyzed**.** (A) n=3, (B) n=2.

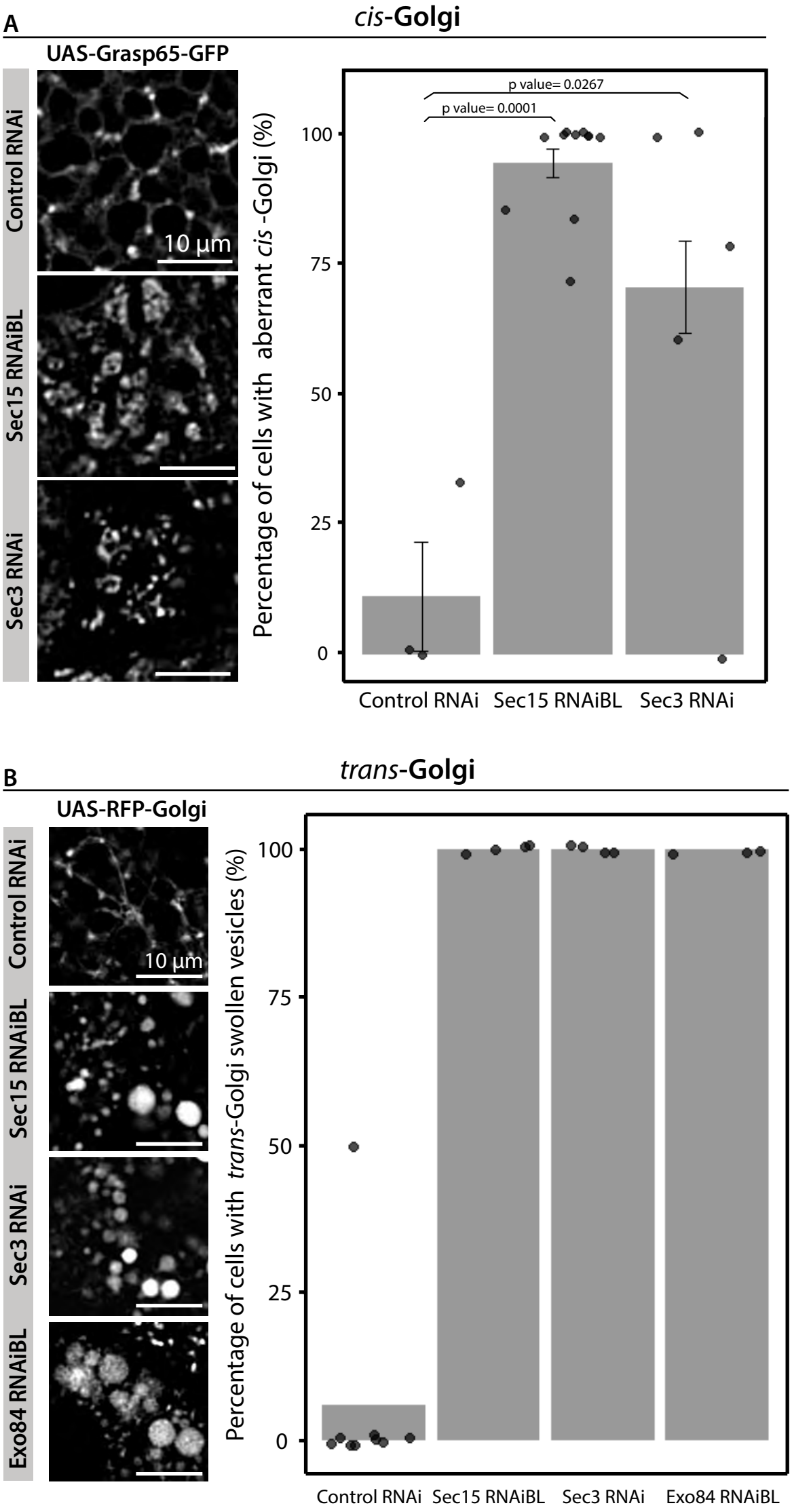
A
cis-Golgi
UAS-Grasp65-GFP
Control RNAi
Sec15 RNAiBL
Sec3 RNAi
10 µm
p value= 0.0267
p value= 0.0001
Percentage of cells with aberrant cis -Golgi (%)
100
75
50
25
0
Control RNAi
Sec15 RNAiBL
Sec3 RNAi
B
trans-Golgi
UAS-RFP-Golgi
Control RNAi
Sec15 RNAiBL
Sec3 RNAi
Exo84 RNAiBL
10 µm
Percentage of cells with trans-Golgi swollen vesicles (%)
100
75
50
25
0
Control RNAi
Sec15 RNAiBL
Sec3 RNAi
Exo84 RNAiBL

Supplementary Figure 9. The exocyst is required to maintain the typical morphology of the Golgi complex. Confocal images of unfixed salivary glands of the indicated genotypes. Larvae were grown at 29 °C to achieve maximal activation of the Gal4-UAS system, and maximal downregulation of exocyst subunits. *cis*-Golgi (*UAS-Grasp65-GFP*) (A) and trans-Golgi (*UAS-RFP-Golgi*) (B) markers were analyzed In control salivary glands (*fkh-Gal4/ UAS-white*^{RNAi}) or in exocyst-down-regulated salivary glands (UAS-sec15^{RNAiBL}, UAS-sec3^{RNAi} or UAS-exo84^{RNAiV}). RNAis were expressed using *fkh*-Gal4. Scale bar 10 μm. Bar graphs show the quantification of the penetrance of the Golgi complex phenotype. Statistical analysis was performed using a Likelihood ratio test followed by Tuckey´s test (p value < 0.05, "ns"=not significant). "n" represents the total number of salivary glands analyzed**.** (A) *control*^{RNAi} (*white*^{RNAi}) n= 3; *sec15*^{RNAiBL} n=11; *sec3*^{RNAi} n=3**.** (B) *control*^{RNAi} (*white*^{RNAi}) n= 9; *sec15*^{RNAiBL} n=4; *sec3*^{RNAi} n=4; *exo84*^{RNAiV} n=3.

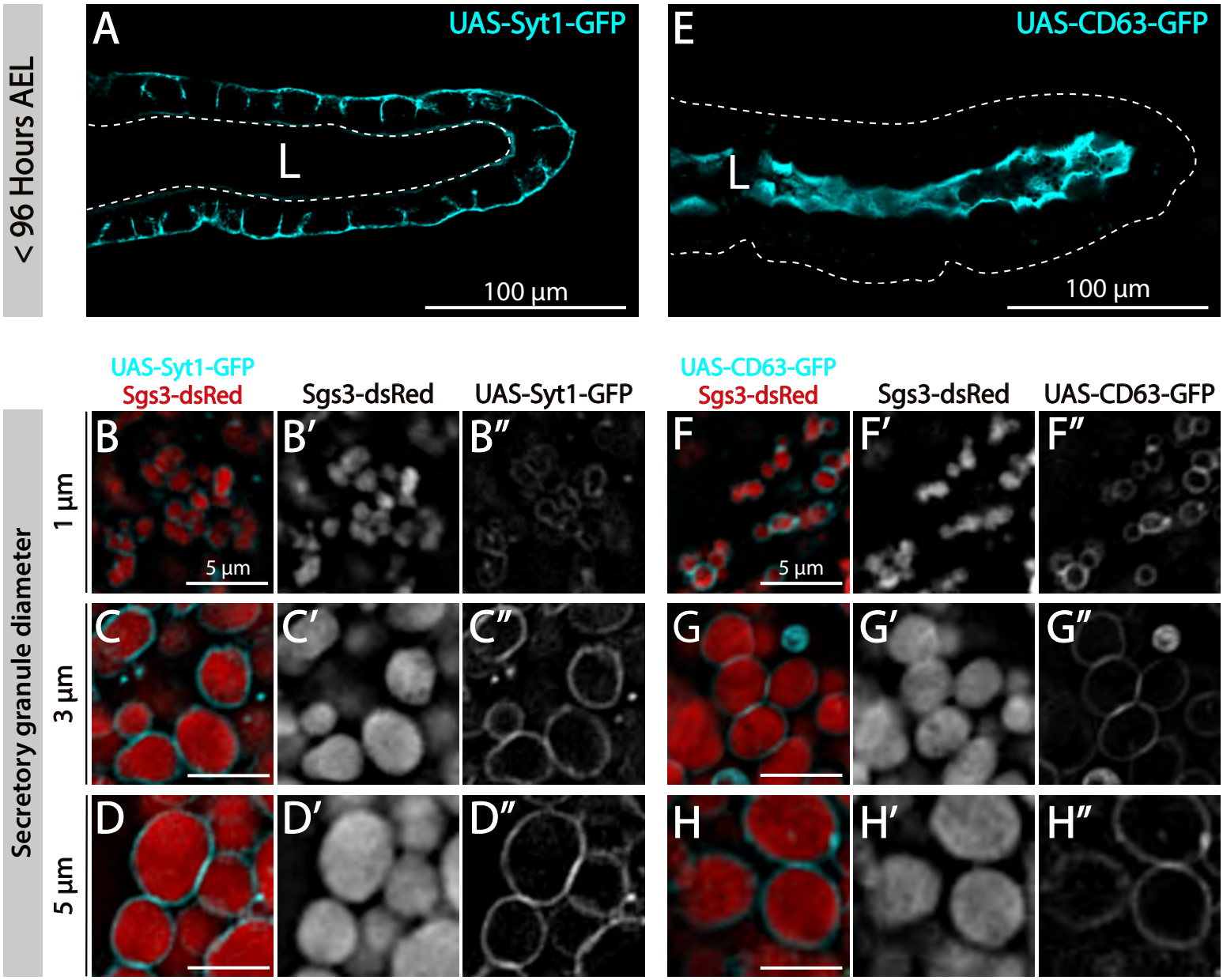
< 96 Hours AEL
A
UAS-Syt1-GFP
L
100 µm
E
UAS-CD63-GFP
L
100 µm
Secretory granule diameter
1 µm
3 µm
5 µm
UAS-Syt1-GFP
Sgs3-dsRed
Sgs3-dsRed
UAS-Syt1-GFP
UAS-CD63-GFP
Sgs3-dsRed
Sgs3-dsRed
UAS-CD63-GFP
B
B′
B″
C
C′
C″
D
D′
D″
F
F′
F″
G
G′
G″
H
H′
H″
5 µm
5 µm

Supplementary Figure 10. Incorporation of maturation markers to SGs in wild type salivary glands. Incorporation of the SG maturation markers Syt1 (*sgs3-dsRed/ UAS-syt1-GFP; fkh-Gal4*), (A-D) and CD63 (*sgs3-dsRed/ UAS-CD63-GFP; fkh-Gal4*), (E-H) to developing granules. Prior to SG biogenesis (<96 hours AEL) Syt1 localized at the basolateral plasma membrane of salivary cells (A), while CD63 localized at the apical plasma membrane (E). Scale bar 100 μm. Both markers localized at the membrane of immature SGs and mature SGs (B-D and F-H). Scale bar 5 μm. Note that Syt1 signal intensity increases around SGs as they mature (compare B", C" and D"), whereas CD63 signal remains fairly stable during SG maturation (compare F", G" and H").

Sgs3-dsRedUAS-Syt1-GFP

Immature SGs (25 °C)

Mature SGs (21 °C)

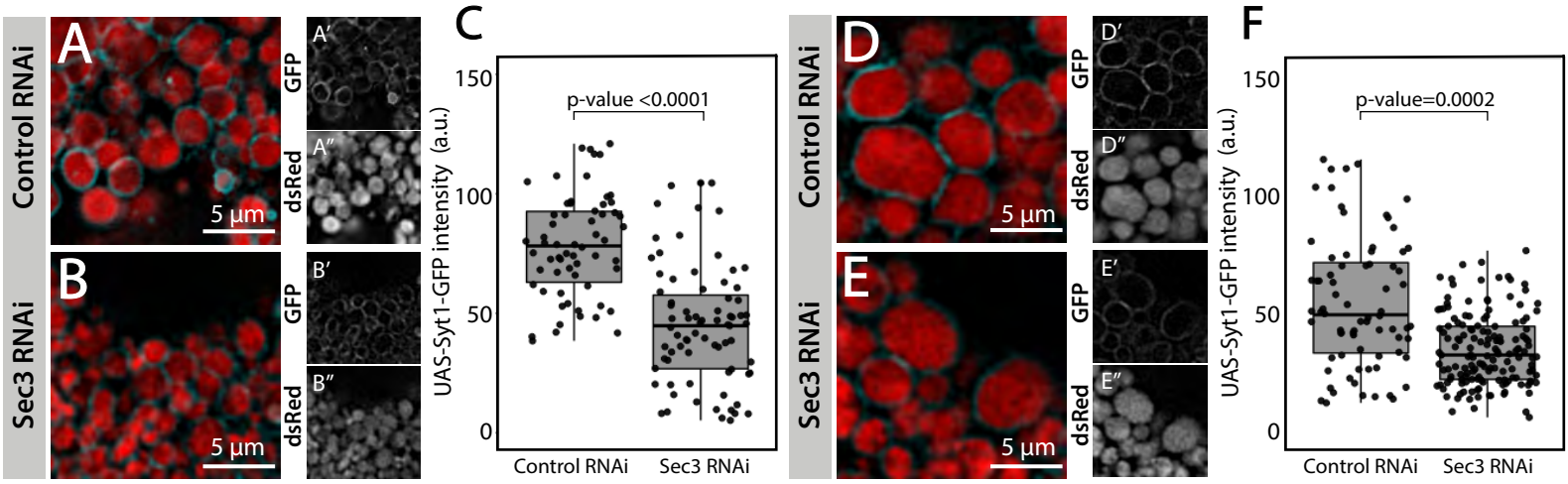

Sgs3-dsRedUAS-CD63-GFP

Immature SGs (25 °C)

Mature SGs (21 °C)

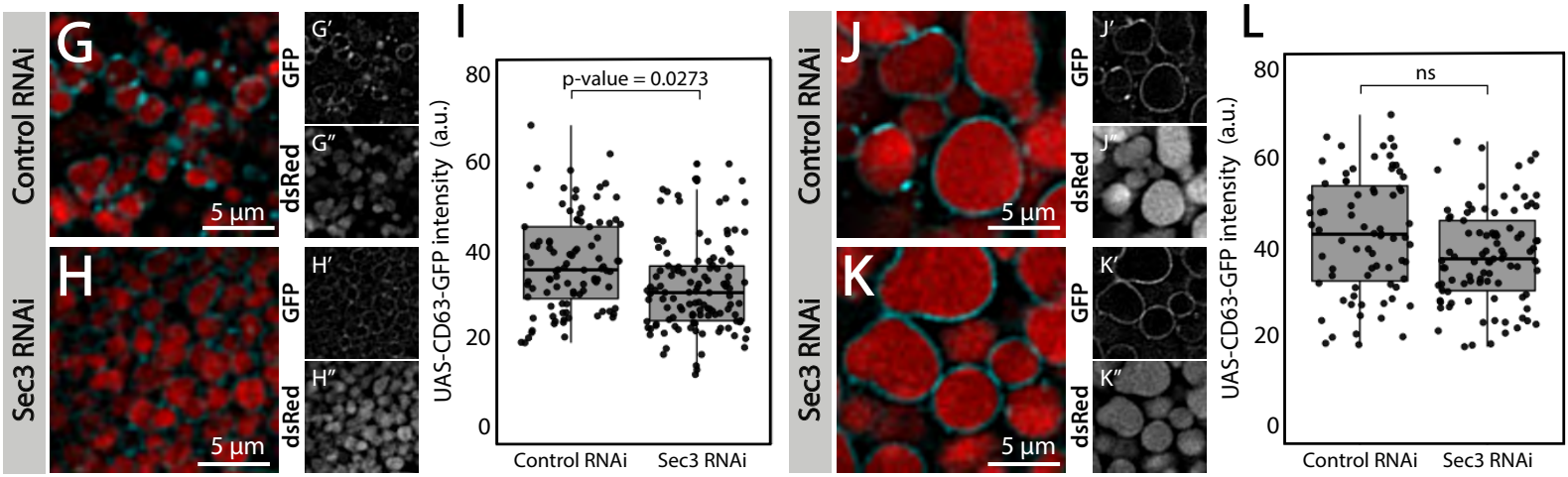

Sgs3-dsRedYFP-Rab11

Immature SGs (25 °C)

Mature SGs (21 °C)

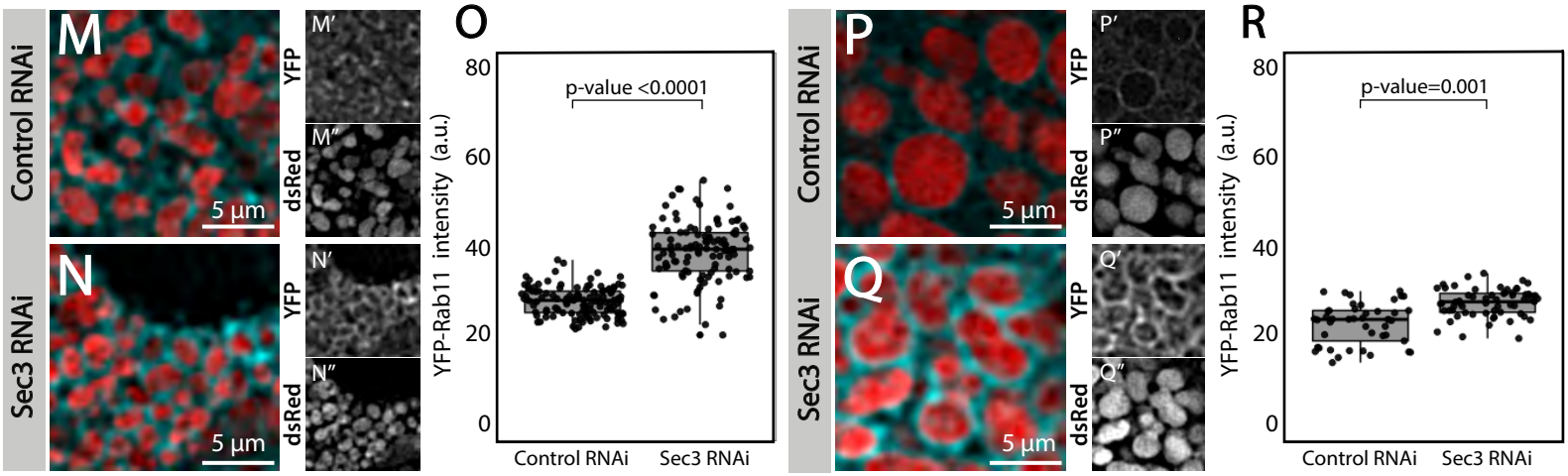

Supplementary Figure 11. The exocyst mediates the acquisition of secretory granule maturation factors. Maturation proteins Syt-1 and CD63 were gradually incorporated to the membrane of SG. Confocal images of unfixed salivary glands of the indicated genotypes. Larvae were grown at 25 or 21 °C to modulate the activity of the Gal4-UAS system and generate a maximal proportion of immature (A, B, G, H, M and N) or mature SGs (D, E, J, K, P and Q) respectively. (A, B, D and E) Recruitment of Syt1-GFP (*UAS-Syt1-GFP*); of (G, H, J and K) CD63-GFP (*UAS-CD63-GFP*); or of (M, N, P and Q) YFP-Rab11 was analyzed in control salivary glands expressing *white*^{RNAi} (*fkh-Gal4/ UAS-white*^{RNAi}) and in salivary glands expressing *sec3*^{RNAi} (*UAS-sec3*^{RNAi}*; fkh-Gal4*). SGs were labelled with Sgs3-dsRed. Fluorescent intensity around SGs of each of the analyzed maturation factors was quantified using the ImageJ software and plotted (C, F, I, L, O and R). Comparison of fluorescence intensity among genotypes, and statistical analysis were performed using one-way analysis of variance (ANOVA). "n" represents the number of salivary glands: (C) *control*^{RNAi} n= 7, *sec3*^{RNAi} n=6; (F) *control*^{RNAi} n=7, *sec3*^{RNAi} n=13; (I) *control*^{RNAi} n= 12, *sec3*^{RNAi} n= 9; (L) *control*^{RNAi} n= 8, *sec3*^{RNAi} n= 8; (O) *control*^{RNAi} n= 7, *sec3*^{RNAi} n= 10; (R) *control*^{RNAi} n= 7, *sec3*^{RNAi} n= 4. Transgenes were expressed using *fkh-Gal4*. "ns" = not significant. Scale bar 5 μm.

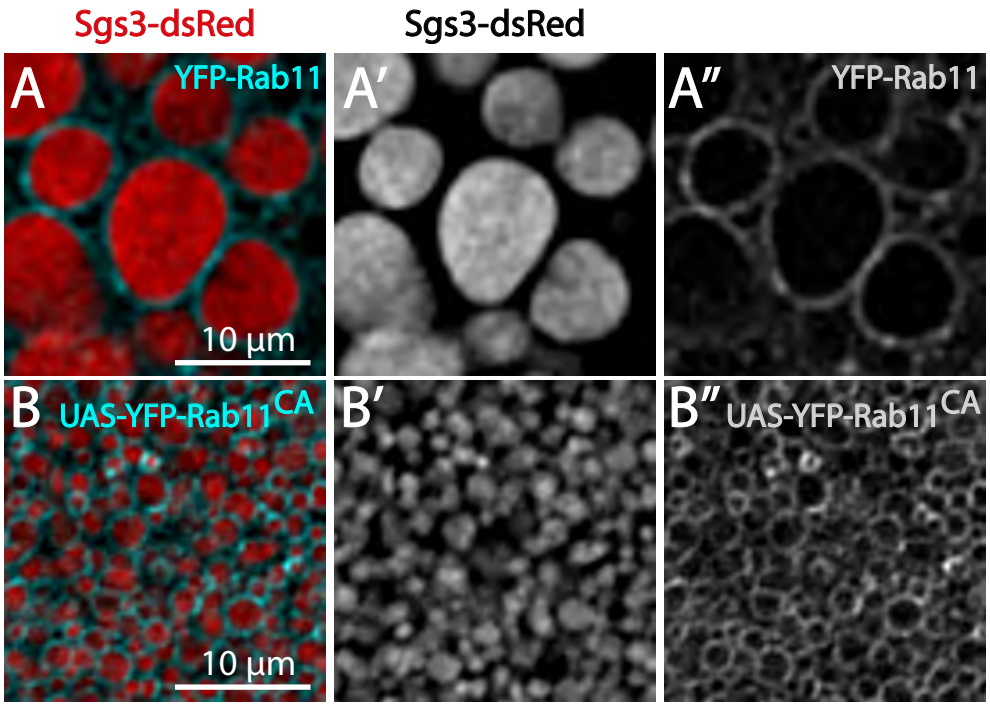
Sgs3-dsRed
Sgs3-dsRed
A
YFP-Rab11
10 µm
A′
A″
YFP-Rab11
B
UAS-YFP-Rab11CA
10 µm
B′
B″
UAS-YFP-Rab11CA

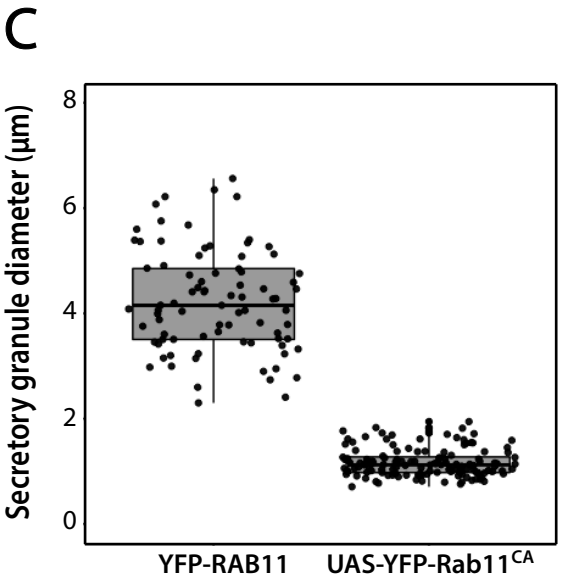
C
Secretory granule diameter (µm)
8
6
4
2
0
YFP-RAB11
UAS-YFP-Rab11CA

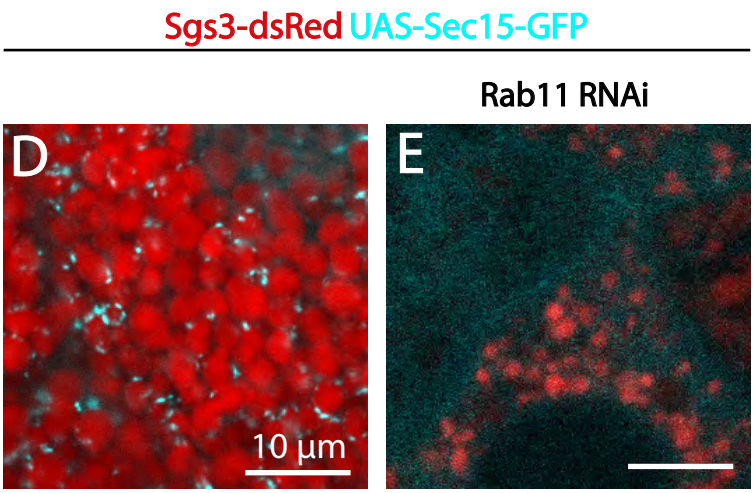
Sgs3-dsRed UAS-Sec15-GFP
Rab11 RNAi
D
10 µm
E

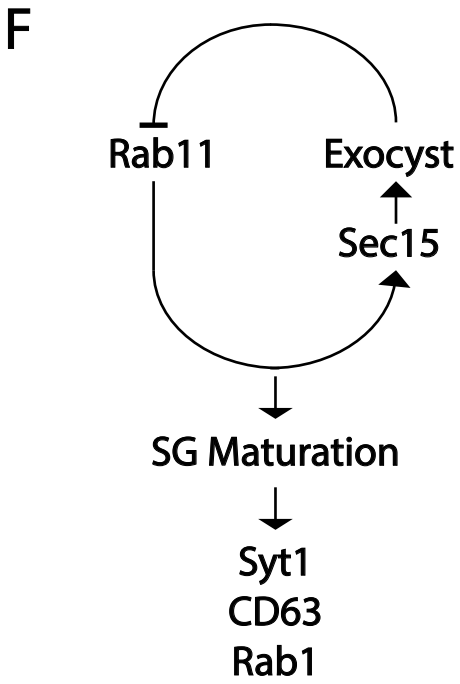
F
Rab11
Exocyst
Sec15
SG Maturation
Syt1
CD63
Rab1

Supplementary Figure 12. The exocyst negatively regulates incorporation of Rab11 to SGs. Salivary gland cells expressing Sgs3-dsRed and endogenously tagged YFP-Rab11 (A), or overexpressing a constitutively active form of Rab11 at 29 °C (*fkh-Gal4/ UAS-YFP-Rab11*^{CA}) (B). YFP-Rab11 localized around mature SGs (A). Overexpression of Rab11^{CA} arrested SG maturation (B), as shown in the quantification of SG diameter (C). YFP-Rab11, n = 6; UAS-YFP-RAB11^{CA}, n = 5. "n" = Number of salivary glands. (D) In control salivary glands, GFP-Sec15 localized as *foci* on the periphery of mature SGs (*sgs3-dsRed/ UAS-GFP-sec15; fkh-Gal4*). (E) Knock-down of Rab11 (*sgs3-dsRed; UAS-rab11*^{RNAi}*/ fkh-Gal4*) generated immature SGs and prevented GFP-Sec15 from localizing on SGs. (F) Proposed mechanism of genetic interactions between Rab11 and Sec15. A single-negative feedback loop regulates the levels of these proteins on the SGs, and recruitment of the maturation factors Syt-1, CD63 and Rab1. Scale bar 10 μm.

Supplementary Movie 1. Real time imaging showing association between the exocyst and the *trans*-Golgi network. A Drosophila early 3rd instar larva salivary gland (~168 hours at 18 °C equivalent to ~72-96 hours at 25 °C) expressing the trans-Golgi marker RFP-Golgi and the exocyst maker GFP-Sec15 in cyan (*UAS-GFP-sec15/UAS-RFP-Golgi; fkh-Gal4*) was imaged. Three-dimensional reconstruction of 6 slides with 0.44 μm spacing was generated using Image J. Frame acquisition time was 2.25 seconds. A total of 78 frames per channel were acquired. Total video time is 77 seconds. Crop size is 8 μm.

Supplementary Movie 2 and 3. Three dimensional reconstruction showing association between the exocyst and the *trans*-Golgi network. A salivary gland from an early 3rd instar larva (~168 hours at 18 °C equivalent to ~72-96 hours at 25 °C) was imaged. The trans-Golgi marker RFP-Golgi (red) and the exocyst maker GFP-Sec15 (cyan) were in close association (*UAS-GFP-sec15/UAS-RFP-Golgi; fkh-Gal4*). Three-dimensional reconstruction of 33 slides with 0.1 μm spacing was generated using Image J. Crop size is 5.57 μm. Corresponds to images shown in Figure 5C 1'.

Supplementary Movie 4. Three dimensional reconstruction showing association between the exocyst and immature secretory granules. A salivary gland from a 3rd instar larva (~186 hours at 18 °C equivalent to ~100 hours at 25 °C) was imaged. SGs with Sgs3-dsRed (red) and the exocyst marker GFP-Sec15 (cyan) were in close association (*sgs3-dsRed/ UAS-GFP-sec15; fkh-Gal4*). Three-dimensional reconstruction of 6 slides with 0.4 μm spacing was generated using image J. Crop size is 10 μm.

Supplementary Movie 5. Three dimensional reconstruction showing association between the exocyst and immature secretory granules. A salivary gland from a 3rd instar larva (~186 hours at 18 °C equivalent to ~104 hours at 25 °C) was imaged. SGs with Sgs3-dsRed (red) and the exocyst marker GFP-Sec15 (cyan) were in close association (*sgs3-dsRed/ UAS-GFP-sec15; fkh-Gal4*). Three-dimensional reconstruction of 12 slides with 0.45 μm spacing was generated using image J. Crop size is 10 μm.

Supplementary Movie 6. Real time imaging of a fusion event between secretory granules. A Drosophila salivary gland expressing Sgs3-dsRed and GFP-Sec15 (*sgs3-dsRed/ UAS-GFP-sec15; fkh-Gal4*) in which a fusion event between SGs was captured (circle). Note that the exocyst (GFP-Sec15) localized at the fusion point between two SGs. The movie was not deconvolved, and represents a maximum intensity projection of three optical slices (total range: 1,6 μm). Scale bar 5 μm.

Supplementary Movie 7. Real time imaging of a fusion event between a secretory granule and the plasma membrane. A Drosophila salivary gland expressing Sgs3-dsRed and GFP-Sec15 (*sgs3-dsRed/ UAS-GFP-sec15; fkh-Gal4*) in which a fusion event between a SGs and the plasma membrane was captured (circle). The granule content was released to the gland lumen (L). The movie shows a single slice of 32 frames comprising a total time of 0.32 seconds. The movie was not deconvolved. Scale bar 5 μm.